


A Global Assessment of the Controls on the Fractionation of Arc Magmas

Journal Article**Author(s):**

Klein, Benjamin Z.; Jagoutz, Oliver; Schmidt, Max W.; [Kueter, Nico](#) 

Publication date:

2023-05

Permanent link:

<https://doi.org/10.3929/ethz-b-000615078>

Rights / license:

[Creative Commons Attribution 4.0 International](#)

Originally published in:

Geochemistry, Geophysics, Geosystems 24(5), <https://doi.org/10.1029/2023GC010888>

Geochemistry, Geophysics, Geosystems®



RESEARCH ARTICLE

10.1029/2023GC010888

Key Points:

- The major element evolution of arc magmas is controlled by the fractionation of pressure and H₂O sensitive mineral assemblages
- We use these relationships to develop two proxies that calculate early fractionation pressure and H₂O contents from magma compositions
- Continental arcs are dominantly H₂O-rich and deeper fractionating, while island arcs are more H₂O-poor and shallower fractionating

Supporting Information:

Supporting Information may be found in the online version of this article.

Correspondence to:

B. Z. Klein,
benjaminzachary.klein@unil.ch

Citation:

Klein, B. Z., Jagoutz, O., Schmidt, M. W., & Kueter, N. (2023). A global assessment of the controls on the fractionation of arc magmas. *Geochemistry, Geophysics, Geosystems*, 24, e2023GC010888. <https://doi.org/10.1029/2023GC010888>

Received 26 JAN 2023



Accepted 17 MAR 2023

Author Contributions:

Conceptualization: Benjamin Z. Klein, Oliver Jagoutz, Max W. Schmidt
Data curation: Benjamin Z. Klein
Formal analysis: Benjamin Z. Klein, Nico Kueter
Funding acquisition: Oliver Jagoutz
Investigation: Benjamin Z. Klein, Oliver Jagoutz, Max W. Schmidt, Nico Kueter
Methodology: Benjamin Z. Klein, Oliver Jagoutz, Max W. Schmidt
Supervision: Oliver Jagoutz
Visualization: Benjamin Z. Klein

© 2023. The Authors. *Geochemistry, Geophysics, Geosystems* published by Wiley Periodicals LLC on behalf of American Geophysical Union. This is an open access article under the terms of the [Creative Commons Attribution License](https://creativecommons.org/licenses/by/4.0/), which permits use, distribution and reproduction in any medium, provided the original work is properly cited.

A Global Assessment of the Controls on the Fractionation of Arc Magmas

Benjamin Z. Klein^{1,2} , Oliver Jagoutz^{1,2}, Max W. Schmidt³ , and Nico Kueter³

¹Institute of Earth Sciences, University of Lausanne, Lausanne, Switzerland, ²Department of Earth, Atmospheric and Planetary Science, Massachusetts Institute of Technology, Cambridge, MA, USA, ³Department of Earth Sciences, ETH, Zurich, Switzerland

Abstract During the differentiation of arc magmas, fractionating liquids follow a series of cotectics, where the co-crystallization of multiple minerals control the melt compositional trajectories, commonly referred to as liquid lines of descent (LLD). These cotectics are sensitive to intensive properties, including fractionation pressure and melt H₂O concentration, and changes in these variables produce systematic differences in the LLDs of arc lavas. Based on a compilation of experimental studies, we develop two major element proxies that exploit differences in LLDs to constrain the fractionation conditions of arc magmas. Near-primary fractionating magmas evolve along the olivine-clinopyroxene cotectic, which is pressure-sensitive. We use this sensitivity to develop a proxy for early fractionation pressure based on the normative mineral compositions of melts with 8 ± 1 wt.% MgO. Fractionation in more evolved magmas is controlled by the clinopyroxene-plagioclase cotectic, which is strongly sensitive to magmatic H₂O contents. We use this relationship to develop an H₂O proxy that is calibrated to the normative mineral components of melts with 2–4 wt.% MgO. These two proxies provide new tools for estimating the variations in pressure and temperature between magmatic systems. We applied these proxies to compiled major element data and phenocryst assemblages from modern volcanic arcs and show that in island arcs early fractionation is relatively shallow and magmas are dominantly H₂O-poor, while continental arcs are characterized by more hydrous and deeper early fractionation. These differences likely reflect variations in the relative contributions of decompression and flux melting in combination with distinct upper plate controls on arc melt generation.

Plain Language Summary Within volcanic arcs, magmas evolve from silica-poor basalts to more silica-rich compositions. This process is dominantly controlled by the minerals that crystallize from the magmas and generates characteristic changes in magma compositions that can be measured in erupted lavas. The crystallizing minerals and evolution in magma composition are sensitive to changes in the conditions at which magmas crystallize including the amount of water dissolved in the magma and the depth of crystallization within the crust. We develop two new methods that use changes in magma composition to understand how these conditions vary between different volcanic arcs. We find that arcs built on continental crust typically erupt lavas that began to crystallize at greater depths and are more water-rich, while arcs built on oceanic crust primarily erupt water-poor lavas that began to crystallize at shallower depths. These differences have important implications for the processes by which new continental crust is created within volcanic arcs.

1. Introduction

Volcanic arcs represent the primary location on Earth for the generation of continental crust (Jagoutz & Schmidt, 2012; Taylor, 1977). Within volcanic arcs, primitive melts originally in equilibrium with mantle olivine and orthopyroxene \pm clinopyroxene differentiate to form erupted products with compositions spanning from basalts to high-silica rhyolites. A range of mechanisms contribute to the observed compositional variations in arc magmas, including partial melting and assimilation of upper plate material (Hildreth & Moorbath, 1988), magma mixing (Eichelberger, 1975; Grove et al., 2004), and crystal fractionation and accumulation (Deering & Bachmann, 2010; Jagoutz, 2010; Wagner et al., 1995). However, multiple lines of evidence show that crystallization differentiation within the arc crust is the dominant control on the compositional variations in arc magmas (Jagoutz & Klein, 2018). These include studies examining erupted arc products globally (Keller et al., 2015; Lee & Bachmann, 2014), studies of exposed arc sections (Greene et al., 2006; Jagoutz, 2010, 2014; Jagoutz et al., 2011; Klein & Jagoutz, 2021; Walker et al., 2015), and experimental studies of arc magma fractionation (Grove et al., 2003; Nandedkar et al., 2014; Ulmer et al., 2018).

Writing – original draft: Benjamin Z. Klein

Writing – review & editing: Benjamin Z. Klein, Oliver Jagoutz, Max W. Schmidt, Nico Kueter

During crystallization, the removal of cumulate minerals from differentiating magmas produces distinct compositional trends that are commonly referred to as liquid lines of descent (LLD). Critically, with progressive fractionation, all melt compositions converge to cotectics where the fractionating mineral assemblages do not vary. The locations and trajectories of these cotectics do not chiefly depend on the initial melt bulk composition but on intensive properties such as pressure, H₂O concentration and oxygen fugacity. Therefore, the major element LLDs along which arc magmas evolve do not primarily depend on the parental melt composition but on the conditions under which the magmas fractionate. Variations in fractionation conditions can therefore be inferred from the distinct compositional trends generated along LLDs (e.g., Parman et al., 2010; Zimmer et al., 2010). In this study, we develop two proxies that relate differences in major element LLDs to melt H₂O contents and fractionation pressure. We then apply these proxies to a global compilation of arc lava compositions to identify first order differences in fractionation conditions among active arcs.

2. Existing Methods to Estimate Magma H₂O Contents and Fractionation Pressure

Several techniques exist to estimate pre-eruptive magmatic H₂O contents and fractionation pressures. These methods can broadly be divided into three groups: (a) direct measurements, typically of melt inclusions; (b) mineral-melt equilibria, based on either the partitioning of hydrogen in nominally anhydrous minerals, or on H₂O-sensitive mineral-liquid exchange reactions; and (c) experimentally constrained liquid lines of descent. We will discuss existing LLD-based methods in the context of our new proxies below, but first offer a brief summary of the other approaches.

The most direct technique to constrain pre-eruptive H₂O contents is to measure the H₂O contents of melt inclusions trapped in phenocrysts (e.g., Portnyagin et al., 2007; Ruscitto et al., 2012; Sisson & Layne, 1993). If the melt inclusion H₂O content is not modified post-entrapment, this approach can directly constrain the original H₂O contents of the magma. Further, when H₂O and CO₂ are both present in melt-inclusions, minimum entrapment and hence fractionation pressures can also be constrained (Newman & Lowenstern, 2002). Primary limitations to this technique are that vapor-saturated melts may degas prior to melt inclusion formation, and melt inclusions are susceptible to rapid post-entrapment diffusive re-equilibration, especially of hydrogen (Bucholz et al., 2013; Gaetani et al., 2012), which modifies the apparent melt H₂O contents and oxidation state. To minimize the effects of diffusive re-equilibration, melt inclusion studies are often restricted to relatively recently erupted ash and scoria (Lloyd et al., 2013).

Mineral-melt partitioning-based hygrometers and barometers provide valuable information on the conditions of magmatic differentiation. The plagioclase-melt hygrometer (Lange et al., 2009; Waters & Lange, 2015), based on the strongly H₂O-dependent distribution of the anorthite component between plagioclase and melt, is the most commonly used mineral-melt hygrometer. A range of mineral-melt barometers have also been developed, many of which are derived from the pressure sensitivity of Al-rich components in pyroxenes (e.g., Neave & Putirka, 2017; Putirka, 2008, 2016). The primary limitation of all mineral-melt approaches lies in the evaluation of primary equilibrium as well as the need for independent temperature estimates. Alternatively, melt H₂O contents can be constrained by directly measuring the hydrogen contents of nominally anhydrous minerals (NAMs, e.g., Mitchell et al., 2017; Urann et al., 2022). For minerals with experimentally constrained hydrogen partition coefficients (i.e., garnet, olivine, clinopyroxene), this method expands our ability to estimate primary H₂O contents to systems that are otherwise difficult to constrain. However, the H₂O contents of NAMs are difficult to measure and re-equilibration due to rapid hydrogen diffusion frequently destroys the record of primary H₂O contents (e.g., Demouchy et al., 2006).

While both melt-inclusion and mineral melt-based estimates of magmatic H₂O contents and pressures provide valuable constraints, their application is restricted by the availability of appropriate samples, that is, lavas containing the necessary phenocrysts and a glassy matrix or melt inclusions. A complementary approach for investigating global arc magma systematics is to use the whole rock compositions of erupted magmas to locate pressure- and H₂O-sensitive cotectics in compositional space.

3. Major Element Proxies for Variations in Liquid Lines of Descent

In this study, we develop two proxies that relate variations in major element liquid lines of descent in arc magmas to differences in their fractionation conditions. We rely on the large number of experimental studies investigating

liquid lines of descent in tholeiitic and calc-alkaline systems to infer the relationships between conditions of fractionation and LLD compositional trajectories (experimental studies summarized in Table S1 of the Supporting Information S1). Many of these studies provide clear examples of how LLDs change in response to different fractionation pressures (Nandedkar et al., 2014 vs. Ulmer et al., 2018; Villiger et al., 2004 vs. Villiger, Ulmer, & Müntener, 2007) and magmatic H₂O contents (Alonso-Perez et al., 2009; Melekhova et al., 2015; Nandedkar et al., 2014 vs. Villiger, Ulmer, & Müntener, 2007).

Based on these experiments, a representative simplified fractionation sequence can be defined for arc basalts across a range of experimental conditions: Most primitive arc magmas last equilibrate with the sub-arc mantle at conditions where they are multiply saturated in olivine, orthopyroxene and clinopyroxene, typically at 10–18 kbars and 1,220–1,350°C (for recent compilations of multiple saturation points see Schmidt & Jagoutz, 2017 and Till, 2017). At pressures greater than this multiple saturation point, clinopyroxene becomes the liquidus phase, while olivine is the liquidus phase at lower pressures. Concomitantly, the temperature difference between the olivine-liquidus and clinopyroxene-in increases with decreasing pressure: at pressures just below the multiple saturation point, clinopyroxene is rapidly added to the fractionating assemblage, while at lower pressures, the olivine liquidus field expands resulting in prolonged olivine-only fractionation prior to clinopyroxene-in. By contrast, in dry magmas fractionating at low pressures (as is typical at many mid-ocean ridges), plagioclase may stabilize before clinopyroxene but only after extensive olivine-only fractionation. Thus, during fractionation at relatively high pressures, the liquid line of descent exhibits only a limited initial enrichment in clinopyroxene-forming oxide components (e.g., CaO), while at lower pressures a much larger CaO-enrichment interval is observed, and this difference persists during differentiation following the olivine-clinopyroxene cotectic (Figure 1a).

As melts continue to evolve along the LLD, plagioclase joins the fractionating assemblage. Continuing silica enrichment during differentiation makes the melts lose olivine-saturation, either by olivine-consuming peritectic reactions that produce orthopyroxene or through fractional crystallization. Numerous prior studies have established that increases in melt H₂O contents cause a decrease in plagioclase stability (Eggler, 1972; Gaetani et al., 1993; Sisson & Grove, 1993a), and that the first appearance of plagioclase is strongly controlled by H₂O contents but is relatively pressure insensitive at crustal pressures (Eggler, 1972). Therefore, plagioclase-forming components such as Al₂O₃ passively increase in fractionating melts until plagioclase joins the crystallizing assemblage (Figure 1b). Consequently, a delay in plagioclase-in will increase the maximum observed Al₂O₃ contents along any liquid line of descent, an observation previously used to constrain melt H₂O contents (Parman et al., 2010; Pichavant & Macdonald, 2007; Sisson & Grove, 1993b). Continuing fractionation proceeds along the clinopyroxene-plagioclase (±amphibole) cotectic for an extended interval, typically until the system reaches at least intermediate SiO₂ contents at temperatures below ~1,050°C in H₂O-poor systems and below ~900°C in H₂O-rich systems.

Additional phases may also be stable during arc magma fractionation: at elevated pressures (>8–10 kbars), garnet may become a fractionating phase, particularly in more evolved compositions (Alonso-Perez et al., 2009; Ulmer et al., 2018). Hornblende plays an important role in the fractionation sequence of hydrous magmas (Nandedkar et al., 2014), but rarely appears before the melt has cooled below 1,050°C (Melekhova et al., 2015; Nandedkar et al., 2014; Ulmer et al., 2018); amphibole appears as a near-liquidus phase only in H₂O-saturated basaltic magmas (Krawczynski et al., 2012; Stern et al., 1975). Orthopyroxene occurs mostly in minor abundances but can become a more important phase in systems with SiO₂-rich primitive compositions (e.g., Grove et al., 2003; Ulmer et al., 2018). Finally, FeTi-oxides are present in evolved arc sequences and stabilize earlier on wet than on dry LLDs (Sisson & Grove, 1993a). Despite potential complications from these additional phases, the early portions of the LLDs of most arc magmas can be readily understood from the fractionation systematics of olivine, clinopyroxene and plagioclase.

The pressure dependency of CaO-enrichment was previously described in dry MORB systems (Langmuir et al., 1992), and the systematics of the olivine-clinopyroxene cotectic form the basis of multiple barometers applied to MORB LLDs (Danyushevsky et al., 1996; Herzberg, 2004; Michael & Cornell, 1998; Villiger, Müntener, & Ulmer, 2007). Melekhova et al. (2015) also used the pressure sensitivity of the olivine-clinopyroxene cotectic in variably hydrated parental magmas from the Lesser Antilles to deduce their pressures of fractionation. Similarly, the suppression of plagioclase crystallization by H₂O has been leveraged to infer magmatic H₂O contents using the relations between melt H₂O contents and either the maximum Al₂O₃ recorded in lavas sampling a common LLD (Parman et al., 2010) or the Al₂O₃ content in melts multiply saturated with olivine,

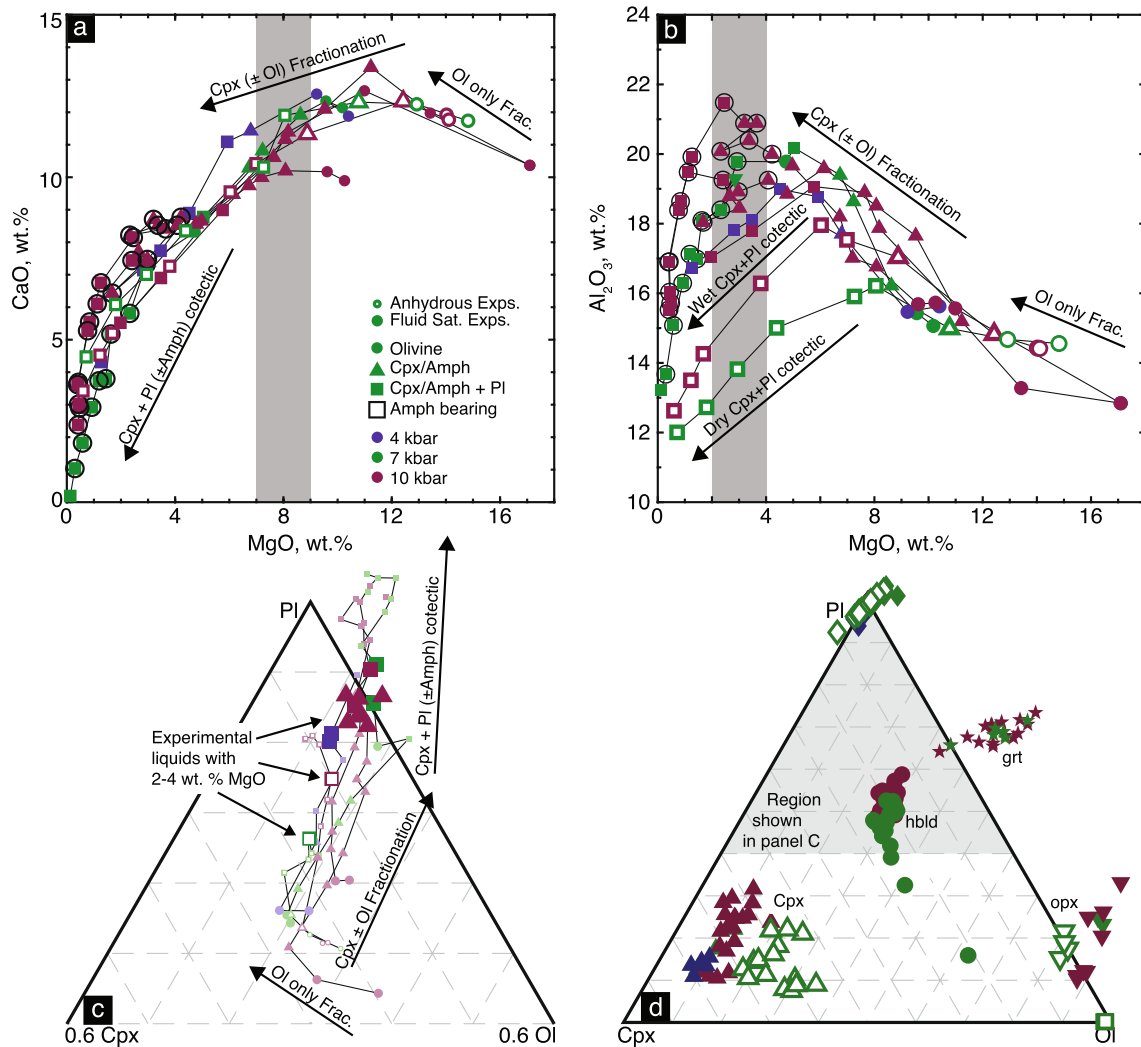


Figure 1. Illustration of liquid lines of descent (LLD) determined from fractional crystallization experiments for basaltic starting compositions at different pressures and initial water contents. In each panel, symbols denote phenocryst assemblage, and color and symbol are used to distinguish experimental pressures and hydration states. (a) The LLD of magmas shown in MgO-CaO space. Three segments are observed in these LLDs, corresponding to olivine only, olivine + clinopyroxene and clinopyroxene + plagioclase ± amphibole cotectics. The gray vertical bar centered on 8 wt. % MgO shows the region sampled by P_{ol-cpx} . (b) LLD of magmas shown in MgO- Al_2O_3 space. The same three fractionation segments are again observable, and the hydrous and dry clinopyroxene-plagioclase cotectics are well-distinguished. Horizontal bar centered on 3 wt. % MgO shows the primary compositional criteria used to identify samples for calculating H_2O_{cpx-pl} . (c) The same experimental series as in a and b projected into the normative plagioclase-clinopyroxene-olivine pseudo-ternary. Here large symbols are used to identify experiments with appropriate compositions for calculating H_2O_{cpx-pl} . (d) Phenocryst mineral compositions from the same experimental series plotted in the plagioclase-clinopyroxene-olivine pseudo-ternary space. Symbols represent different phases and are labeled in the figure. Plotted experimental data in all panels from Nandedkar (2014), Nandedkar et al. (2014), Ulmer et al. (2018), Villiger et al. (2004), and Villiger, Ulmer, and Müntener (2007).

plagioclase, and clinopyroxene or hornblende (Pichavant & Macdonald, 2007; Sisson & Grove, 1993b). Each of these hygrometers is restricted to a relatively narrow range of basaltic to basaltic-andesite compositions where plagioclase first stabilizes. In the following sections we develop proxies for fractionation pressure and melt H_2O contents based on the olivine-clinopyroxene and clinopyroxene-plagioclase cotectics respectively and show that these proxies are robust for a range of arc magma compositions. We begin by first describing the compiled database of experimental liquids and our approach to developing the H_2O and pressure proxies.

3.1. Experimental Liquid Database

A total of 1,248 experimental liquids were compiled from 54 publications (summary of compiled experimental publications available in Table S1 of the Supporting Information S1). Publications with experiments conducted

at ≤ 20 kbars and with tholeiitic to relatively K-rich calc-alkaline and mafic to intermediate starting compositions were prioritized. The compilation includes 528 anhydrous experiments, of which 324 were conducted at 1 atm and 204 at elevated pressures. The remaining 720 experiments were conducted with hydrous bulk compositions, including 333 experiments that were fluid-saturated (either H_2O or a mixed C-O-H fluid) and 387 that were fluid-undersaturated. For each experiment, the melt composition, phenocryst assemblage, and melt fraction were compiled. For nearly all experiments, melt fractions are reported in the original publications and were calculated using mass balance or less commonly by point counting and/or image processing techniques. For a small subset of experiments that do not report melt fractions, we calculated melt fractions assuming that K_2O is perfectly incompatible.

We also compiled the H_2O concentrations of all hydrous melts. Where available, we relied on published directly measured H_2O contents, which included measurements made using various techniques including Raman and Fourier transform infrared spectroscopy, ion microprobe, calibrated electron microprobe measurements and Karl-Fischer titration. When not directly measured, we calculated melt H_2O contents based on mass balance for H_2O -undersaturated experiments and using VESICAL (Iacovino et al., 2021) for fluid-saturated experiments after calculating melt Fe_2O_3 contents from the reported experimental $f\text{O}_2$ using the calibration of Kress and Carmichael (1991). As some biases may be introduced by combining these methods, we used the same approach to calculate H_2O contents in experiments with direct measurements and additionally calculated H_2O contents using the plagioclase-melt hygrometer (Waters & Lange, 2015). Comparisons of all three methods show acceptable agreement given the generally large uncertainties for many of these approaches (Figure S1 in Supporting Information S1), consistent with previous studies (Devine et al., 1995).

In principle, thermodynamic phase equilibria modeling can complement our experimental compilation and help to further refine models for how fractionation pressure and melt H_2O contents control liquid lines of descent. However, when comparing liquid lines of descent calculated with rhyoliteMELTS (Gualda et al., 2012) to representative series of experiments, we found that rhyoliteMELTS consistently fails to accurately reproduce the location of both the olivine-clinopyroxene and clinopyroxene-plagioclase cotectics in both hydrous and anhydrous experiments conducted at pressures above 2 kbars (Text S1 in Supporting Information S1). This is consistent with results from previous experimental studies (e.g., Nandedkar et al., 2014; Villiger et al., 2004) that compared their results to MELTS and shows that both more experiments and better solution models are needed before phase equilibria models can be relied on to model liquid lines of descent at a range of pressures and volatile contents.

3.2. Development of Pressure and H_2O Proxies Based on Mineral Projections

Two requirements must be satisfied before leveraging the compositions of melts crystallizing on cotectics as proxies for fractionation pressure and magmatic H_2O contents: (a) melts in equilibrium with the cotectic mineral assemblages must be identifiable; and (b) the proxies must rely only on melt components buffered by the cotectic assemblages. The first criterium is trivial to evaluate with the experimental data set. However, satisfying this requirement is more challenging in natural lavas, where the crystalline cargoes of erupted lavas may not correspond to the equilibrium fractionating assemblages (see Section 6.1). Therefore, instead of relying on phenocryst assemblages to identify suitable lavas, we used the reported phase assemblages of experimental liquids to identify ranges of magma compositions that are most often in equilibrium with a given cotectic assemblage. By using these same criteria to filter the experimental calibration data set, we incorporate into our proxies the uncertainties that result from including some liquids that are not on the cotectic. We additionally exclude from our calibration experiments where iron or alkali loss was observed, and those with melt fractions below 0.2, where identification and analysis of equilibrium melt becomes difficult, or above 0.95, where the melt composition may still be sensitive to the starting composition. The experimental data used to calibrate the two proxies are provided in Tables S2 and S3.

To satisfy the second requirement, we follow previous workers studying magmatic fractionation (e.g., Grove et al., 1992; Herzberg, 2004; Merzbacher & Egger, 1984; Yang et al., 1996) and use normative mineral components (Tormey et al., 1987) to isolate the melt components most sensitive to the systematics of the olivine-clinopyroxene and clinopyroxene-plagioclase cotectics. This projection recalculates the bulk composition of a liquid as mineral components, which then can be readily identified as enriching or fractionating. The sensitivity of these normative mineral components to cotectic fractionation is enhanced by projecting the normative mineral components into the olivine-clinopyroxene-plagioclase pseudo-ternary space that includes both cotectic assemblages (Figure 1c).

The normative olivine, clinopyroxene and plagioclase components are calculated according to Equations 1–3 (after Grove et al., 1992; Tormey et al., 1987) using molar melt compositions, and subsequently are projected into the olivine-clinopyroxene-plagioclase pseudo-ternary by normalizing the sum of the three components to 1.

$$pl = 2AlO_{1.5} + 2(NaO_{0.5} - KO_{0.5}) \quad (1)$$

$$ol = -TiO_2 + 0.5(AlO_{1.5} - CrO_{1.5}) + FeO + MgO - CaO - 0.5(NaO_{0.5} + KO_{0.5}) + \frac{5}{3}PO_{2.5} \quad (2)$$

$$cpx = -1.5AlO_{1.5} + 3CaO + 1.5(NaO_{0.5} + KO_{0.5}) - 5PO_{2.5} \quad (3)$$

Pseudo-ternary plots of representative experimental liquid lines of descent are shown in Figure 1c, illustrating the systematics of the olivine-clinopyroxene and clinopyroxene-plagioclase cotectics. The initial melts in these experimental series are near-mantle melt compositions, and thus olivine is the liquidus phase at the experimental pressures and H₂O contents. During the initial interval of olivine-only fractionation, melt compositions migrate toward the clinopyroxene-plagioclase join. Experiments conducted at lower pressures undergo more extensive olivine fractionation, and these melts evolve further from the olivine vertex. Subsequently, the melts undergo clinopyroxene-olivine fractionation followed by clinopyroxene-plagioclase (\pm olivine, hornblende) fractionation. Most melt trajectories during clinopyroxene-plagioclase fractionation are parallel and broadly overlapping. However, the rates at which melts evolve along this trajectory differ. Thus, if melts with similar extents of differentiation (highlighted in Figure 1b based on MgO contents) are compared, the differences between hydrous and dry LLDs are readily apparent.

Following projection, the relationship between normative mineral components and P or H₂O was quantified by fitting a piecewise-planar surface defined by equations with the form:

$$P \text{ or } H_2O = \max(aX + bY + c, 0) \quad (4)$$

where X and Y are projected normative mineral components, a , b , and c are fitted coefficients, and $\max(i, j)$ is a function that returns the greater of the two values i and j . This equation defines two portions of the model, a positive planar surface with a gradient determined by a and b , and a constant zero-valued component, and ensures continuity between these components. Given the limited experimental data set, we did not use separate training and test data, but estimated the model uncertainty by repeating this fitting procedure using 10-fold cross validation and calculating the average RMSE of the test fraction from each cross validation. Implementations of both proxies as Excel worksheets are available for download as Tables S4 and S5.

3.3. P_{ol-cpx} : An Early Fractionation Barometer Based on the Olivine-Clinopyroxene Cotectic

As described above, clinopyroxene crystallization begins in most systems after an interval of olivine-only fractionation. However, melts often evolve on the olivine-clinopyroxene cotectic for a relatively limited interval prior to the stabilization of plagioclase. As plagioclase fractionation can obscure the olivine-clinopyroxene systematics, it is essential to restrict the calibration data set for this proxy to a range of melts that maximizes the percentage of compositions in equilibrium with olivine and clinopyroxene while minimizing the number of plagioclase-crystallizing lavas. We found that melts with ~ 8 wt. % MgO best balanced these two objectives as the experimental compilation shows a dramatic increase in the number of melts crystallizing clinopyroxene at this MgO content (Figure 2a), suggesting that melts with this composition are typically near the onset of clinopyroxene-olivine fractionation. To optimize the calibration of this pressure proxy, we used experimental melt compositions linearly interpolated to 8 wt. % MgO, and only included experimental series where the two bracketing experiments with the nearest MgO contents contained between 6 and 10 wt. % MgO. We observe that nearly all experimental series conducted at pressures >4 kbars are on the olivine-clinopyroxene cotectic at 8 wt. % MgO, while several lower pressure experiments had not yet stabilized clinopyroxene but are close to clinopyroxene saturation (Figure 2c). Some anhydrous experiments begin crystallizing plagioclase prior to ~ 8 wt. % MgO, particularly at low pressure, but these experiments have melt compositions consistent with the trend defined by plagioclase-free experiments. This is indicative of limited fractionation immediately upon plagioclase-saturation. Finally, none of the melts with ~ 8 wt. % MgO are saturated in amphibole.

We fit Equation 4 to these data to find the relationship between normative clinopyroxene and olivine contents and pressure (Figure 2b; Equation 5):

$$P_{ol-cpx}(\text{kbars}) \pm 1.8 = \max(7.66Ol - 77.07Cpx + 19.43, 0) \quad (5)$$

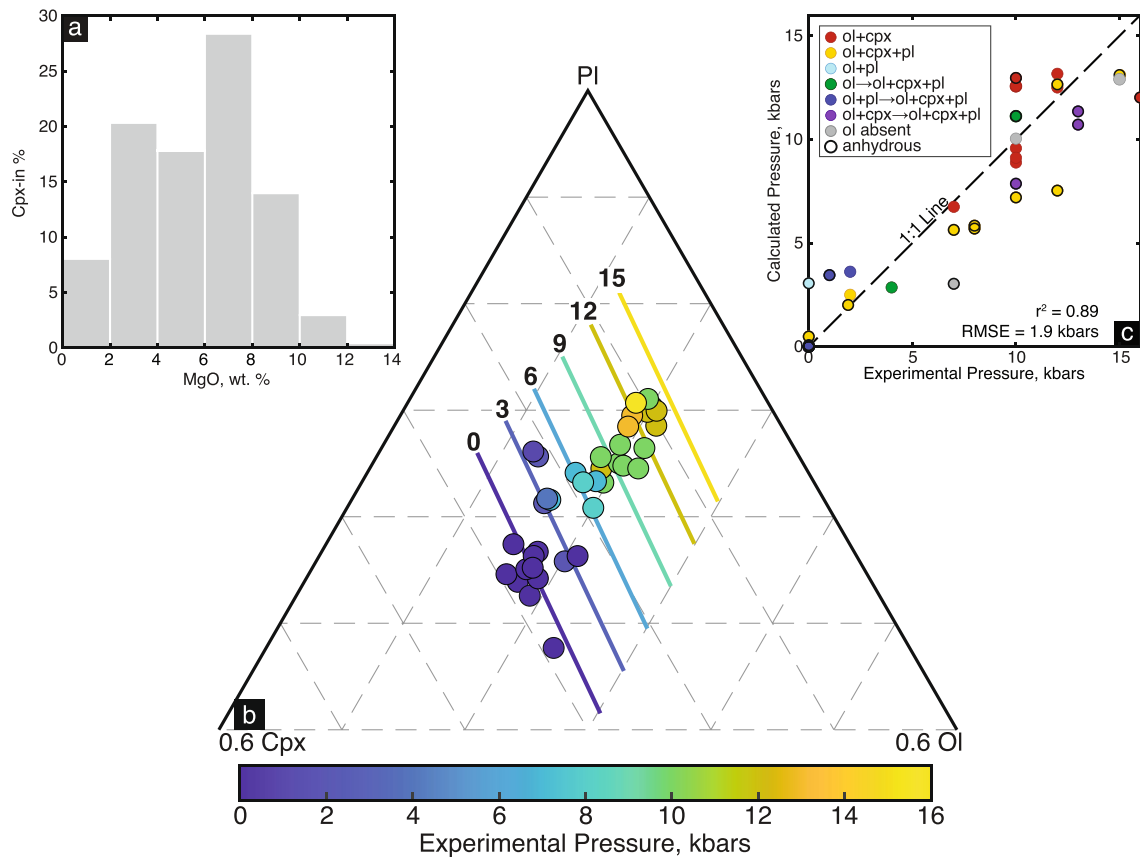


Figure 2. Development of the P_{ol-cpx} proxy based on the olivine-clinopyroxene cotectic. (a) Histogram of the MgO contents at which the experimental fractionation series first crystallize clinopyroxene. A maximum is observed at ~ 8 wt. % MgO, by which point $>50\%$ of all experiments are crystallizing clinopyroxene. Note that this fraction is underestimated as many of the included experimental studies use starting compositions with less than 8 wt. % MgO. (b) Plagioclase-clinopyroxene-olivine pseudo-ternary plot showing the projection of experimental melt compositions interpolated to 8 wt. % MgO. Symbol colors show experimental pressures. Labeled lines indicate isobars derived from the P_{ol-cpx} surface and are similarly colored to show pressure. (c) Comparison of P_{ol-cpx} to experimental pressures. Symbol colors indicate phenocryst assemblages in bracketing experiments. Symbol labels with multiple mineral assemblages indicate experimental series where the phenocryst changes between the two bracketing experiments.

This equation defines the clinopyroxene-olivine cotectic barometer (which we refer to as P_{ol-cpx}) and reflects the expected relationship between fractionation pressure and the olivine-clinopyroxene cotectic: pressure is negatively correlated with clinopyroxene content and is $\sim 10X$ more sensitive to changes in normative clinopyroxene contents than olivine contents. P_{ol-cpx} has an uncertainty of 1.8 kbars estimated based on the average RMSE calculated from 10-fold cross validation. The overall systematics supports a semi-quantitative relationship where normative clinopyroxene content in early fractionating melts correlates with early fractionation pressure. Arc magmas with lower normative clinopyroxene can be inferred to crystallize at shallow pressures, while higher normative clinopyroxene indicates early fractionation at higher pressures. This pressure proxy should only be applied to natural whole rock data with 8.0 ± 1.0 wt. % MgO that fall within the field defined by the experimental calibration data set in the olivine-clinopyroxene-plagioclase pseudoternary.

We note that the approach behind estimating P_{ol-cpx} shares some similarities to the $Ca_{6,0}$ metrics developed in previous studies of arc magmas (Plank & Langmuir, 1988; Turner & Langmuir, 2015) as CaO contents are buffered during fractionation on the olivine-clinopyroxene cotectic. However, the distinction between using melt compositions at 8 versus 6 wt. % MgO is critical. In experiments with liquids with ~ 6 wt. % MgO, nearly all anhydrous compositions crystallize plagioclase, while many H_2O -bearing experiments are still plagioclase free (Figure S2 in Supporting Information S1). This sensitivity to the strongly H_2O -dependent plagioclase stability (see Section 3.4) causes the correlation between fractionation pressure and normative clinopyroxene contents to weaken significantly for melts with 6 wt.% MgO.

3.4. $H_2O_{\text{cpx-pl}}$: A Hygrometer Based on the Clinopyroxene-Plagioclase Cotectic

Melts typically evolve along the clinopyroxene-plagioclase (\pm hornblende) cotectic for an extended temperature interval (Figure 3a) and within this interval the difference in plagioclase-forming oxide components between hydrous and dry melts is broadly constant (Figures 1b and 1c). Therefore, a proxy for magmatic H_2O contents based on this cotectic could potentially be applied to a wide range of melt compositions. Nevertheless, H_2O is continuously enriched during fractionation until reaching fluid-saturation, at which point initial differences in H_2O content converge to (pressure-dependent) saturation values. To isolate differences in magmatic H_2O contents independent of the extent of differentiation, we focus on developing a clinopyroxene-plagioclase cotectic H_2O proxy for melts with 2–4 wt. % MgO, which typically includes andesitic to dacitic compositions. In addition, we restrict the calibration data set to SiO_2 contents between 52 and 65 wt.%, and X_{Mg} below 0.65. The first of these criteria helps to avoid any melts that have evolved past clinopyroxene and/or hornblende stability, while the second ensures that no melts in (near-) equilibrium with mantle olivine are included.

Applying these criteria yields melts from 146 experiments that range in pressure from 1 atm to 12 kbar including 26 anhydrous experiments. To calibrate the H_2O proxy (which we refer to as $H_2O_{\text{cpx-pl}}$), we fit Equation 4 to the clinopyroxene and plagioclase components of these experimental melts, resulting in Equation 6 (Figure 3b):

$$H_2O(\text{wt.}\%) \pm 1.4 = \max(4.88\text{Pl} - 36.74\text{Cpx} + 2.71, 0) \quad (6)$$

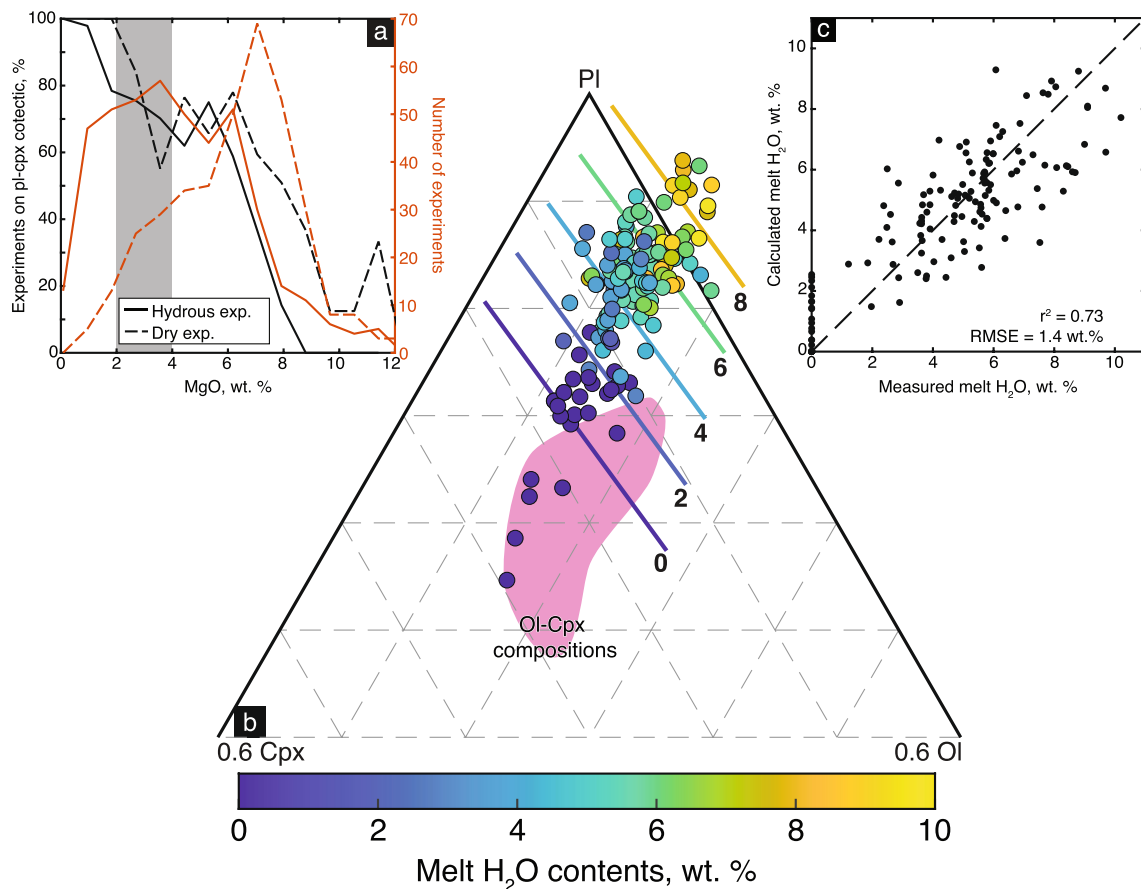


Figure 3. Development of the $H_2O_{\text{cpx-pl}}$ proxy based on the clinopyroxene-plagioclase cotectic. (a) Distribution of experiments crystallizing on the clinopyroxene + plagioclase \pm amphibole cotectic as a function of MgO content. Black lines show the percentage of experiments with cotectic phenocrysts while red lines show the total number of experiments. For both axes, solid lines show data for hydrous experiments and dashed lines represent anhydrous experiments. The percentage of experiments on the cotectic is likely underestimated, primarily due to difficulties with nucleating plagioclase at lower temperatures. (b) Plagioclase-clinopyroxene-olivine pseudo-ternary plot showing projected melt compositions from experiments used to calibrate $H_2O_{\text{cpx-pl}}$. Symbol colors show experimental H_2O contents. Labeled lines show H_2O content isopleths calculated from the $H_2O_{\text{cpx-pl}}$ surface. Compositional field of samples used to calibrate the $P_{\text{ol-cpx}}$ model from Figure 2b shown in pink. (c) Comparison of modeled H_2O contents and experimental H_2O contents. Typical uncertainties on experimental H_2O contents are 1–2 wt. %.

The modeled relationship has an RMSE of 1.4 wt. % H₂O (Figure 3c), indicating relatively strong predictive power. The proxy has stronger sensitivity to the normative clinopyroxene component than the plagioclase component. However, as the normative olivine component remains roughly constant throughout the calibration data set (Figure 3b), the plagioclase and clinopyroxene components must be inversely correlated. Thus, the H₂O_{cpx-pl} is consistent with the hypothesis that normative plagioclase contents and H₂O are correlated, and moreover shows that there is a complimentary inverse correlation between normative clinopyroxene contents and H₂O.

Finally, we also note that the barometer and hygrometer both define relatively similar trends in the olivine-clinopyroxene-plagioclase pseudo-ternary space. It has been observed in past studies that increasing pressure may also inhibit plagioclase crystallization (e.g., Bartels et al., 1991; Bender et al., 1978), raising the possibility that the effects due to changes in pressure and H₂O contents are conflated in our two proxies. However, we are confident that P_{ol-cpx} and H₂O_{cpx-pl} successfully isolate the effects of pressure and H₂O: we found that attempting to model the experimental pressures of the H₂O_{cpx-pl} data set results in a much worse fit compared to the H₂O_{cpx-pl}, and more importantly, the modeled pressure surface is nearly orthogonal to the hygrometer calibration (Figure S3 in Supporting Information S1), showing that the H₂O_{cpx-pl} proxy is insensitive to differences in fractionation pressure. Further, there is essentially no overlap between the compositional fields of the two calibration data sets (Figure 3b), and melts have necessarily undergone significant differentiation from ~8 wt. % to 2–4 wt. % MgO between the two proxies.

3.5. Fe-Mg Systematics: The Tholeiitic Index (THI)

Lastly, an alternative LLD-based proxy for magmatic H₂O contents is the Tholeiitic Index (Zimmer et al., 2010). The Tholeiitic Index leverages the observation that LLDs characterized by Fe-enrichment (tholeiitic) trends are generated in magmas with low H₂O contents, while Fe-depletion (calc-alkaline) LLDs are characteristic of high H₂O contents (Sisson & Grove, 1993a). This difference results from the enhanced stability of FeTi-oxides and amphibole relative to other silicate phases (especially plagioclase) in H₂O-rich magmas (Alonso-Perez et al., 2009; Grove & Baker, 1984; Sisson & Grove, 1993a). Zimmer et al. (2010) quantified the difference in these LLDs by calculating the ratio of Fe4 to Fe8, where Fe[X] is defined as the mean FeO content of magmas with MgO contents equal to X ± 1 wt. %. They show that the Fe4/Fe8 ratio correlates inversely with absolute melt H₂O content, where ratios less than 1 are associated with H₂O-rich magmas. Recently, it was suggested that pressure may also strongly control the tholeiitic versus calc-alkaline fractionation trends, with high pressure fractionation of garnet-rich cumulates generating Fe-depletion LLDs (Chiaradia, 2014; Tang et al., 2018). Nevertheless, the Tholeiitic Index broadly correlates with magmatic H₂O contents (Zimmer et al., 2010), and we calculate arc-scale Tholeiitic Index values to compare to H₂O_{cpx-pl}. In calculating the Tholeiitic Index for arc-scale data sets, we make two small modifications. First, we restrict the range of MgO contents for calculating Fe[X] to X ± 0.5 wt. %, and second, we calculate the median Fe4 and Fe8 rather than the mean to better represent the dominant population in each arc. To note this difference, we subsequently refer to this modified index as THI_m.

3.6. The Significance of Other Fractionating Phases

As described above, the motivation for the P_{ol-cpx} and H₂O_{cpx-pl} is based on the displacements in the compositional space of the olivine-clinopyroxene and clinopyroxene-plagioclase cotectics with changes in magmatic H₂O contents and pressure. However, orthopyroxene, amphibole and garnet are also observed in some of the compiled experiments. Fractionation of these phases influences the normative olivine, clinopyroxene and plagioclase melt components, yet the LLDs that include fractionation of any of these additional phases are similar to those that only fractionate olivine, clinopyroxene and plagioclase.

This insensitivity is in part because orthopyroxene plots similarly in the olivine-clinopyroxene-plagioclase pseudo-ternary space to olivine-rich cumulates, while amphibole and garnet are compositionally like clinopyroxene- and plagioclase-bearing cumulates (Figure 1d). While orthopyroxene fractionation may moderate SiO₂-enrichment, its effect on the clinopyroxene and plagioclase components remains similar to that of olivine. Orthopyroxene has appreciable CaO and Al₂O₃ and therefore does not plot exactly at the olivine vertex (Figure 1d). However, the fractionation of minor amounts of orthopyroxene with low CaO and Al₂O₃ does not meaningfully hinder normative plagioclase enrichments in the magma. Similarly, the fractionation of amphibole and garnet from arc magmas drives rapid SiO₂-enrichment. Yet, typical amphibole and garnet compositions

from arc magmas plot centrally in the olivine-clinopyroxene-plagioclase pseudo-ternary in a similar location to clinopyroxene-plagioclase cumulates (Figure 1d). Therefore, additionally fractionating these phases has a relatively minor impact on the evolution of magmas along the clinopyroxene-plagioclase cotectic. In fact, the amphibole-plagioclase cotectic is often a direct extension of the clinopyroxene-plagioclase cotectic (Grove & Donnelly-Nolan, 1986).

In contrast, crystallization of either hornblende or garnet prior to the melt reaching the clinopyroxene-plagioclase cotectic will have greater impact on the LLD. However, hornblende stability requires ≥ 4 wt. % H_2O in the melt and, more importantly, temperatures below $\sim 1,050^\circ C$ (Blatter et al., 2013; Melekhova et al., 2015). Only very H_2O -rich magmas cool below this temperature prior to reaching the clinopyroxene-plagioclase cotectic and most arc magmas will not stabilize amphibole prior to reaching this cotectic (see also Section 6.1). Similarly, early garnet fractionation occurs only above at least 12 kbars in hydrous magmas (Klein & Müntener, 2023; Müntener et al., 2001), and at even higher pressures in anhydrous systems. While fractionation at these pressures may be important in the thickest arcs, they likely do not represent the dominant fractionation conditions of typical arc magmas. We caution against applying the proxies to locations where significant early garnet fractionation could be expected.

4. Compiled Data Sets

4.1. Global Arc Geochemical Data Set

We compiled whole rock major element compositions of arc volcanic rocks using the precompiled arc and arc seamount data sets from Georoc (<http://georoc.mpch-mainz.gwdg.de/georoc/>) (Figure 4; Table 1). We subdivided some of the Georoc arc data sets, separating the Alaskan Peninsula from the Aleutians data set and dividing the Andes data into Northern, Central, Southern and Austral Volcanic Zones. We filtered all data to include only analyses that were published after 1970 with anhydrous totals between 98 and 102 wt. %, and excluded samples described as altered or with a loss of ignition greater than 5 wt. %. We further restricted the data to volcanic systems that were primarily active in the Pliocene and later. This time window was necessary for arcs with relatively few analyses, yet in all arcs most samples are Pleistocene or younger, allowing comparison of the compiled data to modern arc physical parameters. Additionally, we excluded analyses of fore-arc lavas and of samples from actively spreading back-arcs. Finally, alkaline silica-undersaturated magmas are separated from calc-alkaline and tholeiitic magmas by a thermal divide and thus evolve along a distinct LLD (Schmidt & Weidendorfer, 2018). We therefore excluded the small populations of strongly peralkaline arc volcanics. Our compiled filtered data sets are available as Data Set S1.

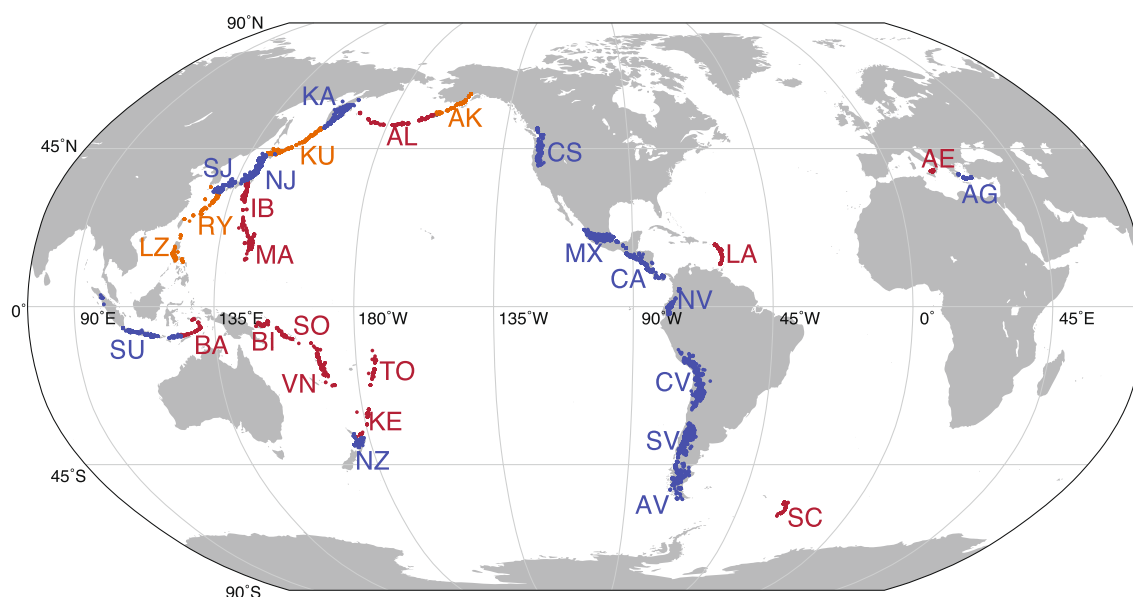


Figure 4. Distribution of global arc whole rock data set. Arcs are labeled according to abbreviations given in Table 1. Colors correspond to arc type: continental arcs are shown in blue, oceanic arcs are shown in red, and arcs that transition between continental and oceanic basements are shown in orange.

Table 1
Arc Parameters and Calculated Proxy Values

Arc	Abbreviation	Arc type	Crustal thickness, km	References ^a	Slab depth, km (H)	Wedge thickness, km	Thermal parameter/100	Slab dip, °	Convergence velocity, mm/yr	Slab age, Ma	Median calculated <i>P</i> , kbars	(<i>n</i>)	Median calculated H ₂ O, wt. %	(<i>n</i>)	THI _m	Fe8(n)	Fe4(n)	Notes
Aleutian ^b	AL	Island	34.6	1–5	101.5	66.9	25.99	54.8	56.8	56	4.7	29	3.1	286	0.96	15	222	1
Alaskan Peninsula	AK	Transitional	40.0	5.6	103.33	63.3	20.62	44.2	57.4	51.53	10.1	13	4.8	661	0.94	4	262	2
Cascades	CS	Continental	40.0	7–12	95	55.0	1.10	21.1	35	8.75	9.3	353	4.8	733	0.81	198	288	3
Mexico	MX	Continental	42.0	13–17	80	38.0	4.05	59.5	47	10	10.2	225	5.1	833	0.71	147	520	
Central America ^c	CA	Continental	34.4	18–21	140.4	106.0	10.34	59.1	69.9	17.1	8.6	44	4.4	591	0.87	20	313	4
Northern Volcanic Zone	NV	Continental	55.0	22–24	155	100.0	4.23	28	60	15	10.5	10	5.3	561	0.78	6	224	
Central Volcanic Zone	CV	Continental	63.0	25–30	125	62.0	14.75	27.2	73.83	43.7	10.2	31	4.5	872	0.80	22	223	5
Southern Volcanic Zone	SV	Continental	43.0	31–36	109	66.0	9.76	28.5	73.15	27.95	9.0	187	4.3	475	0.81	101	302	6
Austral Volcanic Zone	AV	Continental	32.0	36–39	114	82.0	4.34	34.2	74.9	10.3	9.4	94	6.1	43	0.84	54	21	
Kamchatka	KA	Continental	35.0	40–43	111	76.0	53.99	50.7	75.1	92.9	8.7	146	4.2	405	0.96	73	324	
Kuriles	KU	Transitional	27.0	42,44–47	107.3	80.3	60.88	46.23	76.8	109.77	9.8	53	4.2	305	0.96	24	174	7
NE Japan	NJ	Continental	35.0	42,48–52	109	74.0	55.44	31.3	82.15	129.9	11.5	121	5.0	1572	0.87	71	641	8
SW Japan	SJ	Continental	35.0	42,52–55	122	87.0	9.15	42.6	57.5	23.5	9.1	113	5.0	386	0.81	63	189	9
Ryukyu	RY	Transitional	25.0	56–64	105.9	80.9	19.09	50.4	73.2	29.7	8.4	8	4.5	154	0.84	12	90	10
Izu Bonin	IB	Island	25.0	42,65–67	149	124.0	44.08	54.45	38.6	140.35	8.6	104	0.8	347	1.27	56	587	11
Mariana	MA	Island	20.0	68–71	160.8	140.8	41.98	58.3	18.8	149.7	6.4	58	3.3	95	1.08	23	41	12
Luzon	LZ	Transitional	33.0	72,73	142	109.0	23.94	57.4	87.7	32.4	7.3	22	4.3	196	0.86	9	69	
Banda	BA	Island	15.0	74	145.8	130.8	38.54	50.9	45.6	100	8.2	4	3.8	49	0.85	2	30	13
Sunda ^d	SU	Continental	33.7	75–80	142.6	108.9	53.50	48.4	67.4	110.5	5.4	15	3.3	569	0.86	8	202	14
Bismarck	BI	Island	20.0	81	137	117.0	23.30	68.2	100.4	25	3.6	12	3.4	35	0.97	3	27	
Solomon Islands	SO	Island	26.0	82–84	155	129.0	27.33	70.4	93.6	31	0.0	5	3.2	42	0.88	4	21	
Vanuatu ^e	VN	Island	27.0	85–87	133	106.0	33.44	69.1	76.15	47	2.8	52	2.9	112	0.95	25	66	15
Tonga	TO	Island	20.0	88,89	123	103.0	143.18	52.4	165.8	109	3.1	10	0.9	25	1.02	4	48	
Kermadec	KE	Island	17.0	90,91	136.6	119.6	56.62	56.1	55.8	104.2	2.8	37	2.7	63	1.10	22	48	16
New Zealand	NZ	Continental	26.8	92,93	133.3	106.5	23.96	50.3	25.5	100	6.7	71	4.5	371	0.97	35	375	17
Lesser Antilles	LA	Island	30.7	94–96	131.5	100.8	10.85	46.1	17.75	84.8	8.8	26	4.9	746	0.99	15	286	18

Table 1
Continued

Arc	Abbreviation	Arc type	Crustal thickness, km	Slab depth, km (H)	Wedge thickness, km	Thermal parameter/100	Slab dip, °	Convergence velocity, mm/yr	Slab age, Ma	Median calculated P, kbars	Median calculated H ₂ O, wt. %	THI _m (n)	Fe8(n)	Fe4(n)	Notes
Scotia	SC	Island	19.6	97	98.4	32.46	64.6	60.8	59.1	5.9	1.5	59	0.98	8	55
Aegean	AG	Continental	33.0	98	87.0	15.23	30.5	15	200	9.2	3.9	208	0.95	6	124
Aeolian	AE	Island	28.9	99,100	121.1	58.31	43	45	190	6.0	3.1	376	0.93	10	216

Note. Arc Physical Parameter Notes (S2006—Syracuse & Abers, 2006; S2010—Syracuse et al., 2010). 1—Average of Central and western Aleutian segments (S2010). 2—Average of Eastern Aleutians, Alaskan Peninsula and Alaska segments (S2010). 3—Average of North and Central Cascadia segments (S2010). 4—Calculated from all Central America arc-front volcanoes (S2006). 5—Average of Peru, North Chile and North-Central Chile segments (S2010). 6—Average of Central and South-Central Chile segments (S2010). 7—Average of North and South Kurile segments and Hokkaido segment (S2010). 8—Average of North and Central Honshu segments (S2010). 9—Average of Nankai and Kyushu segments (S2010). 10—Average of arc-front volcanoes from Ryukyu and Kyushu south of 32N (S2006). 11—Average of Izu and Bonin segments (S2010). 12—Average of North and South Marianas segments (S2010). 13—Average of arc front volcanoes from East and West Banda Sea between 122.5 and 130E (S2006). 14—Average of arc front volcanoes from Sunda Strait, Java, Bali, Lombok and West Banda Sea west of 122.5E (S2006). 15—Average of North and South Vanuatu segments (S2010). 16—Average of Kermadec arc front volcanoes and Rumble sea mounts (S2006). 17—Average of sub-aerial arc front volcanoes on New Zealand (S2006). 18—Average of North and South Lesser Antilles segments (S2010). 19—Aeolian slab depth not estimated by S2006; 2010. Value taken from Ventura (2013).

^aAll references for crustal thickness listed in Table S7. ^bAleutians calculated excluding the unusual westernmost dredged samples (see text). ^cCentral America calculated excluding the tholeiitic lavas from Nicaragua (see text). ^dSunda calculated excluding recent Taal lavas. ^eVanuatu calculated excluding Matthew and Hunter.

4.2. Compilation of Phenocryst Assemblages for Selected Arcs

An assumption critical to our approach is that melt compositions are controlled by cotectics sensitive to fractionation pressure and H₂O contents. Consequently, the samples used in calculating P_{ol-cpx} and H₂O_{cpx-pl} could be expected to contain the phenocryst assemblages olivine + clinopyroxene (±orthopyroxene) and clinopyroxene + plagioclase (±amphibole), respectively. We thus compiled the reported phenocryst assemblages for the Central America, Cascadia, the Aleutians and Alaskan Peninsula, Izu-Bonin, Marianas, and Sunda arcs from the original publications (Table S6). For each sample, this data set lists the minerals observed and distinguishes between phases that are explicitly documented as opposed to descriptions that are more ambiguous (e.g., a sample described as olivine + plagioclase ± clinopyroxene phyrlic would be recorded as definitely containing olivine and plagioclase and possibly containing clinopyroxene). Here, we focus on the explicitly described phenocryst assemblages, which yield a data set significantly smaller than the complete geochemical data set.

4.3. Arc Physical Parameters

In discussing the significance of the new LLD proxies, we compare the results with various subduction zone physical parameters (Table 1). For these parameters, we rely on the data of Syracuse et al. (2010) when their arc definitions align geographically with the geochemical data sets compiled here. Otherwise, we manually recalculate the subduction zone parameters from Syracuse and Abers (2006) and Syracuse et al. (2010) for geographically appropriate regions, which are noted in Table 1. We also compare the proxy values to the average crustal thickness of each arc, which we compiled from local seismic studies at all arcs, except for the Scotia Arc, for which no local seismic studies exist and where we instead rely on constraints from gravity modeling (Larter et al., 2003). In most arcs the seismic data from multiple independent studies are consistent with relatively invariant crustal thicknesses, but for arcs where there is evidence for trench-parallel variation or significant differences between studies representative average crustal thicknesses were estimated from the available data. Crustal thickness values and consulted references are listed in Table 1 and references for all consulted studies are listed in Table S7.

5. Application of Proxies to Global Arc Database

5.1. Pressures of Early Fractionation

The systematics of fractionation from the olivine-clinopyroxene cotectic and of P_{ol-cpx} are illustrated for representative arcs in Figure 5 (plots of all proxies for each arc are provided in Data Set S2). In the early fractionation interval sampled by P_{ol-cpx}, most continental arcs show constant to slightly decreasing CaO with a decrease in MgO (Figure 5a), consistent with fractionation on the olivine-clinopyroxene cotectic. The relatively low CaO contents (<10 wt. % at 8 wt. % MgO) correspond to lower normative clinopyroxene (Figure 5d). As a result, calculated pressures for continental arcs are consistently higher than 8 kbars and extend up to ~14 kbars (Figure 7a). Island arcs have a less pronounced CaO/MgO slope near 8 wt. % MgO (Figures 5b and 5c) and higher CaO contents corresponding to elevated normative clinopyroxene, suggesting more limited clinopyroxene fractionation in this interval (Figures 5e and 5f). Calculated early fractionation pressures in island arcs are variable, but median values are mostly less than ~7 kbars (Figure 7a). These elevated early fractionation pressures, and the wide variation observed in some arcs are consistent with polybaric fractionation, which may play an important role in arc crust formation (Klein & Jagoutz, 2021; Melekhova et al., 2015).

These results indicate that there is a clear difference between early fractionation depths in continental and island arcs. Two arcs, Central America and the Aleutians, exhibit more complex behavior: both are characterized by a strongly bimodal distribution of calculated pressures (Figures 5e and 7a). Within the Central American Arc, we observe a primary population

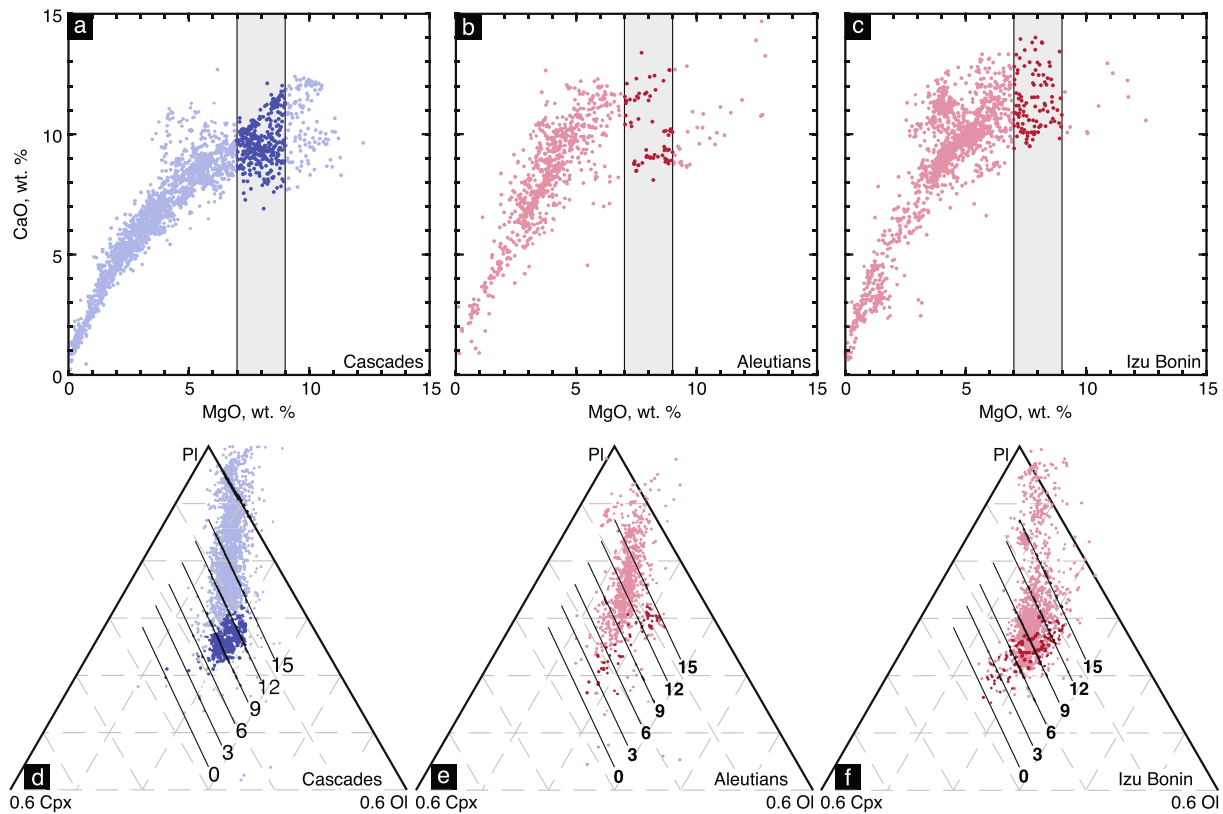


Figure 5. Examples from representative arcs of whole rock arc magma composition data used to calculate P_{ol-cpx} . (a–c) MgO–CaO data presented for three representative arcs: (a) Cascades, (b) Aleutians, and (c) Izu Bonin. Gray bar in each figure shows the range of MgO values used to calculate the P_{ol-cpx} values. (d–f) Same whole rock data projected in the plagioclase–clinopyroxene–olivine pseudo-ternary. Darker colored compositions show data with appropriate compositions for calculating P_{ol-cpx} . Isobars calculated from P_{ol-cpx} are shown in black lines and labeled in kbars.

of samples that yield P_{ol-cpx} estimates above ~ 8 kbars, comparable to other continental arcs, and a second population with calculated P_{ol-cpx} below 5 kbars. Low pressure samples are exclusively produced in a small number of volcanoes erupting tholeiitic basalts in Nicaragua (Walker, 1984). These samples likely represent a LLD that fractionates at lower pressures within the crust, distinct from the broader Central American LLD. As the median P_{ol-cpx} in Central America falls between these two distinct populations, we use the median of the higher pressure population to represent the typical early fractionation pressure dominant in the Central American arc. Similarly, the high pressure (>12 kbars) population in the Aleutians is exclusively from seafloor samples dredged west of the westernmost emergent volcano, where the plate boundary transitions to a nearly strike-slip orientation. These samples may contain significant slab melt components that are not observed elsewhere in the Aleutians (Yogodzinski et al., 2015). We therefore exclude these atypical samples from the calculated Aleutian median pressure.

5.2. H_2O in Fractionating Arc Magmas

Figure 6 illustrates the data used to calculate H_2O_{cpx-pl} for representative arcs. Al_2O_3 contents as a function of MgO are plotted for arcs with LLDs consistent with fractionation of dominantly H_2O -rich (Cascades), intermediate (Aleutians) and relatively dry (Izu Bonin) magmas. In each case, a wide range of Al_2O_3 concentrations is observed at >4 wt. % MgO. Many of these relatively mafic compositions are likely not yet fractionating on the clinopyroxene–plagioclase cotectic, and thus the spread reflects varying extents of olivine \pm clinopyroxene fractionation and variations in the parental melt compositions. As MgO decreases to below ~ 4 wt. %, maximum Al_2O_3 contents are reached, and Al_2O_3 concentrations subsequently decrease for each arc (Figures 6a–6c). As MgO contents decrease to below 2 wt. %, the range of values observed in each arc narrows significantly and most arcs converge toward a single trend, suggesting that the magmas have reached relatively shallow, fluid-saturated conditions by this stage.

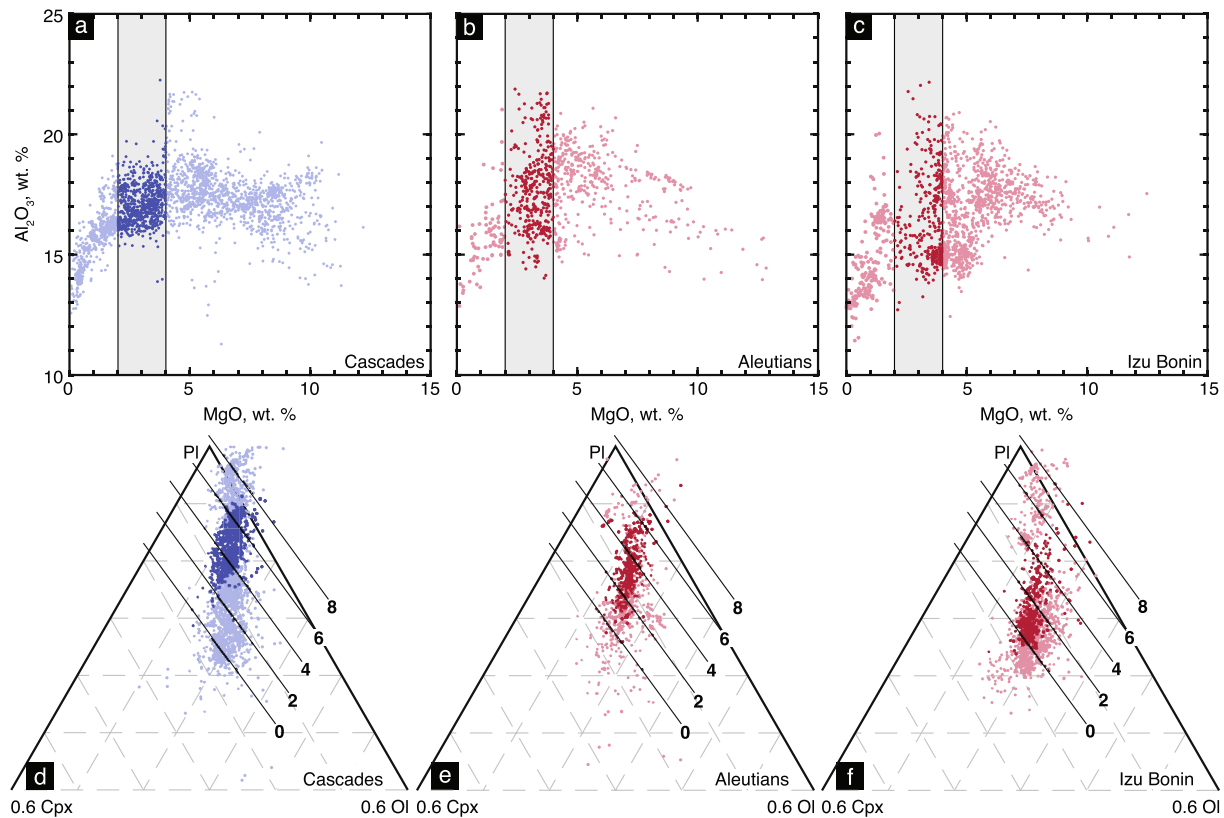


Figure 6. Examples from representative arcs of whole rock arc magma composition data used to calculate $H_2O_{\text{cpx-pl}}$. (a–c) MgO–Al₂O₃ data shown for three representative arcs: (a) Cascades, (b) Aleutians, and (c) Izu Bonin. Gray horizontal bars show the range of MgO contents used to calculate $H_2O_{\text{cpx-pl}}$. (d–f) Same whole rock data projected in the plagioclase–clinopyroxene–olivine pseudo-ternary. Darker colored compositions show data with appropriate compositions for calculating $H_2O_{\text{cpx-pl}}$. H_2O isopleths calculated from $H_2O_{\text{cpx-pl}}$ are shown in black lines and labeled in wt. %.

Consistent with the experimental LLDs (Figure 1c), most arc magmas evolving on the clinopyroxene–plagioclase cotectic follow similar trajectories in the olivine–clinopyroxene–plagioclase pseudo-ternary space. However, magmas with comparable MgO contents from different arcs plot at distinct points along the cotectic LLD due to varying extents of prior plagioclase fractionation and indicative of differing H₂O contents. At 2–4 wt. % MgO, Cascades lavas are relatively Al₂O₃-rich, corresponding to elevated normative plagioclase contents and calculated H₂O contents are dominantly above 4 wt. % (Figure 6d). In contrast, samples from Izu Bonin show a wide range in Al₂O₃ contents, but the dominant population has less than 15 wt. % Al₂O₃ and comparatively little normative plagioclase (Figures 6c and 6f). These samples are consistent with greater extents of plagioclase fractionation and yield-calculated H₂O contents below 2 wt. % (Figure 6f). The Aleutians represent an intermediate case between these two endmembers and have variable intermediate Al₂O₃ contents corresponding to moderate extents of normative plagioclase depletion and H₂O contents dominantly between 2 and 4 wt. % (Figures 6b and 6e).

We find that all arcs are characterized by a broad, but typically unimodal distribution of H₂O contents, and that there are well-resolved differences between arcs (Figures 6 and 7b). Continental arcs generally show elevated H₂O contents (i.e., >4 wt. %; Figure 6a), while several island arcs are dominated by magmas with notably lower calculated H₂O contents (<3 wt. %), including the Aleutians, Izu Bonin, Kermadec, and Marianas (Figure 7b).

To complement $H_2O_{\text{cpx-pl}}$, we examine the Tholeiitic Index (THI_m; Figure 8). While variations in the Tholeiitic Index exist between individual volcanoes within a single arc (Zimmer et al., 2010), large systematic differences are also resolvable between arcs. Some arcs, such as the Cascades (Figure 8a), are dominated by Fe-depletion trends and have Tholeiitic Index values THI_m << 1, while other arcs, including Izu Bonin (Figure 8c), are dominated by marked Fe-enrichment trends and have THI_m >> 1. In the Aleutians (Figure 8b), we observe a large range of both Fe4 and Fe8 values, suggesting that both Fe-enrichment and Fe-depletion trends may be present, likely derived from distinct parental magmas. The low Fe8 compositions in the Aleutians are again restricted to the anomalous westernmost lavas. After excluding these data, a large range of Fe4 values results in an intermediate THI_m near

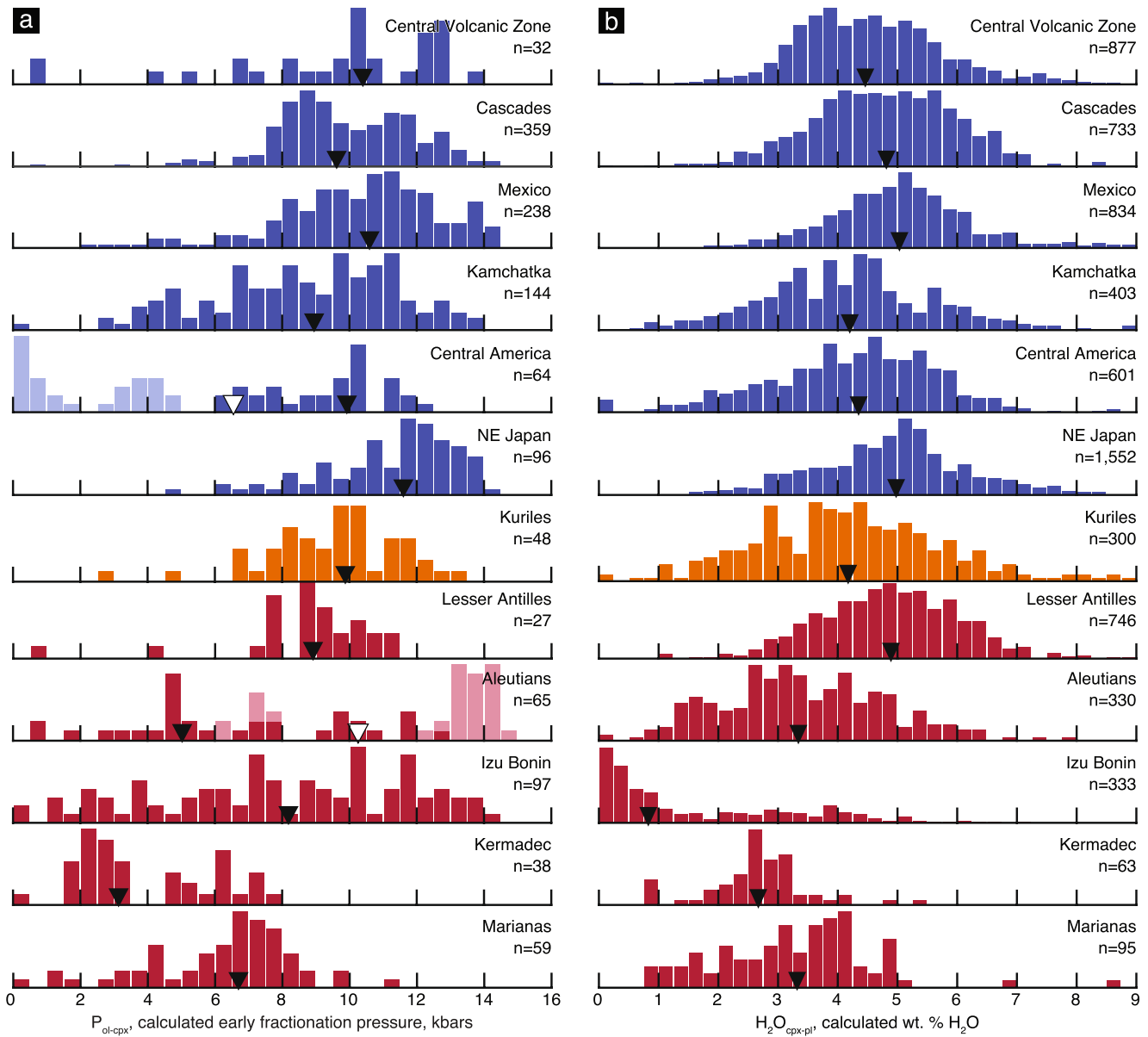


Figure 7. Normalized histograms of (a) P_{ol-cpx} and (b) H_2O_{cpx-pl} proxies calculated from whole rock compositional data of 12 representative arcs. Arcs are sorted in order of decreasing crustal thickness (Table 1) and colored corresponding to arc type as in Figure 4. Median P_{ol-cpx} pressures and H_2O_{cpx-pl} contents are marked with small black triangles. Central America and Aleutians have strongly bi-modal P_{ol-cpx} distributions. As discussed in the main text, in both instances, one of these populations is geographically limited and not taken to be representative of the typical LLD. These populations are shown here in lighter colors and are excluded from the calculated median pressures. Scatter plots and histograms for all arcs are available in Data Set S2.

1 for the Aleutians. Consistent with H_2O_{cpx-pl} , TH_m shows that continental arcs are dominated by Fe-depletion trends consistent with H_2O -rich LLDs, while island arcs are dominated by Fe-enrichment trends consistent with H_2O -poor LLDs (Figure 8d).

6. Discussion

6.1. Liquid Lines of Descent and Phenocryst Populations

The above results are interpreted in terms of cotectic crystallization. Based on this rationale, one might expect that the erupted lavas contain phenocryst assemblages consistent with these cotectics. To evaluate this inference, we compiled a database of reported phenocryst assemblages for six representative arcs.

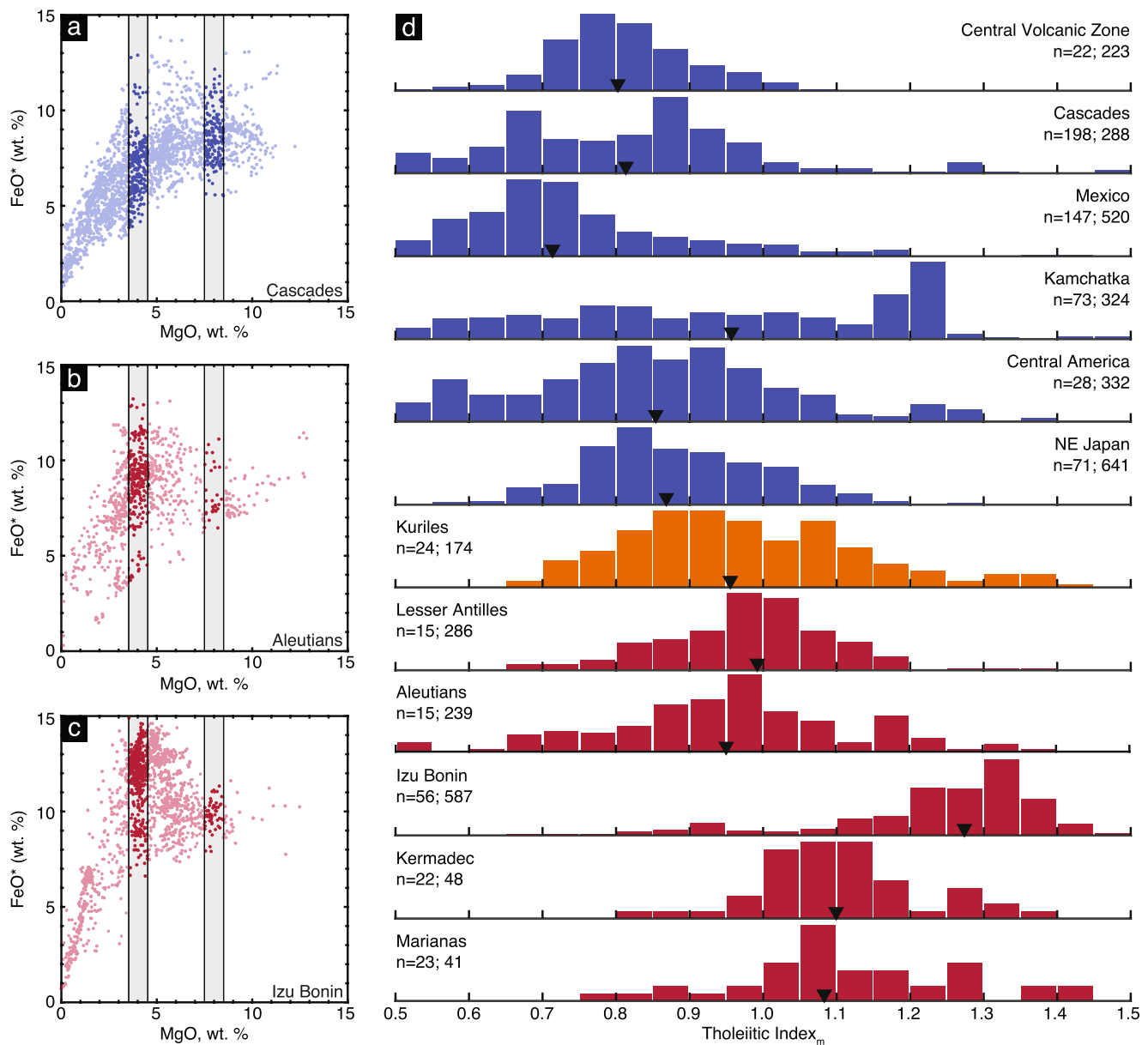


Figure 8. Examples of data used to calculate the (median) Tholeiitic Index for representative arcs. (a–c) FeO*-MgO data shown for three representative arcs: (a) Cascades, (b) Aleutians, and (c) Izu Bonin, with all Fe shown as FeO. Gray vertical bars show ranges of MgO contents used to calculate Fe4 and Fe8 values. (d) Normalized histograms of Fe4 populations divided by median Fe8 values for 12 representative arcs sorted by crustal thickness as in Figure 7. The calculated medians of these populations represent the arc Tholeiitic Index and are marked with black triangles. Sample abundances (*n*) are listed for each arc first for Fe8 and second for Fe4.

6.1.1. Olivine + Clinopyroxene Cotectic

Figure 9 shows plots of MgO and CaO contents for the six arcs with phenocryst data, colored by phenocryst assemblage. We find that there is only a sparse record of samples that are olivine(-only) and olivine + clinopyroxene(-only) phyrlic, and there is no obvious evolution from olivine phyrlic to olivine + clinopyroxene bearing samples. Instead, plagioclase phenocrysts are reported in most samples even at MgO contents above 8 wt. % (Figure 9). Samples with 7–9 wt.% MgO, as used to calculate the pressure proxy, dominantly contain olivine + clinopyroxene + plagioclase phenocrysts in Central America, Sunda, and the Aleutians, while Izu-Bonin, the Marianas, and the Cascades have more variable phenocryst assemblages of olivine, olivine + plagioclase or olivine + clinopyroxene + plagioclase (Figure 9 and Figure S4a in Supporting Information S1). Although the samples used for P_{ol-cpx} chemically lie on the experimentally derived olivine-clinopyroxene cotectic, they rarely exhibit olivine + clinopyroxene

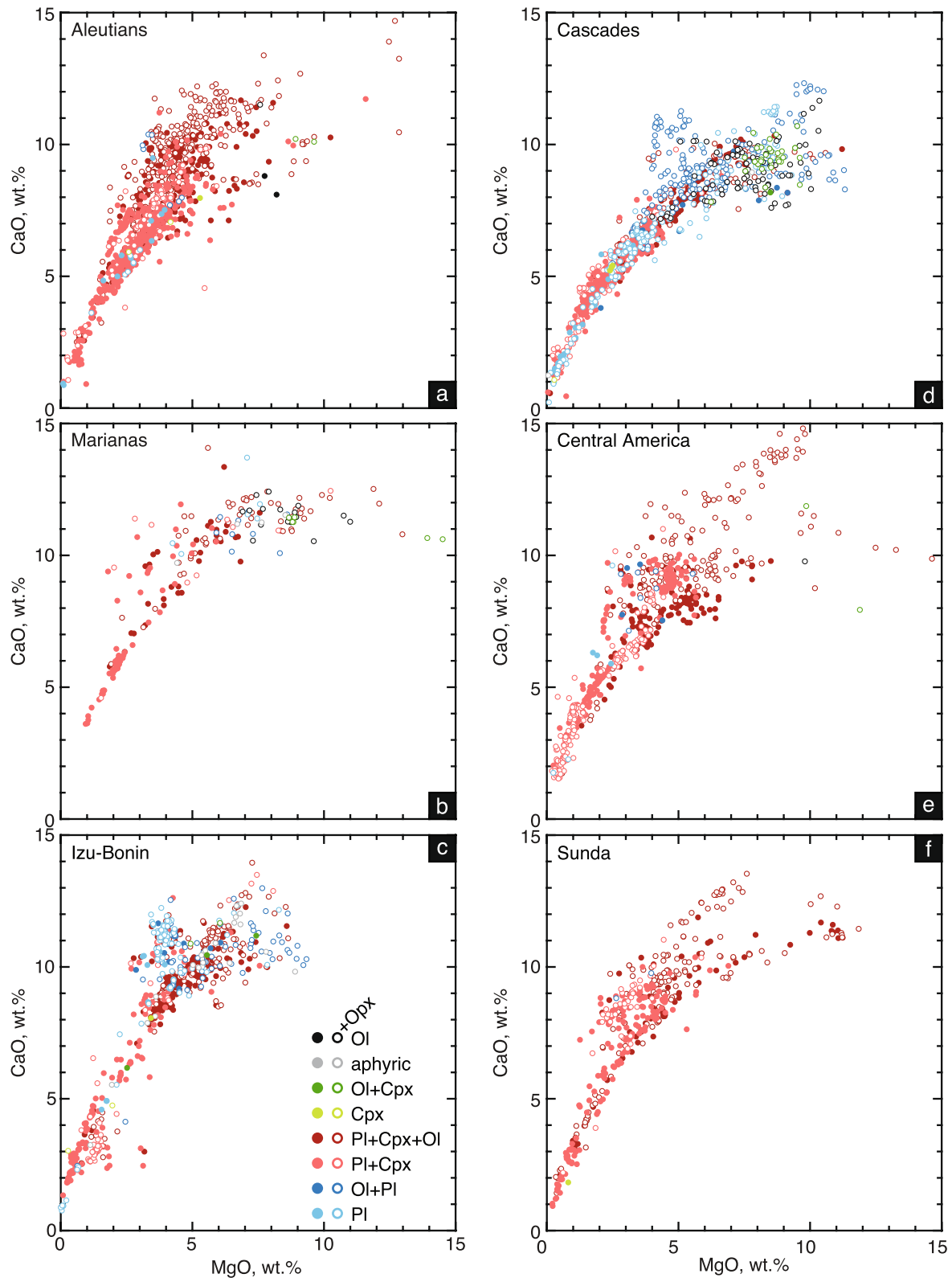


Figure 9. Compiled arc lava phenocryst data sets plotted in MgO-CaO space for the six arcs included in the phenocryst data set: (a) Aleutians, (b) Marianas, (c) Izu-Bonin, (d) Cascades, (e) Central America and (f) Sunda. Plotted data include only samples where the phenocryst assemblages are explicitly described in the original publication. For visibility, symbol colors correspond to phenocryst assemblages only in terms of the dominant phases with regard to Mg-Ca systematics: olivine, clinopyroxene, and plagioclase. Samples that additionally contain orthopyroxene are shown with empty symbols. Additional figures showing the occurrences of amphibole phenocrysts can be found in Figure S5 of the Supporting Information S1.

phenocryst assemblages. This difference shows that fractionation depth and depth of final equilibration within the arc crust are rarely congruent for deeply fractionated erupted magmas. While direct transport from the lower crust to the surface would likely preserve the lower crustal fractionating assemblage, intermittent storage at shallower pressures appears to replace the higher pressure phenocrysts assemblage in favor of a shallower pressure assemblage. With decreasing pressure, the clinopyroxene-stability field shrinks strongly, while the plagioclase and olivine fields expand (Presnall et al., 1978). Consequently, during transport to the surface, intermittent storage and eruption, plagioclase is stabilized at the expense of clinopyroxene.

Critically, while most samples have a low pressure phenocryst assemblage, we suggest that these phases are rarely fractionated. In our phenocryst data set, there is no observable shift in $P_{\text{ol-cpx}}$ between populations with olivine \pm clinopyroxene phenocrysts and samples that also contain plagioclase phenocrysts (Figure S4a in Supporting Information S1), requiring that the plagioclase-bearing shallow pressure assemblage does not appreciably fractionate. Limited fractionation of arc magmas at shallow pressures is also consistent with the observation that mafic cumulates are rare at upper crustal levels in exposed arc sections (Hacker et al., 2008; Jagoutz, 2014; Klein & Jagoutz, 2021), suggesting that most crystal fractionation occurs at high pressures prior to transport to shallower levels. This apparent discrepancy between LLD and phenocryst assemblage is directly analogous to the “pyroxene paradox” in the MORB system (e.g., Dungan & Rhodes, 1978), where clinopyroxene fractionation is inferred from MORB liquid lines of descent but clinopyroxene-bearing MORB samples are rare. This is explained through the same mechanism, with clinopyroxene fractionation at higher pressures and subsequent resorption of clinopyroxene and crystallization of plagioclase upon transport to shallower levels (Grove et al., 1992).

6.1.2. Clinopyroxene-Plagioclase Cotectic

The phenocryst assemblages of samples near the experimentally defined clinopyroxene-plagioclase cotectic generally contain phenocrysts consistent with this cotectic (Figure 10 and Figure S4b in Supporting Information S1). Nearly all samples with less than ~ 5 wt. % MgO contain phenocrysts of both plagioclase and clinopyroxene (Figure 10). Additional phases include orthopyroxene or olivine, and amphibole, which are not expected to significantly alter the clinopyroxene-plagioclase systematics.

In detail, more than 95% of the samples used to calculate $H_2O_{\text{cpx-pl}}$ in Central America, the Aleutians, and Sunda, as well as over 80% of samples from the Marianas and Izu-Bonin contain (at least) the expected plagioclase + clinopyroxene cotectic phenocryst assemblage. The Cascades are an apparent exception, as 280 out of the 406 Cascade samples have assemblages consistent with the clinopyroxene-plagioclase cotectic, but 88 samples ($>20\%$) contain plagioclase without clinopyroxene. As this plagioclase-only sample population is skewed to slightly higher Al_2O_3 contents compared to the clinopyroxene + plagioclase samples (Figure S4b in Supporting Information S1) this may be evidence for plagioclase accumulation in some Cascade magmas. Nevertheless, the near-primitive high- Al_2O_3 and high-CaO lavas in the Cascades have been shown to represent true melt compositions (Baker et al., 1994; Grove et al., 2002).

Finally, in Figure S5 of Supporting Information S1 we identify samples that also contain amphibole phenocrysts. Amphibole is rare in compositions near the olivine-clinopyroxene cotectic due to the elevated temperatures and/or lower H_2O contents below 4 wt. % during the early stages of fractionation. The subsequent appearance of amphibole is strongly correlated with calculated $H_2O_{\text{cpx-pl}}$: lavas erupted at arcs with higher H_2O are more frequently amphibole-phyric, while amphibole is rarely observed at the Marianas and Izu-Bonin, the two arcs with the lowest calculated H_2O contents in the phenocryst compilation. Further, amphibole is rarely observed in samples with less than 3–4 wt. % $H_2O_{\text{cpx-pl}}$, consistent with a minimum H_2O content of ~ 4 wt. % required for amphibole stability (Prouteau & Scaillet, 2003; Sisson & Grove, 1993a). Finally, the samples with amphibole in addition to clinopyroxene + plagioclase still follow the clinopyroxene-plagioclase cotectic (Figure S5 in Supporting Information S1).

6.2. Sensitivity of $P_{\text{ol-cpx}}$ to Primitive Magma Compositions

Several previous studies examined the Ca-Mg systematics in arc magmas (Plank & Langmuir, 1988; Turner & Langmuir, 2015), which in near-primary mafic magmas is primarily controlled by the olivine-clinopyroxene cotectic. In contrast to our approach that focuses on magmas with ~ 8 wt. % MgO, these studies focused on variations in CaO contents at MgO 6 wt. % ($Ca_{6,0}$) and interpreted these variations as reflective of differences in primary melt compositions rather than fractionation conditions. Primitive arc basalts have ~ 9 –13 wt. % MgO (Schmidt

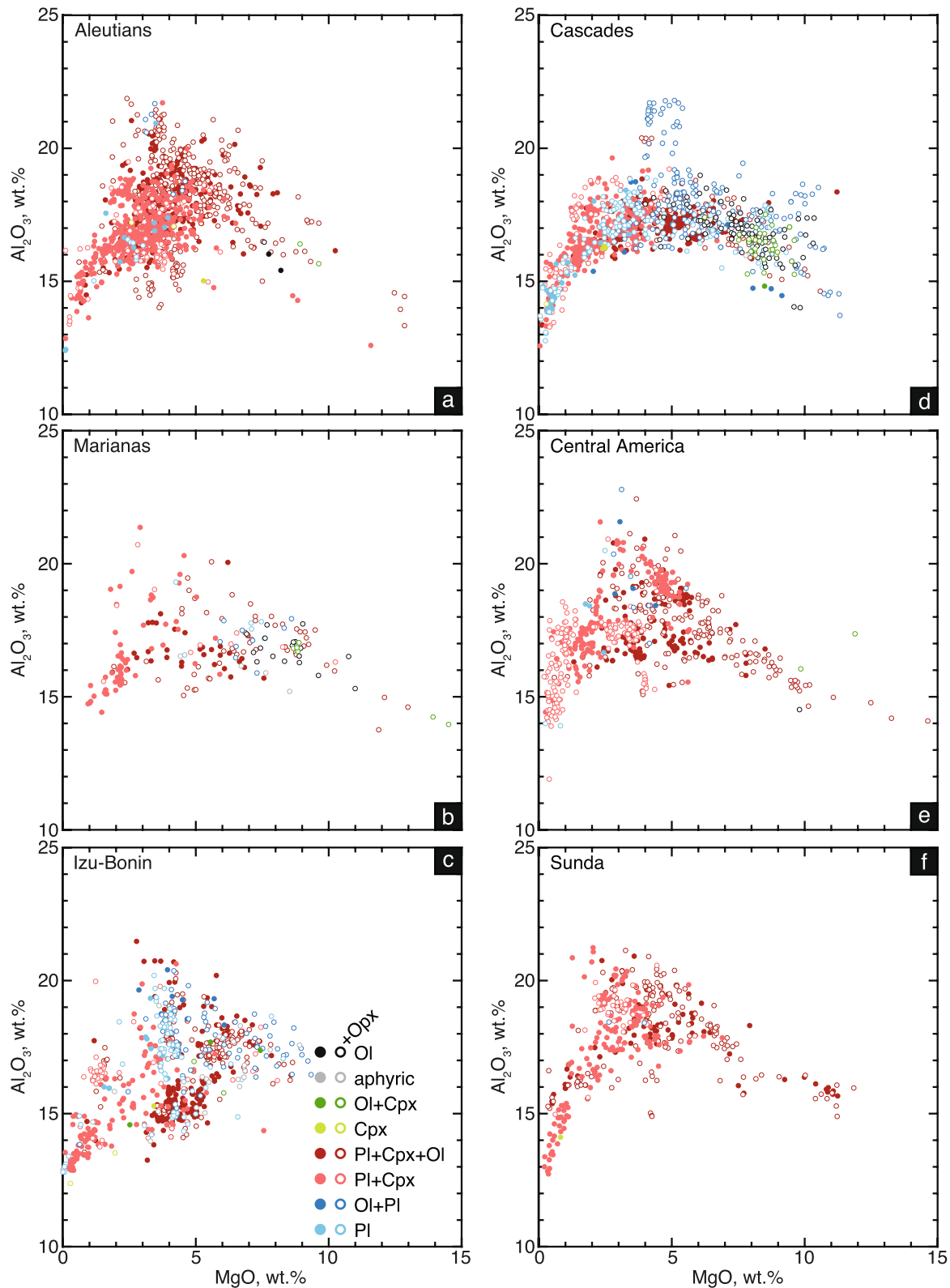


Figure 10. Compiled arc lava phenocryst data sets plotted in MgO-Al₂O₃ space for the six arcs present in the phenocryst compilation: (a) Aleutians, (b) Marianas, (c) Izu-Bonin, (d) Cascades, (e) Central America and (f) Sunda. Plotted data include only samples where the phenocryst assemblages are explicitly described in the original publication. Phenocryst assemblages are colored as in Figure 9. Amphibole-bearing samples are plotted in Figure S5 of the Supporting Information S1.

& Jagoutz, 2017; shown in individual arc plots in Data Set S2). Thus, basaltic samples with ~6 wt. % MgO have undergone significant fractionation relative to primitive basalt compositions. Moreover, the LLD at 6 wt. % MgO is increasingly sensitive to H₂O contents in addition to pressure, as most dry magmas at 6 wt. % MgO are already crystallizing plagioclase (Figures 1b and 3a and Figure S2 in Supporting Information S1). Basaltic compositions with 6 wt. % MgO will therefore have CaO values modified by (unaccounted) fractionation of variable proportions of olivine, clinopyroxene and plagioclase. Consequently, Ca_{6,0} values (and other components normalized to 6 wt. % MgO) are neither robust indicators of primary compositions nor of fractionation pressure. In contrast, the correlation between experimental melt composition at 8 wt. % MgO and pressure is strong, despite a wide range of starting compositions and H₂O contents in the compiled experiments (Figures 3b and 3c), showing that P_{ol-cpx} is a more robust indicator of fractionation pressure for basaltic melts.

In contrast to primitive arc basalts, primitive andesites frequently have MgO contents near 8 wt. % (e.g., Baker et al., 1994; Kelemen, Hanghøj, & Greene, 2003; for a compilation see Schmidt & Jagoutz, 2017) and thus will be included in the population used to calculate P_{ol-cpx}. Although these primitive melts have undergone little crustal differentiation, we argue that their melt compositions are still consistent with olivine-clinopyroxene cotectic control, only that this control is exerted in the mantle. Reaction of primitive basalts with lherzolite in the shallow mantle can produce high-magnesium andesites in equilibrium with a wehrlitic residue (Mitchell & Grove, 2016). These melts are thus effectively controlled by the olivine-clinopyroxene(+orthopyroxene) cotectic while their Mg# remains buffered in equilibrium with mantle olivine. Based on this interpretation, anomalously high P_{ol-cpx} values from locations such as the westernmost Aleutians may be a result of differentiation or reequilibration on the olivine-clinopyroxene(+orthopyroxene) cotectic at mantle pressures.

6.3. Evidence for Multiple Liquid Lines of Descent at Individual Arcs

This contribution focuses on the systematic differences in the dominant LLDs between arcs, but parental melts within a single arc may differ in their H₂O contents and may fractionate at different pressures. Indeed, a large body of work has shown significant variations in LLDs within single arcs (e.g., Jagoutz et al., 2011; Kay & Kay, 1985; Rezeau et al., 2021; Turner et al., 2016), a difference that is already present in the primitive melts (Schmidt & Jagoutz, 2017) and is evident in single volcanoes (Baker et al., 1994; Fujinawa, 1988; Grove et al., 2002; Hunter, 1998; Le Voyer et al., 2010). Similarly, there is significant dispersion within the populations used to calculate each of the proxies utilized here (Figures 7 and 8d), consistent with varying LLDs in most arcs.

To further illustrate the evidence for multiple LLDs, we compare P_{ol-cpx}, H₂O_{cpx-pl} and THI_m to their *Q* statistics (Figure 11), which is a robust estimate of the dispersion (scale) for non-Gaussian and asymmetric data samples (Rousseeuw & Croux, 1991). We used this statistic as many of the arcs have long-tailed distributions, and distributions for arcs with low pressures or H₂O contents are strongly asymmetric. Most arcs exhibit 2–4 kbars of variability in P_{ol-cpx} (Figure 11a) regardless of median value or arc type. A different systematic is present in the two hydration proxies: island arcs that are characterized by the lowest H₂O contents show only limited dispersion (low *Q* statistic values) indicative of a single (relatively dry) LLD. In contrast, most arcs with higher median H₂O contents show greater dispersion and are dominated by magmas that evolve along H₂O-rich LLDs, but also contain magmas that follow less hydrous fractionation paths.

6.4. Correlations Between Proxies

The preceding discussion shows that the new proxies as well as the Tholeiitic Index show resolvable differences between the dominant LLDs at the arc scale. Next, we examine these systematic differences and explore how these proxies relate to arc parameters to constrain the mechanisms and processes that produce the observed range of LLDs. We observe a strong negative correlation between Fe-enrichment and H₂O contents (Figure 12a), consistent with the traditional interpretation that drier magmas evolve on a tholeiitic Fe-enrichment trend, while the calc-alkaline Fe-depletion trend is intimately linked to its hydrous character (Sisson & Grove, 1993a; Zimmer et al., 2010). This strong correlation shows that both the Tholeiitic Index and H₂O_{cpx-pl} constrain the hydration state of differentiating arc magmas. The observed scatter results from the proxies being calculated from different major elements and at different stages of the LLD. Further, calculated THI_m and median H₂O_{cpx-pl} both correlate with median P_{ol-cpx} values (Figures 12b and 12c): arcs with high H₂O contents and calc-alkaline differentiation trends have higher calculated fractionation pressures, while relatively dry tholeiitic arcs show lower fractionation

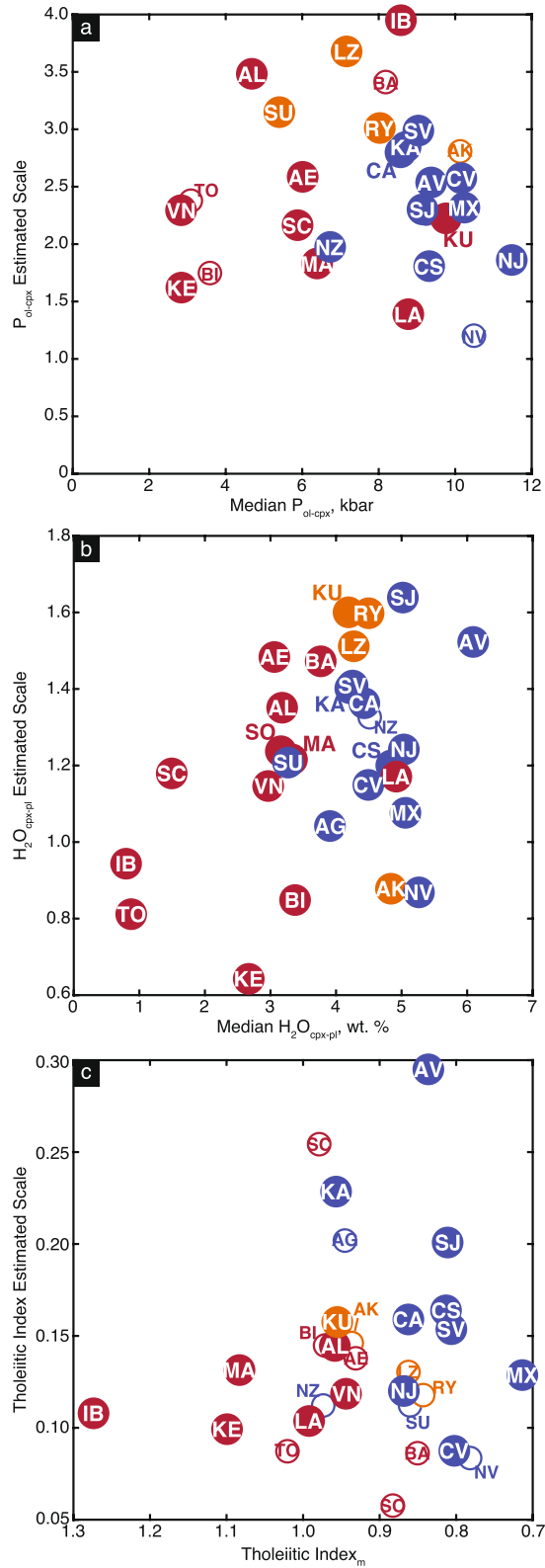


Figure 11.

pressures, suggesting that more calc-alkaline and hydrous magmas begin to differentiate at comparatively higher pressures.

An additional relationship is evident from Figure 12: continental arcs are dominantly characterized by high $H_2O_{\text{cpx-pl}}$ and low THI_m values consistent with wet LLDs, as well as by higher $P_{\text{ol-cpx}}$ indicative of deeper early fractionation. In comparison, the high THI_m index and low $H_2O_{\text{cpx-pl}}$, relatively dry LLDs are mostly observed at island arcs, which also define the shallower early fractionation arc population.

In Figure 13 and Figure S6 in Supporting Information S1, we also compare the three proxies to a range of arc physical parameters. Similar to the comparisons between proxies, in many instances we observe both moderately strong linear correlations between multiple arc parameters and LLD proxies (e.g., crustal thickness and wedge height with most proxies; Figure 13) and also find systematic differences in the systematics of island and continental arcs. In contrast, some proxies show little to no correlation with any of the LLD proxies (e.g., convergence velocity, Figure S6 in Supporting Information S1). In the following sections, we discuss the significance of these relationships.

6.5. The Correlation Between Crustal Thickness and $P_{\text{ol-cpx}}$

The seismically defined crustal thickness (Moho) corresponds in most arcs to the transition from plagioclase-bearing gabbroic cumulates to plagioclase-free ultramafic cumulates (Christensen & Mooney, 1995; Tatsumi et al., 2008), a boundary that is well documented in arc sections where the Moho is exposed (Behn & Kelemen, 2006; Jagoutz & Behn, 2013). $P_{\text{ol-cpx}}$ samples the LLD of arc magmas prior to plagioclase fractionation (Figures 2a and 3a) and thus should reflect fractionation pressures below this boundary. However, at pressures below 10–12 kbars, plagioclase first appears in both hydrous and anhydrous experimental LLDs less than 50°C below the experimental temperatures of melts with 8 wt. % MgO (Figure S7a in Supporting Information S1). Thus, while $P_{\text{ol-cpx}}$ does not directly reflect the plagioclase-in boundary, given the typically steep thermal gradients in the lower arc crust (Klein & Jagoutz, 2021), magmas differentiating in all but the thickest continental arcs reach plagioclase stability shortly after evolving to 8 wt. % MgO, and we expect that calculated $P_{\text{ol-cpx}}$ pressure should closely correlate with Moho depth.

In evaluating this hypothesis, we find that the $P_{\text{ol-cpx}}$ values calculated at most well-studied arcs agree closely with local seismic Moho observations (as indicated by the dashed 1:1 line in Figure 13c), while three arcs have significantly deeper seismic Mohos compared to $P_{\text{ol-cpx}}$: the Central Volcanic Zone (CVZ) in the Andes, the Aleutians and Vanuatu. The CVZ has the thickest crust of any modern arc (>65 km; Yuan et al., 2002), and thus if early fractionation occurs near the seismic Moho, $P_{\text{ol-cpx}}$ should be >18 kbars. These high pressures extend beyond the calibration data set used for $P_{\text{ol-cpx}}$ and at these pressures it is possible that significant garnet fractionation occurs during early fractionation of CVZ magmas, which would interfere with reliable $P_{\text{ol-cpx}}$ estimates. The disagreement in the Aleutians is well-explained by the seismic studies conducted there: the lower crust of the Aleutians is inferred to be dominated by pyroxenites based on high P-wave velocities (V_p) and low V_p/V_s ratios (Shillington et al., 2004, 2013), and thus the Moho depth in these studies corresponds to the petrologic Moho and not the typically measured seismic Moho. An Aleutian seismic Moho assumed to be the boundary between the mid-crust and this pyroxenite-rich lower crust at ~20 km agrees within error with the $P_{\text{ol-cpx}}$ estimate of 4.7 kbars. Finally, the cause of the disagreement at Vanuatu is less clear. While there is a lack of recent detailed seismic studies of this arc, it is also possible that the elevated crustal thickness here is reflective of recent tectonic processes (Meffre & Crawford, 2001) or a relict continental basement in Vanuatu (Buys et al., 2014). If these three arcs are excluded, all 16 of the remaining well-studied arcs show excellent agreement between $P_{\text{ol-cpx}}$ and the seismic Moho within the $P_{\text{ol-cpx}}$ uncertainty.

As noted above, the temperature decrease necessary for melts with ~8 wt. % MgO to subsequently reach plagioclase-in is relatively small in both anhydrous and hydrous LLDs at pressures below 10–12 kbars. However, the absolute temperatures of these melts can vary significantly, primarily as a function of H_2O contents: plagioclase appears in H_2O -poor LLDs at temperatures more than 200°C higher than in H_2O -rich systems (Figure S7b

Figure 11. Estimates of the intra-arc variability in the calculated median $P_{\text{ol-cpx}}$, $H_2O_{\text{cpx-pl}}$, and Tholeiitic Index. Population dispersion is represented using the Q statistic (Rousseeuw & Croux, 1991). For a population of samples, the Q statistic represents an estimate of the scale of a variable that is robust to outliers and asymmetric distributions. Q values are scaled so as to be comparable to the scale of the standard deviation scale of a normal distribution. Systematics in $P_{\text{ol-cpx}}$ (a) show that most arcs exhibit 2–4 kbar variability in early fractionation pressures, while both $H_2O_{\text{cpx-pl}}$ (b), and the Tholeiitic Index (c) show that H_2O -poor arcs often have very restricted populations, while significant dispersion, suggesting a range of hydration states, is observed in most H_2O -rich systems. In each panel, symbol colors represent island (red), transitional (orange) and continental (blue) arcs. Arcs are labeled with a two-letter code, which are listed in Table 1. Proxy values calculated from arcs with less than 15 samples are shown with empty symbols.

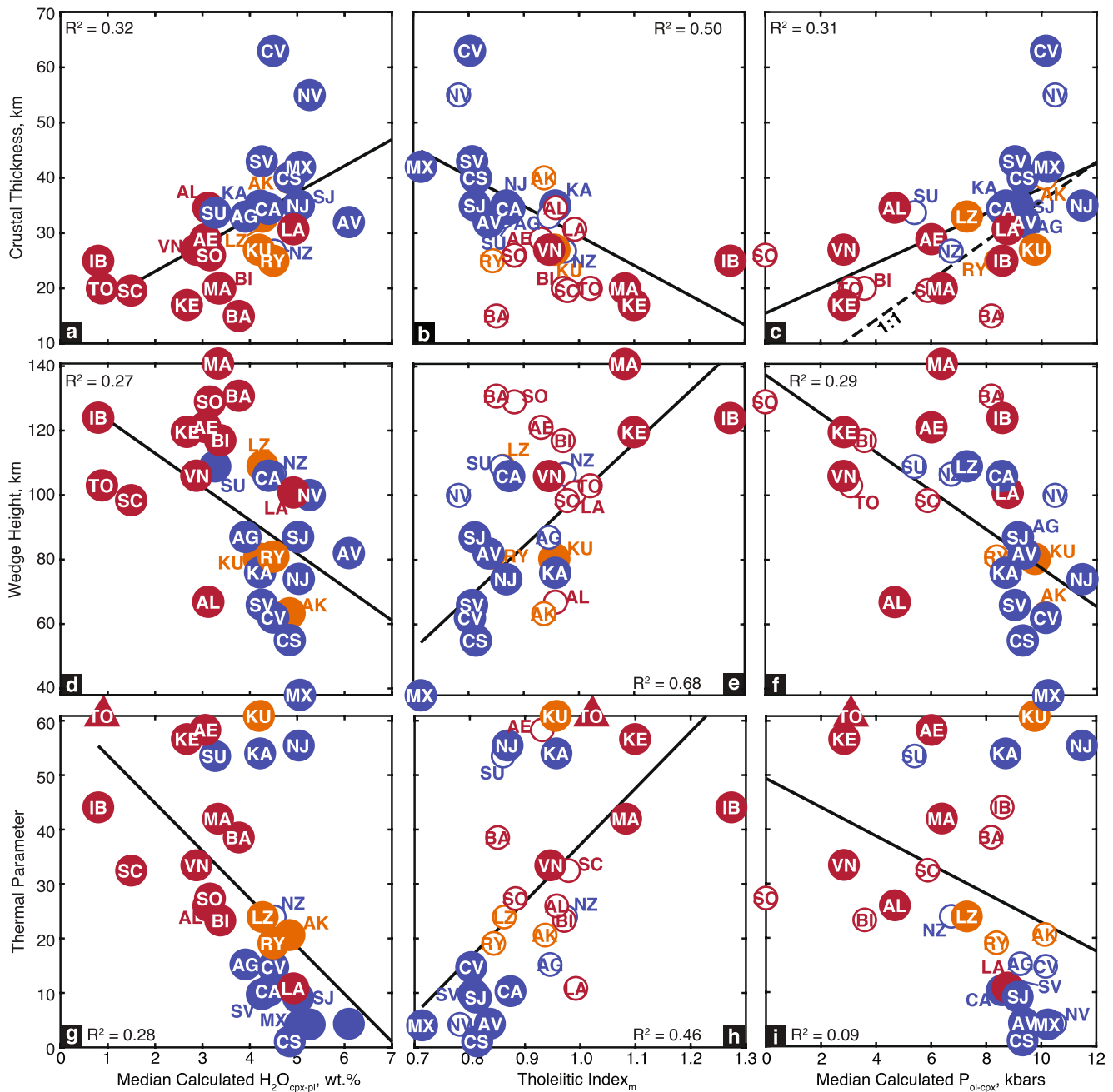


Figure 13. Comparisons of arc proxies to arc physical parameters. (a–c) Comparisons with compiled local crustal thickness measurements. (d–f) Comparisons with mantle wedge height, calculated as the difference between sub-arc slab depth and crustal thickness. (g–i) Comparisons with arc thermal parameters. Linear best-fit lines are shown in black and r^2 values are given for all fits. All proxies are well correlated with crustal thickness, and THI_m and P_{ol-cpx} are also well correlated with wedge heights. While the linear fit between wedge height and $H_2O_{cp-x-pl}$ is comparatively poor, there is a clear systematic clustering of these data for wedge heights above and below ~ 100 km. Similar clustering is also present in comparisons between crustal thickness and $H_2O_{cp-x-pl}$, as well as between both wedge height and crustal thickness and THI_m . In comparison, poor correlations with no evident systematics are observed between all three proxies and the arc thermal parameter. Arc symbols and labels as in Figure 11. Tonga (marked with a triangle) has an extreme thermal parameter value (~ 160) and is omitted from the plots for visibility and also excluded from the calculated fits.

in Supporting Information S1). As there are large variations in the hydration state of magmas within individual arcs (Figures 11b and 11c), the temperatures of magmas corresponding to plagioclase-in and P_{ol-cpx} must vary strongly within single arcs. These differences in LLDs likely contribute to the broad, poorly resolved Moho in many arcs (e.g., Shillington et al., 2004; Takahashi et al., 2008), and are consistent with the observed variability in P_{ol-cpx} values within individual arcs (Figure 11a). As most arcs erupt a range of variably hydrated magmas

including at least some H₂O-poor magmas (Figures 7 and 11), the base of this broadly defined Moho likely corresponds to the earliest plagioclase-in boundary at temperatures of 1,150–1,200°C (Figure S7b in Supporting Information S1).

6.6. The Relationship Between H₂O Proxies and Physical Arc Parameters

The above observations highlight a dichotomy in arc systems: continental arcs dominantly produce H₂O-rich magmas that begin to differentiate at high pressures, while island arcs are characterized by more H₂O-poor magmas that differentiate at shallower levels. However, when interpreting variations in calculated H₂O contents, one needs to determine whether the estimated H₂O contents reflect fluid-saturated conditions. If so, the calculated H₂O contents reflect magma storage and differentiation pressures of intermediate-felsic magmas but do not retain a memory of primary H₂O contents. If magmas are fluid-saturated, the cluster of continental arcs with median H₂O contents of 4–6 wt. % only reflects typical fractionation depths at ~1–2 kbars (Newman & Lowenstern, 2002; see also Plank et al., 2013). Although we cannot exclude that some arc magmas reach fluid-saturation relatively early, we contend that the systematic differences in H₂O_{cpx-pl} and THI_m distributions between relatively H₂O-poor and H₂O-rich arcs (Figure 11) argue against fluid-saturation as a primary control on magmatic H₂O contents. Similarly, the observed correlations between hydration proxies, crustal thickness and early fractionation pressure (Figures 12b, 12c, 13a, and 13b) seem difficult to explain if the hydration proxies are simply reflective of relatively evolved magmas reaching fluid-saturation at shallow pressures.

If fluid-saturation is not a primary control, the dichotomy between continental and island arcs raises a question: what is the fundamental mechanism that leads to these different behaviors? Is the range of H₂O contents in arc magmas dominantly controlled by processes during magma generation such as variable contributions of H₂O-rich slab material (Grove et al., 2002; Ruscitto et al., 2012) or variations in mantle wedge melting (Plank & Langmuir, 1988; Turner et al., 2016)? Alternatively, in what ways does arc crust itself influence these variations?

The correlations between magma hydration proxies and arc physical parameters allow for two distinct interpretations, (1) one that results from considering all arcs together, and (2) one motivated by considering continental and island arcs as distinct populations. These two interpretations suggest somewhat contrasting answers to the above questions.

1. If all arcs are considered together, H₂O_{cpx-pl} and THI_m are only modestly correlated with the thermal state of the slab as characterized by the thermal parameter (Figures 13g and 13h), suggesting that this is not a primary control on the hydration state of arc magmas. In contrast, a strong correlation is observed between mantle wedge height and THI_m (Figure 13e). While the correlation between H₂O_{cpx-pl} and wedge height is weak (Figure 13d), there are pronounced clusters in the data: arcs with primarily low H₂O content magmas (<4 wt.%) are dominantly observed in arcs with mantle wedge heights greater than 100 km, while arcs with wedge heights below 100 km have median H₂O_{cpx-pl} values of at least 4 wt. %. Similarly, both hydration proxies exhibit weak to moderate linear correlations with crustal thickness and a similar threshold is present, where H₂O-poor LLDs are only found when crustal thickness is less than ~25 km, and H₂O-rich LLDs are restricted to crust thicker than 20 km (Figures 13a and 13b). These observations suggest that there is a significant control between either wedge height or upper plate thickness and the hydration state of arc magmas.
2. Alternatively, if continental and island arcs are examined separately, two distinct relationships are apparent (Figure 13): Continental arcs span a wide range of crustal thicknesses and wedge heights, but have nearly invariant, elevated H₂O_{cpx-pl} and low THI_m values consistent with H₂O-rich LLDs. The median H₂O contents in continental arcs cluster between 4 and 6 wt. %, with maximum values typically ≤8 wt. %. Conversely, island arcs span a limited range of the wedge heights and crustal thicknesses and H₂O_{cpx-pl} varies from 1 to 5 wt. %, while THI_m values span a wide range from values consistent with H₂O-poor to H₂O-rich LLDs. By contrast, there is no clear relationship between continental or island arcs and the arc thermal parameter. Compared to the previous interpretations, the distinct continental and island arc systematics imply that neither wedge height nor crustal thickness directly controls variations in the arc hydration state, but instead that other fundamental differences between continental and island arcs generate the distinct dominant LLDs and are the primary cause for the range of observed arc magmas.

6.7. Mechanisms for the Generation of H₂O-Rich and H₂O-Poor Arc Magmas

The above two interpretations of the hydration proxy data require distinct mechanisms to generate the observed range of arc magmas. Similar to previous studies (Chin et al., 2018; Plank & Langmuir, 1988; Turner et al., 2016),

one explanation consistent with the combined global systematics relates the observed range of arc magmas to differences in the relative contributions of decompression (dry) and flux (wet) melting. In these models, the amount of decompression melting is positively correlated with melting column height. Greater extents of decompression melting in the mantle wedge dilute the slab-derived flux of H₂O, yielding on average lower H₂O arc melts. The decompression melting component may include a large contribution from adiabatic decompression melting (e.g., Conder et al., 2002) or from initially H₂O-fluxed melts ascending into the hot core of the mantle wedge where the extent of melting increases to maintain equilibrium with the surrounding mantle (Grove et al., 2002). This process could produce the observed spectrum of arcs ranging from thin-crust island arcs associated with dominantly low-H₂O magmas to thick-crust continental arcs fluxed with more hydrous magmas.

This wedge-height dependent model predicts a continuum of LLDs with primary H₂O contents varying inversely with mantle wedge melting column heights but cannot explain the dichotomy between continental and island arcs. While several properties differ between these settings, we focus here on three possible mechanisms: (a) The shallowest slab dips are exclusively observed at continental arcs and may be a direct result of either enhanced slab suction or plate coupling as crustal thickness increases (Sharples et al., 2014; Tovish et al., 1978). Although shallow slab dips are not necessarily correlated with shorter mantle wedge melting columns, they may hinder corner flow and limit the contribution of decompression melting to arc magmas (England & Wilkins, 2004); (b) Continental arcs likely subduct significantly more crustal material than island arcs. Crustal recycling at subduction zones is primarily estimated using sedimentary sections sampled by oceanic drill cores, which do not show a systematic difference between continental and island arcs (Plank & Langmuir, 1998). However, these drill cores are typically located hundreds of kilometers from trenches, and therefore underestimate near-trench additions of crustal material. These contributions are important for continental arcs, where enhanced subaerial erosion from coastal cordilleras deposits terrigenous sediments in the trench (e.g., Collinet & Jagoutz, 2017; Lee et al., 2015) but are essentially absent in intra-oceanic arcs. The greater crustal thicknesses at continental arcs may also lead to enhanced subduction erosion (e.g., Heuret et al., 2012; Straub et al., 2020). These terrigenous materials can carry a significant volume of H₂O to sub-arc depths (Hacker, 2008) and may contribute to differences in the amounts of slab-derived fluids supplied to continental arcs compared to island arcs, independent of slab thermal parameter. (c) Finally, lower crustal fractionation within thick arcs may allow for a greater role of deep magmatic recharge (Lee et al., 2014). Models have shown that this process can introduce additional feedbacks that lead to greater enrichments in incompatible elements (including H₂O) in melts that are eventually extracted from these deep crustal magma systems (Lee et al., 2014).

6.8. Implications for the Growth of Arc Crust and Continental Crust Formation

The discussion to this point has focused on modern physical parameters of arcs, which implies a relatively static view of arc systems. In this view, the differentiation in arcs with more hydrous magmas begins deeper than in arcs dominated by drier magmas and more hydrous arcs follow calc-alkaline, Fe-depletion trends typical of continental crust. Moreover, high pressure differentiation in hydrous arcs will produce garnet and amphibole-rich, silica-poor cumulates (Alonso-Perez et al., 2009; Müntener et al., 2001) that are density-unstable and readily removed by delamination (Jagoutz et al., 2011; Jull & Kelemen, 2001; Müntener et al., 2001), leaving a more evolved bulk arc crust composition that is similar to estimates of bulk continental crust (Jagoutz & Kelemen, 2015; Rudnick & Gao, 2003). Thus, more hydrous, thicker arcs appear well-suited to create new continental crust, while thin-crust, dominantly tholeiitic, island arcs would seem inefficient. Yet, subduction geometry and arc crustal thickness evolve over the lifespan of an arc (e.g., Kay et al., 2005) and long-lived island arcs can generate new continental crust (Jagoutz & Schmidt, 2012; Kodaira et al., 2007). How do H₂O-poor island arcs with a thin oceanic upper plate such as Tonga or Scotia evolve to generate continental crust, or do some island arcs never generate continental crust?

As discussed above, the upper plate thermal structure and specifically the depth to the temperatures at which magmas cool sufficiently to crystallize plagioclase fundamentally controls arc crustal thickness. We suggest that the flux of magma itself exerts a strong control on the temperature structure of arc crust. While the geotherm that magmas are exposed to is a function of the pre-existing upper plate thickness and thermal structure (e.g., Kelemen, Rilling, et al., 2003), the upper plate thermal structure is also strongly influenced by the sensible and latent heat advected by magmas (England & Katz, 2010; Rees Jones et al., 2018). Thus, a decrease in magma flux should result in cooler temperatures and enhanced fractionation at depth, leading to deeper early fractionation

pressures, deeper plagioclase stability, and thus increased seismic Moho depths. In this model, the flux of magma to arc crust is inversely correlated with Moho depth and exerts a strong control on the petrologic and thermal structure of the arc crust (cf., Till et al., 2019). Long-term estimates of magmatic fluxes in modern arcs appear to broadly support this inverse relationship between magma flux and crustal thickness: in comparison to continental arcs, island arcs are characterized by both thinner crust and also elevated average (felsic) magmatic fluxes of at least 60–80 km³/km/Myr (Jicha & Jagoutz, 2015)—rates that are matched in continental arcs only during magmatic flare-up events (Ducea et al., 2017; Klein et al., 2021; Paterson & Ducea, 2015).

Tectonic processes may also help to maintain the continental and island arc dichotomy. Most modern island arcs are extensional (due to slab pull and trench retreat; Lallemand et al., 2005), which serves to maintain high arc crust temperatures, and may directly reduce crustal thicknesses, in some cases resulting in intra-arc rifting and arc-relocation. A prime example of extensional arc failure is the Marianas, where the construction of the third iteration of arc crust is currently underway (the first two resulting in the Kyushu-Palau and West Mariana Ridges; Beccaluva et al., 1980). Tectonic processes may similarly be important in generating the thickest arcs today. Cumulates produced at pressures above 10–12 kbars are garnet-rich (Ducea et al., 2021; Jagoutz et al., 2011; Lee & Anderson, 2015) and have high densities and fast seismic velocities. These cumulates may delaminate and will also have seismic velocities comparable to mantle peridotite (Jagoutz & Behn, 2013; Müntener & Ulmer, 2006), and thus arc magmatism alone should struggle to produce seismically observable arc crust thicker than ~42 km. Instead, tectonic shortening and underplating must play an important role in producing the thickest continental arcs observed today.

Distinct mechanisms may counteract both factors to improve the efficiency of continental crust construction at island arcs. As in thick continental arcs, if island arcs transition to compressional settings, tectonic overthickening or underplating could increase crustal thickness and depress upper plate temperature profiles. This newly thickened and cooler crust would cause future magmas to differentiate deeper, generating a durable increase in crustal thickness. However, as most modern island arcs are extensional, tectonic shortening may mostly become relevant during island arc collision events (Niu et al., 2013). Alternatively, if island arcs transition to more continent-like magmatism, that is, lower magmatic fluxes and more H₂O-rich magmas, crustal thickening may also occur. Factors otherwise characteristic of continental arcs that promote more hydrous magmas are shallowing slab dips or trench-ward arc migration. Both reduce the mantle wedge melting column beneath the arcs and thus reduce the decompression melting productivity, which should in turn increase H₂O contents in parental magmas.

The Aleutian Arc provides a compelling example of how these processes can interact to produce continent-like crust at an island arc. Among island arcs the Aleutian arc has an unusually shallow sub-arc slab depth (Figure 13) and as discussed above, may have thicker than typical island arc crust and is well-known for producing continental crust-like calc-alkaline magmas (e.g., Kay & Kay, 1985). The Aleutian arc is also unusual in that it is a comparatively long-lived island arc that has never undergone intra-arc rifting (Jicha et al., 2006). It has been shown that subduction zone age correlates with slab dip (Hu & Gurnis, 2020), and thus the unusual long-term survival of the Aleutian arc may have primed it to evolve to a more hydrous, thicker arc. Finally, if the flux of subducted crustal material is a critical factor in continental arc magmatism, island arcs proximal to continents may subduct larger volumes of terrigenous sediments, as is currently occurring in the southern Lesser Antilles.

7. Conclusion

Our new proxies show that for arc magmas, the olivine-clinopyroxene and clinopyroxene-plagioclase cotectics are dominantly controlled by (early) fractionation pressure and H₂O content, respectively. These proxies reveal that arcs with hydrous, deeper fractionating melts evolve toward the calc-alkaline compositions characteristic of continental crust as opposed to drier, shallower fractionating arc systems that typically follow Fe-enrichment trends in island arcs. Governing factors appear to relate to the upper plate crustal thickness and to a lesser extent mantle wedge height.

The strong correlation between early fractionation pressure and arc crustal thickness points to strong control of the plagioclase-in boundary and highlights the importance of the upper plate temperature in controlling the differentiation pressures of arc magmas. The relationships between hydration proxies and subduction zone physical parameters allow for two opposing interpretations: (a) when all arcs are taken together, an apparent inverse relationship between mantle wedge height and magma hydration state indicates that the relative contribution

of decompression melting to arc magmatism decreases with decreasing melting column height; or (b) when continental and island arcs are considered separately, continental and island arcs are quite distinct. Specifically, continental arcs have restricted proxy values consistent with H₂O-rich LLDs but span a range of mantle wedge heights and crustal thicknesses, while island arcs have a wide range of hydration states but quite limited ranges of mantle wedge heights and crustal thicknesses. This dichotomy suggests that fundamental differences exist in magma generation processes between continental and island arcs. Finally, these distinct models suggest contrasting processes by which thick, calc-alkaline continental crust can be generated at initially thin and dominantly tholeiitic island arcs.

Data Availability Statement

No new data were produced during this project. All data compiled as part of this research are available on figshare at <https://dx.doi.org/10.6084/m9.figshare.22621027>.

Acknowledgments

The authors thank George Bergantz, an anonymous reviewer and editor Marie Edmonds for evaluating this work. Detailed comments on a previous version of this manuscript by editor Jane Blichert-Toft, Tom Sisson and an anonymous reviewer helped to significantly refine this work. BZK and OJ were supported by NSF Grant EAR-1552202, and BZK acknowledges additional funding from the University of Lausanne.

References

- Alonso-Perez, R., Müntener, O., & Ulmer, P. (2009). Igneous garnet and amphibole fractionation in the roots of island arcs: Experimental constraints on andesitic liquids. *Contributions to Mineralogy and Petrology*, *157*(4), 541–558. <https://doi.org/10.1007/s00410-008-0351-8>
- Baker, M. B., Grove, T. L., & Price, R. (1994). Primitive basalts and andesites from the Mt. Shasta region, N. California: Products of varying melt fraction and water content. *Contributions to Mineralogy and Petrology*, *118*(2), 111–129. <https://doi.org/10.1007/BF01052863>
- Bartels, K. S., Kinzler, R. J., & Grove, T. L. (1991). High pressure phase relations of primitive high-alumina basalts from Medicine Lake volcano, northern California. *Contributions to Mineralogy and Petrology*, *108*(3), 253–270. <https://doi.org/10.1007/BF00285935>
- Beccaluva, L., Macciotta, G., Savelli, C., Serri, G., & Zeda, O. (1980). Geochemistry and K/Ar ages of volcanics dredged in the Philippine Sea (Mariana, Yap, and Palau trenches and Parece Vela Basin). In D. E. Hayes (Ed.), *The tectonic and geologic evolution of southeast Asian seas and islands, geophysical monograph series* (Vol. 23, pp. 247–268). American Geophysical Union. <https://doi.org/10.1029/GM023p0247>
- Behn, M. D., & Kelemen, P. B. (2006). Stability of arc lower crust: Insights from the Talkeetna arc section, south central Alaska, and the seismic structure of modern arcs. *Journal of Geophysical Research*, *111*(B11), B11207. <https://doi.org/10.1029/2006JB004327>
- Bender, J. F., Hodges, F. N., & Bence, A. E. (1978). Petrogenesis of basalts from the project FAMOUS area: Experimental study from 0 to 15 kbars. *Earth and Planetary Science Letters*, *41*(3), 277–302. [https://doi.org/10.1016/0012-821X\(78\)90184-X](https://doi.org/10.1016/0012-821X(78)90184-X)
- Blatter, D. L., Sisson, T. W., & Hankins, W. B. (2013). Crystallization of oxidized, moderately hydrous arc basalt at mid- to lower-crustal pressures: Implications for andesite genesis. *Contributions to Mineralogy and Petrology*, *166*(3), 861–886. <https://doi.org/10.1007/s00410-013-0920-3>
- Bucholz, C. E., Gaetani, G. A., Behn, M. D., & Shimizu, N. (2013). Post-entrapment modification of volatiles and oxygen fugacity in olivine-hosted melt inclusions. *Earth and Planetary Science Letters*, *374*, 145–155. <https://doi.org/10.1016/j.epsl.2013.05.033>
- Buys, J., Spandler, C., Holm, R. J., & Richards, S. W. (2014). Remnants of ancient Australia in Vanuatu: Implications for crustal evolution in island arcs and tectonic development of the southwest Pacific. *Geology*, *42*(11), 939–942. <https://doi.org/10.1130/G36155.1>
- Chiaradia, M. (2014). Copper enrichment in arc magmas controlled by overriding plate thickness. *Nature Geoscience*, *7*(1), 43–46. <https://doi.org/10.1038/ngeo2028>
- Chin, E. J., Shimizu, K., Bybee, G. M., & Erdman, M. E. (2018). On the development of the calc-alkaline and tholeiitic magma series: A deep crustal cumulate perspective. *Earth and Planetary Science Letters*, *482*, 277–287. <https://doi.org/10.1016/j.epsl.2017.11.016>
- Christensen, N. I., & Mooney, W. D. (1995). Seismic velocity structure and composition of the continental crust: A global view. *Journal of Geophysical Research*, *100*(B6), 9761–9788. <https://doi.org/10.1029/95JB00259>
- Collinet, M., & Jagoutz, O. (2017). Influence of sediment recycling on the trace element composition of primitive arc lavas. In *Abstract #T231-02, presented at 2017 fall meeting* (pp. 11–15). AGU.
- Conder, J. A., Wiens, D. A., & Morris, J. (2002). On the decompression melting structure at volcanic arcs and back-arc spreading centers. *Geophysical Research Letters*, *29*(15), 17-1–17-4. <https://doi.org/10.1029/2002GL015390>
- Danyushevsky, L. V., Sobolev, A. V., & Dmitriev, L. V. (1996). Estimation of the pressure of crystallization and H₂O content of MORB and BABB glasses: Calibration of an empirical technique. *Mineralogy and Petrology*, *57*(3), 185–204. <https://doi.org/10.1007/BF01162358>
- Deering, C. D., & Bachmann, O. (2010). Trace element indicators of crystal accumulation in silicic igneous rocks. *Earth and Planetary Science Letters*, *297*(1–2), 324–331. <https://doi.org/10.1016/j.epsl.2010.06.034>
- Demouchy, S., Jacobsen, S. D., Gaillard, F., & Stern, C. R. (2006). Rapid magma ascent recorded by water diffusion profiles in mantle olivine. *Geology*, *34*(6), 429–432. <https://doi.org/10.1130/G22386.1>
- Devine, J. D., Gardner, J. E., Brack, H. P., Layne, G. D., & Rutherford, M. J. (1995). Comparison of microanalytical methods for estimating H₂O contents of silicic volcanic glasses. *American Mineralogist*, *80*(3–4), 319–328. <https://doi.org/10.2138/am-1995-3-413>
- Ducea, M. N., Bergantz, G. W., Crowley, J. L., & Otamendi, J. (2017). Ultrafast magmatic buildup and diversification to produce continental crust during subduction. *Geology*, *45*(3), 235–238. <https://doi.org/10.1130/G38726.1>
- Ducea, M. N., Chapman, A. D., Bowman, E., & Triantafyllou, A. (2021). Arclogites and their role in continental evolution: part 1: Background, locations, petrography, geochemistry, chronology and thermobarometry. *Earth-Science Reviews*, *214*, 103375. <https://doi.org/10.1016/j.earscirev.2020.103375>
- Dungan, M. A., & Rhodes, J. M. (1978). Residual glasses and melt inclusions in basalts from DSDP Legs 45 and 46: Evidence for magma mixing. *Contributions to Mineralogy and Petrology*, *67*(4), 417–431. <https://doi.org/10.1007/BF00383301>
- Eggler, D. H. (1972). Water-saturated and undersaturated melting relations in a Paricutin andesite and an estimate of water content in the natural magma. *Contributions to Mineralogy and Petrology*, *34*(4), 261–271. <https://doi.org/10.1007/BF00373757>
- Eichelberger, J. C. (1975). Origin of andesite and dacite: Evidence of mixing at Glass Mountain in California and at other circum-Pacific volcanoes. *Geological Society of America Bulletin*, *86*(10), 1381–1391. [https://doi.org/10.1130/0016-7606\(1975\)86<1381:OOAADE>2.0.CO;2](https://doi.org/10.1130/0016-7606(1975)86<1381:OOAADE>2.0.CO;2)
- England, P. C., & Katz, R. F. (2010). Melting above the anhydrous solidus controls the location of volcanic arcs. *Nature*, *467*(7316), 700–703. <https://doi.org/10.1038/nature09417>

- England, P. C., & Wilkins, C. (2004). A simple analytical approximation to the temperature structure in subduction zones. *Geophysical Journal International*, 159(3), 1138–1154. <https://doi.org/10.1111/j.1365-246X.2004.02419.x>
- Fujinawa, A. (1988). Tholeiitic and calc-alkaline magma series at Adataro volcano, northeast Japan: 1. Geochemical constraints on their origin. *Lithos*, 22(2), 135–158. [https://doi.org/10.1016/0024-4937\(88\)90022-9](https://doi.org/10.1016/0024-4937(88)90022-9)
- Gaetani, G. A., Grove, T. L., & Bryan, W. B. (1993). The influence of water on the petrogenesis of subduction related igneous rocks. *Nature*, 365(6444), 332–334. <https://doi.org/10.1038/365332a0>
- Gaetani, G. A., O'Leary, J. A., Shimizu, N., Bucholz, C. E., & Newville, M. (2012). Rapid reequilibration of H₂O and oxygen fugacity in olivine-hosted melt inclusions. *Geology*, 40(10), 915–918. <https://doi.org/10.1130/G32992.1>
- Greene, A. R., DeBari, S. M., Kelemen, P. B., Blusztajn, J., & Clift, P. D. (2006). A detailed geochemical study of island arc crust: The Talkeetna arc section, south-central Alaska. *Journal of Petrology*, 47(6), 1051–1093. <https://doi.org/10.1093/ptrology/eg1002>
- Grove, T. L., & Baker, M. B. (1984). Phase equilibrium controls on the tholeiitic versus calc-alkaline differentiation trends. *Journal of Geophysical Research*, 89(B5), 3253–3274. <https://doi.org/10.1029/JB089iB05p03253>
- Grove, T. L., Baker, M. B., Price, R. C., Parman, S. W., Elkins-Tanton, L. T., Chatterjee, N., & Müntener, O. (2004). Magnesian andesite and dacite lavas from Mt. Shasta, northern California: Products of fractional crystallization of H₂O-rich mantle melts. *Contributions to Mineralogy and Petrology*, 148(5), 542–565. <https://doi.org/10.1007/s00410-004-0619-6>
- Grove, T. L., & Donnelly-Nolan, J. M. (1986). The evolution of young silicic lavas at Medicine Lake Volcano, California: Implications for the origin of compositional gaps in calc-alkaline series lavas. *Contributions to Mineralogy and Petrology*, 92(3), 281–302. <https://doi.org/10.1007/BF00572157>
- Grove, T. L., Elkins-Tanton, L. T., Parman, S. W., Chatterjee, N., Müntener, O., & Gaetani, G. A. (2003). Fractional crystallization and mantle-melting controls on calc-alkaline differentiation trends. *Contributions to Mineralogy and Petrology*, 145(5), 515–533. <https://doi.org/10.1007/s00410-003-0448-z>
- Grove, T. L., Kinzler, R. J., & Bryan, W. B. (1992). Fractionation of mid-ocean ridge basalt (MORB). In J. P. Morgan, D. K. Blackman, & J. M. Sinton (Eds.), *Mantle flow and melt generation at mid-ocean ridges, Geophysical monograph series* (Vol. 71, pp. 281–310). American Geophysical Union. <https://doi.org/10.1029/GM071p0281>
- Grove, T. L., Parman, S., Bowring, S., Price, R., & Baker, M. (2002). The role of an H₂O-rich fluid component in the generation of primitive basaltic andesites and andesites from the Mt. Shasta region, N California. *Contributions to Mineralogy and Petrology*, 142(4), 375–396. <https://doi.org/10.1007/s004100100299>
- Gualda, G. A. R., Ghiorsio, M. S., Lemons, R. V., & Carley, T. L. (2012). Rhyolite-MELTS: A modified calibration of MELTS optimized for silica-rich, fluid-bearing magmatic systems. *Journal of Petrology*, 53(5), 875–890. <https://doi.org/10.1093/ptrology/egr080>
- Hacker, B. R. (2008). H₂O subduction beyond arcs. *Geochemistry, Geophysics, Geosystems*, 9(3), Q03001. <https://doi.org/10.1029/2007GC001707>
- Hacker, B. R., Mehl, L., Kelemen, P. B., Rioux, M., Behn, M. D., & Luffi, P. (2008). Reconstruction of the Talkeetna intraoceanic arc of Alaska through thermobarometry. *Journal of Geophysical Research*, 113(B3), B03204. <https://doi.org/10.1029/2007JB005208>
- Herzberg, C. (2004). Partial crystallization of mid-ocean ridge basalts in the crust and mantle. *Journal of Petrology*, 45(12), 2389–2405. <https://doi.org/10.1093/ptrology/egh040>
- Heuret, A., Conrad, C. P., Funicello, F., Lallemand, S., & Sandri, L. (2012). Relation between subduction megathrust earthquakes, trench sediment thickness and upper plate strain. *Geophysical Research Letters*, 39(5), L05304. <https://doi.org/10.1029/2011GL050712>
- Hildreth, W., & Moorbath, S. (1988). Crustal contributions to arc magmatism in the Andes of central Chile. *Contributions to Mineralogy and Petrology*, 98(4), 455–489. <https://doi.org/10.1007/BF00372365>
- Hu, J., & Gurnis, M. (2020). Subduction duration and slab dip. *Geochemistry, Geophysics, Geosystems*, 21(4), e2019GC008862. <https://doi.org/10.1029/2019GC008862>
- Hunter, A. G. (1998). Intracrustal controls on the coexistence of tholeiitic and calc-alkaline magma series at Aso Volcano, SW Japan. *Journal of Petrology*, 39(7), 1255–1284. <https://doi.org/10.1093/ptrology/39.7.1255>
- Iacovino, K., Matthews, S., Wieser, P. E., Moore, G. M., & Bégué, F. (2021). VESJcal part I: An open-source thermodynamic model engine for mixed volatile (HCO₂CO₂) solubility in silicate melts. *Earth and Space Science*, 8(11), e2020EA001584. <https://doi.org/10.1029/2020EA001584>
- Jagoutz, O. (2010). Construction of the granitoid crust of an island arc. Part II: A quantitative petrogenetic model. *Contributions to Mineralogy and Petrology*, 160(3), 359–381. <https://doi.org/10.1007/s00410-009-0482-6>
- Jagoutz, O. (2014). Arc crustal differentiation mechanisms. *Earth and Planetary Science Letters*, 396, 267–277. <https://doi.org/10.1016/j.epsl.2014.03.060>
- Jagoutz, O., & Behn, M. D. (2013). Foundering of lower island-arc crust as an explanation for the origin of the continental Moho. *Nature*, 504(7478), 131–134. <https://doi.org/10.1038/nature12758>
- Jagoutz, O., & Kelemen, P. B. (2015). Role of arc processes in the formation of continental crust. *Annual Review of Earth and Planetary Sciences*, 43(1), 363–404. <https://doi.org/10.1146/annurev-earth-040809-152345>
- Jagoutz, O., & Klein, B. (2018). On the importance of crystallization-differentiation for the generation of SiO₂-rich melts and the compositional build-up of arc (and continental) crust. *American Journal of Science*, 318(1), 29–63. <https://doi.org/10.2475/01.2018.03>
- Jagoutz, O., Müntener, O., Schmidt, M. W., & Burg, J.-P. (2011). The roles of flux- and decompression melting and their respective fractionation lines for continental crust formation: Evidence from the Kohistan arc. *Earth and Planetary Science Letters*, 303(1–2), 25–36. <https://doi.org/10.1016/j.epsl.2010.12.017>
- Jagoutz, O., & Schmidt, M. W. (2012). The formation and bulk composition of modern juvenile continental crust: The Kohistan arc. *Chemical Geology*, 298–299, 79–96. <https://doi.org/10.1016/j.chemgeo.2011.10.022>
- Jicha, B. R., & Jagoutz, O. (2015). Magma production rates for intraoceanic arcs. *Elements*, 11(2), 105–111. <https://doi.org/10.2113/gselements.11.2.105>
- Jicha, B. R., Scholl, D. W., Singer, B. S., Yagodinski, G. M., & Kay, S. M. (2006). Revised age of Aleutian Island Arc formation implies high rate of magma production. *Geology*, 34(8), 661–664. <https://doi.org/10.1130/g22433.1>
- Jull, M., & Kelemen, P. B. (2001). On the conditions for lower crustal convective instability. *Journal of Geophysical Research*, 106(B4), 6423–6446. <https://doi.org/10.1029/2000JB900357>
- Kay, S. M., Godoy, E., & Kurtz, A. (2005). Episodic arc migration, crustal thickening, subduction erosion, and magmatism in the south-central Andes. *Geological Society of America Bulletin*, 117(1–2), 67–88. <https://doi.org/10.1130/B25431.1>
- Kay, S. M., & Kay, R. W. (1985). Aleutian tholeiitic and calc-alkaline magma series I: The mafic phenocrysts. *Contributions to Mineralogy and Petrology*, 90(2–3), 276–290. <https://doi.org/10.1007/BF00378268>
- Kelemen, P. B., Hanghøj, K., & Greene, A. R. (2003). 3.18—One view of the geochemistry of subduction-related magmatic arcs, with an emphasis on primitive andesite and lower crust. In H. D. Holland, & K. K. Turekian (Eds.), *Treatise on geochemistry* (Vol. 3, pp. 1–70). Pergamon. <https://doi.org/10.1016/B0-08-043751-6/03035-8>

- Kelemen, P. B., Rilling, J. L., Parmentier, E. M., Mehl, L., & Hacker, B. R. (2003). Thermal structure due to solid-state flow in the mantle wedge beneath arcs. In J. Eiler (Ed.), *Inside the subduction factory, geophysical monograph series* (Vol. 71, pp. 293–311). American Geophysical Union. <https://doi.org/10.1029/138GM13>
- Keller, C. B., Schoene, B., Barboni, M., Samperton, K. M., & Husson, J. M. (2015). Volcanic-plutonic parity and the differentiation of the continental crust. *Nature*, *523*(7560), 301–307. <https://doi.org/10.1038/nature14584>
- Klein, B. Z., & Jagoutz, O. (2021). Construction of a trans-crustal magma system: Building the Bear Valley Intrusive Suite, southern Sierra Nevada, California. *Earth and Planetary Science Letters*, *553*, 116624. <https://doi.org/10.1016/j.epsl.2020.116624>
- Klein, B. Z., Jagoutz, O., & Ramezani, J. (2021). High-precision geochronology requires that ultrafast mantle-derived magmatic fluxes built the transcrustal Bear Valley Intrusive Suite, Sierra Nevada, California, USA. *Geology*, *49*(1), 106–110. <https://doi.org/10.1130/G47952.1>
- Klein, B. Z., & Müntener, O. (2023). MnO/MgO ratios of arc basalts highlight the role of early garnet fractionation. *Geochemical Perspectives Letters*, *25*, 18–24. <https://doi.org/10.7185/geochemlet.2309>
- Kodaira, S., Sato, T., Takahashi, N., Miura, S., Tamura, Y., Tatsumi, Y., & Kaneda, Y. (2007). New seismological constraints on growth of continental crust in the Izu-Bonin intra-oceanic arc. *Geology*, *35*(11), 1031–1034. <https://doi.org/10.1130/G23901A.1>
- Krawczynski, M., Grove, T. L., & Behrens, H. (2012). Amphibole stability in primitive arc magmas: Effects of temperature, H₂O content, and oxygen fugacity. *Contributions to Mineralogy and Petrology*, *164*(2), 317–339. <https://doi.org/10.1007/s00410-012-0740-x>
- Kress, V. C., & Carmichael, I. S. E. (1991). The compressibility of silicate liquids containing Fe₂O₃ and the effect of composition, temperature, oxygen fugacity and pressure on their redox states. *Contributions to Mineralogy and Petrology*, *108*(1), 82–92. <https://doi.org/10.1007/BF00307328>
- Lallemand, S., Heuret, A., & Boutelier, D. (2005). On the relationships between slab dip, back-arc stress, upper plate absolute motion, and crustal nature in subduction zones. *Geochemistry, Geophysics, Geosystems*, *6*(9), Q09006. <https://doi.org/10.1029/2005GC000917>
- Lange, R. A., Frey, H. M., & Hecton, J. (2009). A thermodynamic model for the plagioclase-liquid hygrometer/thermometer. *American Mineralogist*, *94*(4), 494–506. <https://doi.org/10.2138/am.2009.3011>
- Langmuir, C. H., Klein, E. M., & Plank, T. (1992). Petrological systematics of mid-ocean ridge basalts: Constraints on melt generation beneath ocean ridges. In J. P. Morgan, D. K. Blackman, & J. M. Sinton (Eds.), *Mantle flow and melt generation at mid-ocean ridges, Geophysical monograph series* (Vol. 71, pp. 183–280). American Geophysical Union. <https://doi.org/10.1029/GM071p0183>
- Larter, R. D., Vanneste, L. E., Morris, P., & Smythe, D. K. (2003). Structure and tectonic evolution of the South Sandwich arc. *Geological Society, London, Special Publications*, *219*(1), 255–284. <https://doi.org/10.1144/gsl.sp.2003.219.01.13>
- Lee, C.-T. A., & Anderson, D. L. (2015). Continental crust formation at arcs, the arclogite “delamination” cycle, and one origin for fertile melting anomalies in the mantle. *Science Bulletin*, *60*(13), 1141–1156. <https://doi.org/10.1007/s11434-015-0828-6>
- Lee, C.-T. A., & Bachmann, O. (2014). How important is the role of crystal fractionation in making intermediate magmas? Insights from Zr and P systematics. *Earth and Planetary Science Letters*, *393*, 266–274. <https://doi.org/10.1016/j.epsl.2014.02.044>
- Lee, C.-T. A., Lee, T. C., & Wu, C.-T. (2014). Modeling the compositional evolution of recharging, evacuating, and fractionating (REFC) magma chambers: Implications for differentiation of arc magmas. *Geochimica et Cosmochimica Acta*, *143*, 8–22. <https://doi.org/10.1016/j.gca.2013.08.009>
- Lee, C.-T. A., Thurner, S., Paterson, S., & Cao, W. (2015). The rise and fall of continental arcs: Interplays between magmatism, uplift, weathering, and climate. *Earth and Planetary Science Letters*, *425*, 105–119. <https://doi.org/10.1016/j.epsl.2015.05.045>
- Le Voyer, M., Rose-Koga, E. F., Shimizu, N., Grove, T. L., & Schiano, P. (2010). Two contrasting H₂O-rich components in primary melt inclusions from Mount Shasta. *Journal of Petrology*, *51*(7), 1571–1595. <https://doi.org/10.1093/petrology/egq030>
- Lloyd, A. S., Plank, T., Ruprecht, P., Hauri, E. H., & Rose, W. (2013). Volatile loss from melt inclusions in pyroclasts of differing sizes. *Contributions to Mineralogy and Petrology*, *165*(1), 129–153. <https://doi.org/10.1007/s00410-012-0800-2>
- Meffre, S., & Crawford, A. J. (2001). Collision tectonics in the New Hebrides arc (Vanuatu). *Island Arc*, *10*(1), 33–50. <https://doi.org/10.1046/j.1440-1738.2001.00292.x>
- Melekhova, E., Blundy, J., Robertson, R., & Humphreys, M. C. S. (2015). Experimental evidence for polybaric differentiation of primitive arc basalt beneath St. Vincent, Lesser Antilles. *Journal of Petrology*, *56*(1), 161–192. <https://doi.org/10.1093/petrology/egu074>
- Merzbacher, C., & Egglar, D. H. (1984). A magmatic geohygrometer: Application to Mount St. Helens and other dacitic magmas. *Geology*, *12*(10), 587–590. [https://doi.org/10.1130/0091-7613\(1984\)12<587:AMGATM>2.0.CO;2](https://doi.org/10.1130/0091-7613(1984)12<587:AMGATM>2.0.CO;2)
- Michael, P. J., & Cornell, W. C. (1998). Influence of spreading rate and magma supply on crystallization and assimilation beneath mid-ocean ridges: Evidence from chlorine and major element chemistry of mid-ocean ridge basalts. *Journal of Geophysical Research*, *103*(B8), 18325–18356. <https://doi.org/10.1029/98JB00791>
- Mitchell, A. L., Gaetani, G. A., O’Leary, J. A., & Hauri, E. H. (2017). H₂O solubility in basalt at upper mantle conditions. *Contributions to Mineralogy and Petrology*, *172*(10), 85. <https://doi.org/10.1007/s00410-017-1401-x>
- Mitchell, A. L., & Grove, T. L. (2016). Experiments on melt–rock reaction in the shallow mantle wedge. *Contributions to Mineralogy and Petrology*, *171*(12), 107. <https://doi.org/10.1007/s00410-016-1312-2>
- Müntener, O., Kelemen, P., & Grove, T. L. (2001). The role of H₂O during crystallization of primitive arc magmas under uppermost mantle conditions and genesis of igneous pyroxenites: An experimental study. *Contributions to Mineralogy and Petrology*, *141*(6), 643–658. <https://doi.org/10.1007/s004100100266>
- Müntener, O., & Ulmer, P. (2006). Experimentally derived high-pressure cumulates from hydrous arc magmas and consequences for the seismic velocity structure of lower arc crust. *Geophysical Research Letters*, *33*(21), L21308. <https://doi.org/10.1029/2006GL027629>
- Nandedkar, R. H. (2014). *Evolution of hydrous mantle-derived calc-alkaline liquids by fractional crystallization at 0.7 and 0.4 Gpa* (Doctoral dissertation). ETH-Zürich. <https://doi.org/10.3929/ethz-a-010093734>
- Nandedkar, R. H., Ulmer, P., & Müntener, O. (2014). Fractional crystallization of primitive, hydrous arc magmas: An experimental study at 0.7 GPa. *Contributions to Mineralogy and Petrology*, *167*(6), 1–27. <https://doi.org/10.1007/s00410-014-1015-5>
- Neave, D. A., & Putirka, K. D. (2017). A new clinopyroxene-liquid barometer, and implications for magma storage pressures under Icelandic rift zones. *American Mineralogist*, *102*(4), 777–794. <https://doi.org/10.2138/am-2017-5968>
- Newman, S., & Lowenstern, J. B. (2002). VolatileCalc: A silicate melt–H₂O–CO₂ solution model written in visual basic for excel. *Computers & Geosciences*, *28*(5), 597–604. [https://doi.org/10.1016/S0098-3004\(01\)00081-4](https://doi.org/10.1016/S0098-3004(01)00081-4)
- Niu, Y., Zhao, Z., Zhu, D.-C., & Mo, X. (2013). Continental collision zones are primary sites for net continental crust growth—A testable hypothesis. *Earth-Science Reviews*, *127*, 96–110. <https://doi.org/10.1016/j.earscirev.2013.09.004>
- Parman, S. W., Grove, T. L., Kelley, K. A., & Plank, T. (2010). Along-arc variations in the pre-eruptive H₂O contents of Mariana Arc magmas inferred from fractionation paths. *Journal of Petrology*, *52*(2), 257–278. <https://doi.org/10.1093/petrology/egq079>
- Paterson, S. R., & Ducea, M. N. (2015). Arc magmatic tempos: Gathering the evidence. *Elements*, *11*(2), 91–98. <https://doi.org/10.2113/gselements.11.2.91>

- Pichavant, M., & Macdonald, R. (2007). Crystallization of primitive basaltic magmas at crustal pressures and genesis of the calc-alkaline igneous suite: Experimental evidence from St Vincent, Lesser Antilles arc. *Contributions to Mineralogy and Petrology*, 154(5), 535–558. <https://doi.org/10.1007/s00410-007-0208-6>
- Plank, T., Kelley, K. A., Zimmer, M. M., Hauri, E. H., & Wallace, P. J. (2013). Why do mafic arc magmas contain ~4wt% water on average? *Earth and Planetary Science Letters*, 364, 168–179. <https://doi.org/10.1016/j.epsl.2012.11.044>
- Plank, T., & Langmuir, C. H. (1988). An evaluation of the global variations in the major element chemistry of arc basalts. *Earth and Planetary Science Letters*, 90(4), 349–370. [https://doi.org/10.1016/0012-821X\(88\)90135-5](https://doi.org/10.1016/0012-821X(88)90135-5)
- Plank, T., & Langmuir, C. H. (1998). The chemical composition of subducting sediment and its consequences for the crust and mantle. *Chemical Geology*, 145(3–4), 325–394. [https://doi.org/10.1016/S0009-2541\(97\)00150-2](https://doi.org/10.1016/S0009-2541(97)00150-2)
- Portnyagin, M., Hoernle, K., Plechov, P., Mironov, N., & Khubunaya, S. (2007). Constraints on mantle melting and composition and nature of slab components in volcanic arcs from volatiles (H₂O, S, Cl, F) and trace elements in melt inclusions from the Kamchatka Arc. *Earth and Planetary Science Letters*, 255(1–2), 53–69. <https://doi.org/10.1016/j.epsl.2006.12.005>
- Presnall, D. C., Dixon, S. A., Dixon, J. R., O'Donnell, T. H., Brenner, N. L., Schrock, R. L., & Dycus, D. W. (1978). Liquidus phase relations on the join diopside-forsterite-anorthite from 1 atm to 20 kbar: Their bearing on the generation and crystallization of basaltic magma. *Contributions to Mineralogy and Petrology*, 66(2), 203–220. <https://doi.org/10.1007/BF00372159>
- Prouteau, G., & Scaillet, B. (2003). Experimental constraints on the origin of the 1991 Pinatubo dacite. *Journal of Petrology*, 44(12), 2203–2241. <https://doi.org/10.1093/ptrology/egg075>
- Putirka, K. D. (2008). Thermometers and barometers for volcanic systems. *Reviews in Mineralogy and Geochemistry*, 69(1), 61–120. <https://doi.org/10.2138/rmg.2008.69.3>
- Putirka, K. D. (2016). Amphibole thermometers and barometers for igneous systems and some implications for eruption mechanisms of felsic magmas at arc volcanoes. *American Mineralogist*, 101(4), 841–858. <https://doi.org/10.2138/am-2016-5506>
- Rees Jones, D. W., Katz, R. F., Tian, M., & Rudge, J. F. (2018). Thermal impact of magmatism in subduction zones. *Earth and Planetary Science Letters*, 481, 73–79. <https://doi.org/10.1016/j.epsl.2017.10.015>
- Rezeau, H., Klein, B. Z., & Jagoutz, O. (2021). Mixing dry and wet magmas in the lower crust of a continental arc: New petrological insights from the Bear Valley Intrusive Suite, southern Sierra Nevada, California. *Contributions to Mineralogy and Petrology*, 176(9), 73. <https://doi.org/10.1007/s00410-021-01832-2>
- Rousseuw, P. J., & Croux, C. (1991). Alternatives to the median absolute deviation. *Journal of the American Statistical Association*, 88(424), 1273–1283. <https://doi.org/10.1080/01621459.1993.10476408>
- Rudnick, R. L., & Gao, S. (2003). 3.01—Composition of the continental crust. In H. D. Holland & K. K. Turekian (Eds.), *Treatise on geochemistry* (Vol. 3, pp. 1–64). Pergamon Press. <https://doi.org/10.1016/B0-08-043751-6/03016-4>
- Ruscitto, D. M., Wallace, P. J., Cooper, L. B., & Plank, T. (2012). Global variations in H₂O/Ce: 2. Relationships to arc magma geochemistry and volatile fluxes. *Geochemistry, Geophysics, Geosystems*, 13(3), Q03025. <https://doi.org/10.1029/2011GC003887>
- Schmidt, M. W., & Jagoutz, O. (2017). The global systematics of primitive arc melts. *Geochemistry, Geophysics, Geosystems*, 18(8), 2817–2854. <https://doi.org/10.1002/2016GC006699>
- Schmidt, M. W., & Weidendorfer, D. (2018). Carbonatites in oceanic hotspots. *Geology*, 46(5), 435–438. <https://doi.org/10.1130/G39621.1>
- Sharples, W., Jadamec, M. A., Moresi, L. N., & Capitanio, F. A. (2014). Overriding plate controls on subduction evolution. *Journal of Geophysical Research: Solid Earth*, 119(8), 6684–6704. <https://doi.org/10.1002/2014JB011163>
- Shillington, D. J., Van Avendonk, H. J. A., Behn, M. D., Kelemen, P. B., & Jagoutz, O. (2013). Constraints on the composition of the Aleutian arc lower crust from V_p/V_s. *Geophysical Research Letters*, 40(11), 2579–2584. <https://doi.org/10.1002/grl.50375>
- Shillington, D. J., Van Avendonk, H. J. A., Holbrook, W. S., Kelemen, P. B., & Hornbach, M. J. (2004). Composition and structure of the central Aleutian island arc from arc-parallel wide-angle seismic data. *Geochemistry, Geophysics, Geosystems*, 5(10), Q10006. <https://doi.org/10.1029/2004GC000715>
- Sisson, T. W., & Grove, T. L. (1993a). Experimental investigations of the role of H₂O in calc-alkaline differentiation and subduction zone magmatism. *Contributions to Mineralogy and Petrology*, 113(2), 143–166. <https://doi.org/10.1007/BF00283225>
- Sisson, T. W., & Grove, T. L. (1993b). Temperatures and H₂O contents of low-MgO high-alumina basalts. *Contributions to Mineralogy and Petrology*, 113(2), 167–184. <https://doi.org/10.1007/BF00283226>
- Sisson, T. W., & Layne, G. D. (1993). H₂O in basalt and basaltic andesite glass inclusions from four subduction-related volcanoes. *Earth and Planetary Science Letters*, 117(3–4), 619–635. [https://doi.org/10.1016/0012-821X\(93\)90107-K](https://doi.org/10.1016/0012-821X(93)90107-K)
- Stern, C. R., Huang, W. L., & Wyllie, P. J. (1975). Basalt-andesite-rhyolite-H₂O: Crystallization intervals with excess H₂O and H₂O-undersaturated liquidus surfaces to 35 kilobars, with implications for magma genesis. *Earth and Planetary Science Letters*, 28(2), 189–196. [https://doi.org/10.1016/0012-821X\(75\)90226-5](https://doi.org/10.1016/0012-821X(75)90226-5)
- Straub, S. M., Gómez-Tuena, A., & Vannucchi, P. (2020). Subduction erosion and arc volcanism. *Nature Reviews Earth & Environment*, 1(11), 574–589. <https://doi.org/10.1038/s43017-020-0095-1>
- Syracuse, E. M., & Abers, G. A. (2006). Global compilation of variations in slab depth beneath arc volcanoes and implications. *Geochemistry, Geophysics, Geosystems*, 7(5), Q05017. <https://doi.org/10.1029/2005GC001045>
- Syracuse, E. M., van Keken, P. E., & Abers, G. A. (2010). The global range of subduction zone thermal models. *Physics of the Earth and Planetary Interiors*, 183(1–2), 73–90. <https://doi.org/10.1016/j.pepi.2010.02.004>
- Takahashi, N., Kodaira, S., Tsumami, Y., Kaneda, Y., & Suyehiro, K. (2008). Structure and growth of the Izu-Bonin-Mariana arc crust: 1. Seismic constraint on crust and mantle structure of the Mariana arc-back-arc system. *Journal of Geophysical Research*, 113(B1), B01104. <https://doi.org/10.1029/2007JB005120>
- Tang, M., Erdman, M., Eldridge, G., & Lee, C.-T. A. (2018). The redox “filter” beneath magmatic orogens and the formation of continental crust. *Science Advances*, 4(5), eaar4444. <https://doi.org/10.1126/sciadv.aar4444>
- Tatsumi, Y., Shukuno, H., Tani, K., Takahashi, N., Kodaira, S., & Kogiso, T. (2008). Structure and growth of the Izu-Bonin-Mariana arc crust: 2. Role of crust-mantle transformation and the transparent Moho in arc crust evolution. *Journal of Geophysical Research*, 113(B2), B02203. <https://doi.org/10.1029/2007JB005121>
- Taylor, S. R. (1977). Island arc models and the composition of the continental crust. In M. Talwani & W. C. Pitman III (Eds.), *Island arcs, deep sea trenches and back-arc basins, Maurice Ewing series* (Vol. 1, pp. 325–335). American Geophysical Union. <https://doi.org/10.1029/ME001p0325>
- Till, C. B. (2017). A review and update of mantle thermobarometry for primitive arc magmas. *American Mineralogist*, 102(5), 931–947. <https://doi.org/10.2138/am-2017-5783>
- Till, C. B., Kent, A. J. R., Abers, G. A., Janiszewski, H. A., Gaherty, J. B., & Pitcher, B. W. (2019). The causes of spatiotemporal variations in erupted fluxes and compositions along a volcanic arc. *Nature Communications*, 10(1), 1350. <https://doi.org/10.1038/s41467-019-09113-0>

- Tormey, D. R., Grove, T. L., & Bryan, W. B. (1987). Experimental petrology of normal MORB near the Kane Fracture Zone: 22°–25°N, mid-Atlantic ridge. *Contributions to Mineralogy and Petrology*, 96(2), 121–139. <https://doi.org/10.1007/bf00375227>
- Tovish, A., Schubert, G., & Luyendyk, B. P. (1978). Mantle flow pressure and the angle of subduction: Non-Newtonian corner flows. *Journal of Geophysical Research*, 83(B12), 5892–5898. <https://doi.org/10.1029/JB083iB12p05892>
- Turner, S. J., & Langmuir, C. H. (2015). The global chemical systematics of arc front stratovolcanoes: Evaluating the role of crustal processes. *Earth and Planetary Science Letters*, 422, 182–193. <https://doi.org/10.1016/j.epsl.2015.03.056>
- Turner, S. J., Langmuir, C. H., Katz, R. F., Dungan, M. A., & Escrig, S. (2016). Parental arc magma compositions dominantly controlled by mantle-wedge thermal structure. *Nature Geoscience*, 9(10), 772–776. <https://doi.org/10.1038/ngeo2788>
- Ulmer, P., Kaegi, R., & Müntener, O. (2018). Experimentally derived intermediate to silica-rich arc magmas by fractional and equilibrium crystallization at 1.0 GPa: An evaluation of phase relationships, compositions, liquid lines of descent and oxygen fugacity. *Journal of Petrology*, 59(1), 11–58. <https://doi.org/10.1093/petrology/egy017>
- Urann, B. M., Le Roux, V., Jagoutz, O., Behn, M. D., & Chin, E. J. (2022). High water contents of arc magmas recorded in cumulates from subduction zone lower crust. *Nature Geoscience*, 15(6), 501–508. <https://doi.org/10.1038/s41561-022-00947-w>
- Ventura, G. (2013). Chapter 2: Kinematics of the Aeolian volcanism (southern Tyrrhenian Sea) from geophysical and geological data. In F. Lucchi, A. Peccerillo, J. Keller, C. A. Tranne, & P. L. Rossi (Eds.), *The Aeolian islands volcanoes: Geological society* (Vol. 37, pp. 3–11). Geological Society. <https://doi.org/10.1144/M37.2>
- Villiger, S., Müntener, O., & Ulmer, P. (2007). Crystallization pressures of mid-ocean ridge basalts derived from major element variations of glasses from equilibrium and fractional crystallization experiments. *Journal of Geophysical Research*, 112(B1), B01202. <https://doi.org/10.1029/2006JB004342>
- Villiger, S., Ulmer, P., & Müntener, O. (2007). Equilibrium and fractional crystallization experiments at 0.7 GPa; the Effect of pressure on phase relations and liquid compositions of tholeiitic magmas. *Journal of Petrology*, 48(1), 159–184. <https://doi.org/10.1093/petrology/egl058>
- Villiger, S., Ulmer, P., Müntener, O., & Thompson, A. B. (2004). The liquid line of descent of anhydrous, mantle-derived, tholeiitic liquids by fractional and equilibrium crystallization—An experimental study at 1.0 GPa. *Journal of Petrology*, 45(12), 2369–2388. <https://doi.org/10.1093/petrology/egh042>
- Wagner, T. P., Donnelly-Nolan, J. M., & Grove, T. L. (1995). Evidence of hydrous differentiation and crystal accumulation in the low-MgO, high-Al₂O₃ Lake Basalt from Medicine Lake volcano, California. *Contributions to Mineralogy and Petrology*, 121(2), 201–216. <https://doi.org/10.1007/s004100050099>
- Walker, B. A., Jr., Bergantz, G. W., Otamendi, J. E., Ducea, M. N., & Cristofolini, E. A. (2015). A MASH zone revealed: The mafic complex of the Sierra Valle Fértil. *Journal of Petrology*, 56(9), 1863–1896. <https://doi.org/10.1093/petrology/egv057>
- Walker, J. A. (1984). Volcanic rocks from the Nejapa and Granada cinder cone alignments, Nicaragua, Central America. *Journal of Petrology*, 25(2), 299–342. <https://doi.org/10.1093/petrology/25.2.299>
- Waters, L. E., & Lange, R. A. (2015). An updated calibration of the plagioclase-liquid hygrometer-thermometer applicable to basalts through rhyolites. *American Mineralogist*, 100(10), 2172–2184. <https://doi.org/10.2138/am-2015-5232>
- Yang, H.-J., Kinzler, R. J., & Grove, T. L. (1996). Experiments and models of anhydrous, basaltic olivine-plagioclase-augite saturated melts from 0.001 to 10 kbar. *Contributions to Mineralogy and Petrology*, 124(1), 1–18. <https://doi.org/10.1007/s004100050169>
- Yogodzinski, G. M., Brown, S. T., Kelemen, P. B., Vervoort, J. D., Portnyagin, M., Sims, K. W. W., et al. (2015). The role of subducted basalt in the source of island arc magmas: Evidence from seafloor lavas of the Western Aleutians. *Journal of Petrology*, 56(3), 441–492. <https://doi.org/10.1093/petrology/egv006>
- Yuan, X., Sobolev, S. V., & Kind, R. (2002). Moho topography in the central Andes and its geodynamic implications. *Earth and Planetary Science Letters*, 199(3–4), 389–402. [https://doi.org/10.1016/s0012-821x\(02\)00589-7](https://doi.org/10.1016/s0012-821x(02)00589-7)
- Zimmer, M. M., Plank, T., Hauri, E. H., Yogodzinski, G. M., Stelling, P., Larsen, J., et al. (2010). The role of water in generating the calc-alkaline trend: New volatile data for Aleutian magmas and a new Tholeiitic Index. *Journal of Petrology*, 51(12), 2411–2444. <https://doi.org/10.1093/petrology/egq062>

References From the Supporting Information

- Abe, Y., Ohkura, T., Hirahara, K., & Shibutani, T. (2013). Along-arc variation in water distribution in the uppermost mantle beneath Kyushu, Japan, as derived from receiver function analyses. *Journal of Geophysical Research: Solid Earth*, 118(7), 3540–3556. <https://doi.org/10.1002/jgrb.50257>
- Agostinetti, N. P., & Amato, A. (2009). Moho depth and Vp/Vs ratio in peninsular Italy from teleseismic receiver functions. *Journal of Geophysical Research*, 114(B6), B06303. <https://doi.org/10.1029/2008jb005899>
- Almeev, R. R., Holtz, F., Ariskin, A. A., & Kimura, J.-I. (2013). Storage conditions of Bezymianny Volcano parental magmas: Results of phase equilibria experiments at 100 and 700 MPa. *Contributions to Mineralogy and Petrology*, 166(5), 1389–1414. <https://doi.org/10.1007/s00410-013-0934-x>
- Arai, R., Takahashi, T., Kodaira, S., Kaiho, Y., Nakanishi, A., Fujie, G., et al. (2016). Structure of the tsunamigenic plate boundary and low-frequency earthquakes in the southern Ryukyu Trench. *Nature Communications*, 7(1), 12255. <https://doi.org/10.1038/ncomms12255>
- Arai, R., Kodaira, S., Yamada, T., Takahashi, T., Miura, S., Kaneda, Y., et al. (2017). Subduction of thick oceanic plateau and high-angle normal-fault earthquakes intersecting the slab. *Geophysical Research Letters*, 44(12), 6109–6115. <https://doi.org/10.1002/2017gl073789>
- Arai, R., Kodaira, S., Yuka, K., Takahashi, T., Miura, S., & Kaneda, Y. (2017). Crustal structure of the southern Okinawa Trough: Symmetrical rifting, submarine volcano, and potential mantle accretion in the continental back-arc basin. *Journal of Geophysical Research: Solid Earth*, 122(1), 622–641. <https://doi.org/10.1002/2016jb013448>
- Avellaneda-Jiménez, D. S., & Monsalve, G. (2022). Arclite nature of the Colombian Andes magmatic arc root: A receiver-function approach. *Tectonophysics*, 836, 229417. <https://doi.org/10.1016/j.tecto.2022.229417>
- Baillard, C., Crawford, W. C., Ballu, V., Régnier, M., Pelletier, E., & Garaebiti, E. (2015). Seismicity and shallow slab geometry in the central Vanuatu subduction zone. *Journal of Geophysical Research: Solid Earth*, 120(8), 5606–5623. <https://doi.org/10.1002/2014jb011853>
- Baker, D. R., & Egglar, D. H. (1987). Compositions of anhydrous and hydrous melts coexisting with plagioclase, augite, and olivine or low-Ca pyroxene from 1 atm to 8 kbar; application to the Aleutian volcanic center of Atka. *American Mineralogist*, 72(1–2), 12–28.
- Bannister, S., Bryan, C. J., & Bibby, H. M. (2004). Shear wave velocity variation across the Taupo Volcanic Zone, New Zealand, from receiver function inversion. *Geophysical Journal International*, 159(1), 291–310. <https://doi.org/10.1111/j.1365-246x.2004.02384.x>
- Barclay, J., & Carmichael, I. S. E. (2004). A hornblende basalt from western Mexico: Water-saturated phase relations constrain a pressure-temperature window of eruptibility. *Journal of Petrology*, 45(3), 485–506. <https://doi.org/10.1093/petrology/egg091>

- Bassett, D., Kopp, H., Sutherland, R., Henrys, S., Watts, A. B., Timm, C., et al. (2016). Crustal structure of the Kermadec arc from MANGO seismic refraction profiles. *Journal of Geophysical Research: Solid Earth*, *121*(10), 7514–7546. <https://doi.org/10.1002/2016jb013194>
- Berndt, J., Koepke, J., & Holtz, F. (2005). An experimental investigation of the influence of water and oxygen fugacity on differentiation of MORB at 200 MPa. *Journal of Petrology*, *46*(1), 135–167. <https://doi.org/10.1093/ptrology/egh066>
- Beck, S. L., Zandt, G., Myers, S. C., Wallace, T. C., Silver, P. G., & Drake, L. (1996). Crustal-thickness variations in the central Andes. *Geology*, *24*(5), 407–410. [https://doi.org/10.1130/0091-7613\(1996\)024<0407:ctvite>2.3.co;2](https://doi.org/10.1130/0091-7613(1996)024<0407:ctvite>2.3.co;2)
- Besana, G. M., Shibusaki, T., Hirano, N., Ando, M., Bautista, B., Narag, I., & Punongbayan, R. S. (2012). The shear wave velocity structure of the crust and uppermost mantle beneath Tagaytay, Philippines inferred from receiver function analysis. *Geophysical Research Letters*, *22*(23), 3143–3146. <https://doi.org/10.1029/95gl03319>
- Bishop, J. W., Lees, J. M., Biryol, C. B., Mikesell, T. D., & Franco, L. (2018). Examining the interior of Llaima Volcano with receiver functions. *Journal of Volcanology and Geothermal Research*, *352*, 1–9. <https://doi.org/10.1016/j.jvolgeores.2017.11.022>
- Blatter, D. L., & Carmichael, I. S. E. (2001). Hydrous phase equilibria of a Mexican high-silica andesite: A candidate for a mantle origin? *Geochimica et Cosmochimica Acta*, *65*(21), 4043–4065. [https://doi.org/10.1016/S0016-7037\(01\)00708-6](https://doi.org/10.1016/S0016-7037(01)00708-6)
- Botcharnikov, R. E., Holtz, F., Almeev, R. A., Sato, H., & Behrens, H. (2008). Storage conditions and evolution of andesitic magma prior to the 1991–95 eruption of Unzen Volcano: Constraints from natural samples and phase equilibria experiments. *Journal of Volcanology and Geothermal Research*, *175*(1–2), 168–180. <https://doi.org/10.1016/j.jvolgeores.2008.03.026>
- Buffoni, C., Schimmel, M., Sabbione, N. C., Rosa, M. L., & Connon, G. (2019). Crustal structure beneath Tierra del Fuego, Argentina, inferred from seismic P-wave receiver functions and ambient noise autocorrelations. *Tectonophysics*, *751*, 41–53. <https://doi.org/10.1016/j.tecto.2018.12.013>
- Calvert, A. J., Klemperer, S. L., Takahashi, N., & Kerr, B. C. (2008). Three-dimensional crustal structure of the Mariana island arc from seismic tomography. *Journal of Geophysical Research*, *113*(B1), B01406. <https://doi.org/10.1029/2007jb004939>
- Castellanos, J. C., Clayton, R. W., & Pérez-Campos, X. (2018). Imaging the eastern trans-Mexican Volcanic Belt with ambient seismic noise: Evidence for a slab tear. *Journal of Geophysical Research: Solid Earth*, *123*(9), 7741–7759. <https://doi.org/10.1029/2018jb015783>
- Chen, Z., Xu, G., & Kubeka, Z. O. (2022). The crustal structure inferred from gravity data and seismic profiles beneath the Okinawa Trough in the western Pacific. *Journal of Asian Earth Sciences*, *238*, 105375. <https://doi.org/10.1016/j.jseas.2022.105375>
- Christeson, G. L., Mann, P., Escalona, A., & Aitken, T. J. (2008). Crustal structure of the Caribbean–northeastern South America arc-continent collision zone. *Journal of Geophysical Research*, *113*(B8), B08104. <https://doi.org/10.1029/2007jb005373>
- Clowes, R. M., Baird, D. J., & Dehler, S. A. (1997). Crustal structure of the Cascadia subduction zone, southwestern British Columbia, from potential field and seismic studies. *Canadian Journal of Earth Sciences*, *34*(3), 317–335. <https://doi.org/10.1139/e17-028>
- Contreras-Reyes, E., Grevemeyer, I., Watts, A. B., Flueh, E. R., Peirce, C., Moeller, S., & Papenberg, C. (2011). Deep seismic structure of the Tonga subduction zone: Implications for mantle hydration, tectonic erosion, and arc magmatism. *Journal of Geophysical Research*, *116*(B10), B10103. <https://doi.org/10.1029/2011jb008434>
- Coudert, E., Cardwell, R. K., Isacks, B. L., & Chatelain, J.-L. (1984). P-wave velocity of the uppermost mantle and crustal thickness in the central Vanuatu Islands (New Hebrides Island arc). *Bulletin of the Seismological Society of America*, *74*(3), 913–924. <https://doi.org/10.1785/bssa0740030913>
- Crawford, W. C., Hildebrand, J. A., Dorman, L. M., Webb, S. C., & Wiens, D. A. (2003). Tonga Ridge and Lau Basin crustal structure from seismic refraction data. *Journal of Geophysical Research*, *108*(B4), 2195. <https://doi.org/10.1029/2001jb001435>
- Draper, D. S., & Johnston, A. D. (1992). Anhydrous PT phase relations of an Aleutian high-MgO basalt: An investigation of the role of olivine-liquid reaction in the generation of arc high-alumina basalts. *Contributions to Mineralogy and Petrology*, *112*(4), 501–519. <https://doi.org/10.1007/BF00310781>
- Eagar, K. C., Fouch, M. J., James, D. E., & Carlson, R. W. (2011). Crustal structure beneath the High Lava Plains of eastern Oregon and surrounding regions from receiver function analysis. *Journal of Geophysical Research*, *116*(B2), B02313. <https://doi.org/10.1029/2010jb007795>
- Feig, S. T., Koepke, J., & Snow, J. E. (2006). Effect of water on tholeiitic basalt phase equilibria: An experimental study under oxidizing conditions. *Contributions to Mineralogy and Petrology*, *152*(5), 611–638. <https://doi.org/10.1007/s00410-006-0123-2>
- Finlayson, D. M., & Cull, J. P. (1973). Time-term analysis of New Britain—New Ireland island arc structures. *Geophysical Journal of the Royal Astronomical Society*, *33*(3), 265–280. <https://doi.org/10.1111/j.1365-246x.1973.tb03421.x>
- Fliedner, M. M., & Klemperer, S. L. (2000). Crustal structure transition from oceanic arc to continental arc, eastern Aleutian Islands and Alaska Peninsula. *Earth and Planetary Science Letters*, *179*(3–4), 567–579. [https://doi.org/10.1016/s0012-821x\(00\)00142-4](https://doi.org/10.1016/s0012-821x(00)00142-4)
- France, L., Koepke, J., Ildefonse, B., Cichy, S. B., & Deschamps, F. (2010). Hydrous partial melting in the sheeted dike complex at fast spreading ridges: Experimental and natural observations. *Contributions to Mineralogy and Petrology*, *160*(5), 683–704. <https://doi.org/10.1007/s00410-010-0502-6>
- Gans, C. R., Beck, S. L., Zandt, G., Gilbert, H., Alvarado, P., Anderson, M., & Linkimer, L. (2011). Continental and oceanic crustal structure of the Pampean flat slab region, western Argentina, using receiver function analysis: New high-resolution results. *Geophysical Journal International*, *186*(1), 45–58. <https://doi.org/10.1111/j.1365-246x.2011.05023.x>
- Gazel, E., Flores, K. E., & Carr, M. J. (2021). Architectural and tectonic control on the segmentation of the Central American volcanic arc. *Annual Review of Earth and Planetary Sciences*, *49*(1), 1–27. <https://doi.org/10.1146/annurev-earth-082420-055108>
- Gilbert, H., Beck, S., & Zandt, G. (2006). Lithospheric and upper mantle structure of central Chile and Argentina. *Geophysical Journal International*, *165*(1), 383–398. <https://doi.org/10.1111/j.1365-246x.2006.02867.x>
- Grove, T. L., Gerlach, D. C., & Sando, T. W. (1982). Origin of calc-alkaline series lavas at Medicine Lake volcano by fractionation, assimilation and mixing. *Contributions to Mineralogy and Petrology*, *80*(2), 160–182. <https://doi.org/10.1007/BF00374893>
- Grove, T. L., & Bryan, W. B. (1983). Fractionation of pyroxene-phyrlic MORB at low pressure: An experimental study. *Contributions to Mineralogy and Petrology*, *84*(4), 293–309. <https://doi.org/10.1007/BF01160283>
- Grove, T. L., & Juster, T. C. (1989). Experimental investigations of low-Ca pyroxene stability and olivine-pyroxene-liquid equilibria at 1-atm in natural basaltic and andesitic liquids. *Contributions to Mineralogy and Petrology*, *103*(3), 287–305. <https://doi.org/10.1007/BF00402916>
- Gunawan, A., Tilmann, F., Lange, D., Collings, R., Rietbrock, A., Natakijaja, D., & Widiyantoro, S. (2011). *Moho depth estimation beneath Sumatera and Mentawai islands using receiver functions recorded with a temporary array*. (Vol. 13, pp. EGU2011–8072). General Assembly European Geosciences Union.
- Gust, D. A., & Perfit, M. R. (1987). Phase relations of a high-Mg basalt from the Aleutian Island Arc: Implications for primary island arc basalts and high-Al basalts. *Contributions to Mineralogy and Petrology*, *97*(1), 7–18. <https://doi.org/10.1007/BF00375210>
- Hamada, M., & Fujii, T. (2007). Experimental constraints on the effects of pressure and H₂O on the fractional crystallization of high-Mg island arc basalt. *Contributions to Mineralogy and Petrology*, *155*(6), 767–790. <https://doi.org/10.1007/s00410-007-0269-6>

- Hammer, J. E., Rutherford, M. J., & Hildreth, W. (2002). Magma storage prior to the 1992 eruption at Novarupta, Alaska. *Contributions to Mineralogy and Petrology*, 144(2), 144–162. <https://doi.org/10.1007/s00410-002-0393-2>
- Hayes, J. L., Holbrook, W. S., Lizarralde, D., Van Avendonk, H. J. A., Bullock, A. D., Mora, M., et al. (2013). Crustal structure across the Costa Rican volcanic arc. *Geochemistry, Geophysics, Geosystems*, 14(4), 1087–1103. <https://doi.org/10.1002/ggge.20079>
- Heit, B., Bianchi, M., Yuan, X., Kay, S. M., Sandvol, E., Kumar, P., et al. (2014). Structure of the crust and the lithosphere beneath the southern Puna plateau from teleseismic receiver functions. *Earth and Planetary Science Letters*, 385, 1–11. <https://doi.org/10.1016/j.epsl.2013.10.017>
- Heit, B., Yuan, X., Bianchi, M., Sodoudi, F., & Kind, R. (2008). Crustal thickness estimation beneath the southern central Andes at 30°S and 36°S from S wave receiver function analysis. *Geophysical Journal International*, 174(1), 249–254. <https://doi.org/10.1111/j.1365-246x.2008.03780.x>
- Husen, A., Almeev, R. R., & Holtz, F. (2016). The effect of H₂O and pressure on multiple saturation and liquid lines of descent in basalt from the Shatsky Rise. *Journal of Petrology*, 57(2), 309–344. <https://doi.org/10.1093/petrology/egw008>
- Ibrahim, A. K., Pontoise, B., Latham, G., Larue, M., Chen, T., Isacks, B., et al. (1980). Structure of the New Hebrides arc-trench system. *Journal of Geophysical Research*, 85(B1), 253–266. <https://doi.org/10.1029/jb085ib01p00253>
- Iwasaki, T., Hirata, N., Kanazawa, T., Melles, J., Suyehiro, K., Urabe, T., et al. (1990). Crustal and upper mantle structure in the Ryukyu Island Arc deduced from deep seismic sounding. *Geophysical Journal International*, 102(3), 631–651. <https://doi.org/10.1111/j.1365-246x.1990.tb04587.x>
- Iwasaki, T., Levin, V., Nikulin, A., & Idaka, T. (2013). Constraints on the Moho in Japan and Kamchatka. *Tectonophysics*, 609, 184–201. <https://doi.org/10.1016/j.tecto.2012.11.023>
- Iwasaki, T., Yoshii, T., Ito, T., Sato, H., & Hirata, N. (2002). Seismological features of island arc crust as inferred from recent seismic expeditions in Japan. *Tectonophysics*, 355(1–4), 53–66. [https://doi.org/10.1016/s0040-1951\(02\)00134-8](https://doi.org/10.1016/s0040-1951(02)00134-8)
- Janiszewski, H. A., Abers, G. A., Shillington, D. J., & Calkins, J. A. (2013). Crustal structure along the Aleutian island arc: New insights from receiver functions constrained by active-source data. *Geochemistry, Geophysics, Geosystems*, 14(8), 2977–2992. <https://doi.org/10.1002/ggge.20211>
- Jia, X., & Sun, D. (2021). Imaging the crustal interfaces along the Ryukyu arc-trough system using precursors to teleseismic sP and pP. *Journal of Geophysical Research: Solid Earth*, 126(2), e2020JB020413. <https://doi.org/10.1029/2020jb020413>
- Kawamoto, T. (1996). Experimental constraints on differentiation and H₂O abundance of calc-alkaline magmas. *Earth and Planetary Science Letters*, 144(3–4), 577–589. [https://doi.org/10.1016/S0012-821X\(96\)00182-3](https://doi.org/10.1016/S0012-821X(96)00182-3)
- Kashubin, S. N., Petrov, O. V., Rybalka, A. V., Milshtein, E. D., Shokalsky, S. P., Verba, M. L., & Petrov, E. O. (2017). Earth's crust model of the South-Okhotsk Basin by wide-angle OBS data. *Tectonophysics*, 710, 37–55. <https://doi.org/10.1016/j.tecto.2016.11.021>
- Katsumata, A. (2010). Depth of the Moho discontinuity beneath the Japanese islands estimated by traveltimes analysis. *Journal of Geophysical Research*, 115(B4), B04303. <https://doi.org/10.1029/2008jb005864>
- Kennedy, A. W., Grove, T. L., & Johnson, R. J. (1990). Experimental and major element constraints on the evolution of lavas from Lihir Island, Papua New Guinea. *Contributions to Mineralogy and Petrology*, 104(6), 722–734. <https://doi.org/10.1007/BF01167289>
- Kieling, K., Roessler, D., & Krueger, F. (2011). Receiver function study in northern Sumatra and the Malaysian peninsula. *Journal of Seismology*, 15(2), 235–259. <https://doi.org/10.1007/s10950-010-9222-7>
- Kim, Y., Clayton, R. W., & Jackson, J. M. (2010). Geometry and seismic properties of the subducting Cocos plate in central Mexico. *Journal of Geophysical Research*, 115(B6), B06310. <https://doi.org/10.1029/2009jb006942>
- Kinzler, R. J., & Grove, T. L. (1985). Crystallization and differentiation of Archean komatiite lavas from northeast Ontario: Phase equilibrium and kinetic studies. *American Mineralogist*, 70(1–2), 40–51.
- Kinzler, R. J., & Grove, T. L. (1992). Primary magmas of mid-ocean ridge basalts 1. Experiments and methods. *Journal of Geophysical Research*, 97(B5), 6885–6906. <https://doi.org/10.1029/91JB02840>
- Klingelhoefer, F., Berthet, T., Lallemand, S., Schnurle, P., Lee, C.-S., Liu, C.-S., et al. (2012). P-wave velocity structure of the southern Ryukyu margin east of Taiwan: Results from the ACTS wide-angle seismic experiment. *Tectonophysics*, 578, 50–62. <https://doi.org/10.1016/j.tecto.2011.10.010>
- Koch, C. D., Delph, J., Beck, S. L., Lynner, C., Ruiz, M., Hernandez, S., et al. (2021). Crustal thickness and magma storage beneath the Ecuadorian arc. *Journal of South American Earth Sciences*, 110, 103331. <https://doi.org/10.1016/j.jsames.2021.103331>
- Kodaira, S., Sato, T., Takahashi, N., Ito, A., Tamura, Y., Tatsumi, Y., & Kaneda, Y. (2007). Seismological evidence for variable growth of crust along the Izu intraoceanic arc. *Journal of Geophysical Research*, 112(B5), B05104. <https://doi.org/10.1029/2006jb004593>
- Kogiso, T., & Hirschmann, M. M. (2001). Experimental study of clinopyroxenite partial melting and the origin of ultra-calcic melt inclusions. *Contributions to Mineralogy and Petrology*, 142(3), 347–360. <https://doi.org/10.1007/s004100100295>
- Koulakov, I. Y. (2022). Seismic tomography of Kamchatkan Volcanoes. *Russian Geology and Geophysics*, 63(11), 1207–1244. <https://doi.org/10.2113/rgg20214380>
- Ku, C., Kuo, Y., Chao, W., You, S., Huang, B., Chen, Y., et al. (2018). A first-layered crustal velocity model for the western Solomon islands: Inversion of the measured group velocity of surface waves using ambient noise. *Seismological Research Letters*, 89(6), 2274–2283. <https://doi.org/10.1785/0220180126>
- Ku, C.-S., Kuo, Y.-T., Huang, B.-S., Chen, Y.-G., & Wu, Y.-M. (2020). Seismic velocity structure beneath the western Solomon Islands from the joint inversion of receiver functions and surface-wave dispersion curves. *Journal of Asian Earth Sciences*, 195, 104378. <https://doi.org/10.1016/j.jseas.2020.104378>
- Lange, D., Tilmann, F., Henstock, T., Rietbrock, A., Natawidjaja, D., & Kopp, H. (2018). Structure of the central Sumatran subduction zone revealed by local earthquake travel-time tomography using an amphibious network. *Solid Earth*, 9(4), 1035–1049. <https://doi.org/10.5194/se-9-1035-2018>
- Lawrence, J. F., & Wiens, D. A. (2004). Combined receiver-function and surface wave phase-velocity inversion using a niching genetic algorithm: Application to Patagonia. *Bulletin of the Seismological Society of America*, 94(3), 977–987. <https://doi.org/10.1785/0120030172>
- Levin, V., Park, J., Brandon, M., Lees, J., Peyton, V., Gordeev, E., & Ozerov, A. (2002). Crust and upper mantle of Kamchatka from teleseismic receiver functions. *Tectonophysics*, 358(1–4), 233–265. [https://doi.org/10.1016/s0040-1951\(02\)00426-2](https://doi.org/10.1016/s0040-1951(02)00426-2)
- Lizarralde, D., Holbrook, W. S., McGeary, S., Bangs, N. L., & Diebold, J. B. (2002). Crustal construction of a volcanic arc, wide-angle seismic results from the western Alaska Peninsula. *Journal of Geophysical Research*, 107(B8), EPM4-1–EPM4-21. <https://doi.org/10.1029/2001jb000230>
- Lücke, O. H., & Arroyo, I. G. (2015). Density structure and geometry of the Costa Rican subduction zone from 3-D gravity modeling and local earthquake data. *Solid Earth*, 6(4), 1169–1183. <https://doi.org/10.5194/se-6-1169-2015>
- MacKenzie, L., Abers, G. A., Fischer, K. M., Syracuse, E. M., Protti, J. M., Gonzalez, V., & Strauch, W. (2008). Crustal structure along the southern Central American volcanic front. *Geochemistry, Geophysics, Geosystems*, 9(8), Q08S09. <https://doi.org/10.1029/2008gc001991>

- Mandler, B. E., Donnelly-Nolan, J. M., & Grove, T. L. (2014). Straddling the tholeiitic/calc-alkaline transition: The effects of modest amounts of water on magmatic differentiation at Newberry Volcano, Oregon. *Contributions to Mineralogy and Petrology*, 168(4), 57. <https://doi.org/10.1007/s00410-014-1066-7>
- Maurice, S. D. R., Wiens, D. A., Koper, K. D., & Vera, E. (2003). Crustal and upper mantle structure of southernmost South America inferred from regional waveform inversion. *Journal of Geophysical Research*, 108(B1), 2038. <https://doi.org/10.1029/2002jb001828>
- Marxer, F., & Ulmer, P. (2019). Crystallisation and zircon saturation of calc-alkaline tonalite from the Adamello Batholith at upper crustal conditions: An experimental study. *Contributions to Mineralogy and Petrology*, 174(10), 84. <https://doi.org/10.1007/s00410-019-1619-x>
- Matsubara, M., Sato, H., Ishiyama, T., & Horne, A. V. (2017). Configuration of the Moho discontinuity beneath the Japanese Islands derived from three-dimensional seismic tomography. *Tectonophysics*, 710, 97–107. <https://doi.org/10.1016/j.tecto.2016.11.025>
- McGlashan, N., Brown, L., & Kay, S. (2008). Crustal thickness in the central Andes from teleseismically recorded depth phase precursors. *Geophysical Journal International*, 175(3), 1013–1022. <https://doi.org/10.1111/j.1365-246x.2008.03897.x>
- Meen, J. K. (1990). Elevation of potassium content of basaltic magma by fractional crystallization: The effect of pressure. *Contributions to Mineralogy and Petrology*, 104(3), 309–331. <https://doi.org/10.1007/BF00321487>
- Melekhova, E., Blundy, J., Martin, R., Arculus, R., & Pichavant, M. (2017). Petrological and experimental evidence for differentiation of water-rich magmas beneath St. Kitts, Lesser Antilles. *Contributions to Mineralogy and Petrology*, 172(11–12), 1234. <https://doi.org/10.1007/s00410-017-1416-3>
- Melekhova, E., Schlaphorst, D., Blundy, J., Kendall, J.-M., Connolly, C., McCarthy, A., & Arculus, R. (2019). Lateral variation in crustal structure along the Lesser Antilles arc from petrology of crustal xenoliths and seismic receiver functions. *Earth and Planetary Science Letters*, 516, 12–24. <https://doi.org/10.1016/j.epsl.2019.03.030>
- Métrich, N., & Rutherford, M. J. (1998). Low pressure crystallization paths of H₂O-saturated Basaltic-Hawaiitic melts from Mt. Etna: Implications for open-system degassing of basaltic volcanoes. *Geochimica et Cosmochimica Acta*, 62(7), 1195–1205. [https://doi.org/10.1016/S0016-7037\(98\)00048-9](https://doi.org/10.1016/S0016-7037(98)00048-9)
- Miura, S., Suyehiro, K., Shinohara, M., Takahashi, N., Araki, E., & Taira, A. (2004). Seismological structure and implications of collision between the Ontong Java Plateau and Solomon Island Arc from ocean bottom seismometer–airgun data. *Tectonophysics*, 389(3–4), 191–220. <https://doi.org/10.1016/j.tecto.2003.09.029>
- Moore, G., & Carmichael, I. S. E. (1998). The hydrous phase equilibria (to 3 kbar) of an andesite and basaltic andesite from western Mexico: Constraints on water content and conditions of phenocryst growth. *Contributions to Mineralogy and Petrology*, 130(3–4), 304–319. <https://doi.org/10.1007/s004100050367>
- Nakamura, M., & Umedu, N. (2009). Crustal thickness beneath the Ryukyu arc from travel-time inversion. *Earth Planets and Space*, 61(10), 1191–1195. <https://doi.org/10.1186/bf03352971>
- Nakanishi, A., Kurashimo, E., Tatsumi, Y., Yamaguchi, H., Miura, S., Kodaira, S., et al. (2009). Crustal evolution of the southwestern Kuril Arc, Hokkaido Japan, deduced from seismic velocity and geochemical structure. *Tectonophysics*, 472(1–4), 105–123. <https://doi.org/10.1016/j.tecto.2008.03.003>
- Nakajima, J., Matsuzawa, T., & Hasegawa, A. (2002). Moho depth variation in the central part of northeastern Japan estimated from reflected and converted waves. *Physics of the Earth and Planetary Interiors*, 130(1–2), 31–47. [https://doi.org/10.1016/s0031-9201\(01\)00307-7](https://doi.org/10.1016/s0031-9201(01)00307-7)
- Nakajima, J., Matsuzawa, T., Hasegawa, A., & Zhao, D. (2001). Three-dimensional structure of Vp, Vs, and Vp/Vs beneath northeastern Japan: Implications for arc magmatism and fluids. *Journal of Geophysical Research*, 106(B10), 21843–21857. <https://doi.org/10.1029/2000jb000008>
- Nikulin, A., Levin, V., Shuler, A., & West, M. (2010). Anomalous seismic structure beneath the Klyuchevskoy Group, Kamchatka. *Geophysical Research Letters*, 37(14), L14311. <https://doi.org/10.1029/2010gl043904>
- Nishizawa, A., Kaneda, K., Oikawa, M., Horiuchi, D., Fujioka, Y., & Okada, C. (2019). Seismic structure of rifting in the Okinawa Trough, an active backarc basin of the Ryukyu (Nansei-Shoto) island arc–trench system. *Earth Planets and Space*, 71(1), 21. <https://doi.org/10.1186/s40623-019-0998-6>
- Nurfiani, D., Wang, X., Gunawan, H., Triastuty, H., Hidayat, D., Wei, S. J., et al. (2021). Combining petrology and seismology to unravel the plumbing system of a typical arc volcano: An example from Marapi, West Sumatra, Indonesia. *Geochemistry, Geophysics, Geosystems*, 22(4), e2020GC009524. <https://doi.org/10.1029/2020gc009524>
- Obrebski, M., Abers, G. A., & Foster, A. (2015). Magmatic arc structure around Mount Rainier, WA, from the joint inversion of receiver functions and surface wave dispersion. *Geochemistry, Geophysics, Geosystems*, 16(1), 178–194. <https://doi.org/10.1002/2014gc005581>
- Oda, H., & Ushio, T. (2007). Topography of the Moho and Conrad discontinuities in the Kyushu district, southwest Japan. *Journal of Seismology*, 11(2), 221–233. <https://doi.org/10.1007/s10950-007-9049-z>
- Parsons, T., Blakely, R. J., Brocher, T. M., Christensen, N. I., Fisher, M. A., Flueh, E., et al. (2005). Crustal structure of the Cascadia fore arc of Washington. USGS Professional Paper, 1661. <https://doi.org/10.3133/pp1661d>
- Pavlenkova, N. I., Kashubin, S. N., Sakoulina, T. S., & Pavlenkova, G. A. (2020). Geodynamic nature of the Okhotsk Sea lithosphere. An overview of seismic constraints. *Tectonophysics*, 777, 228320. <https://doi.org/10.1016/j.tecto.2020.228320>
- Pérez-Campos, X., Kim, Y., Husker, A., Davis, P. M., Clayton, R. W., Iglesias, A., et al. (2008). Horizontal subduction and truncation of the Cocos Plate beneath central Mexico. *Geophysical Research Letters*, 35(18), L18303. <https://doi.org/10.1029/2008gl035127>
- Pertermann, M., & Lundstrom, C. C. (2006). Phase equilibrium experiments at 0.5 GPa and 1100–1300°C on a basaltic andesite from Arenal Volcano, Costa Rica. *Journal of Volcanology and Geothermal Research*, 157(1–3), 222–235. <https://doi.org/10.1016/j.jvolgeores.2006.03.043>
- Phillips, K., Clayton, R. W., Davis, P., Tavera, H., Guy, R., Skinner, S., et al. (2012). Structure of the subduction system in southern Peru from seismic array data. *Journal of Geophysical Research*, 117(B11), B11306. <https://doi.org/10.1029/2012jb009540>
- Pichavant, M., Martel, C., Bourdier, J.-L., & Scailliet, B. (2002). Physical conditions, structure, and dynamics of a zoned magma chamber: Mount Pelée (Martinique, Lesser Antilles Arc). *Journal of Geophysical Research*, 107(B5), 2093. <https://doi.org/10.1029/2001JB000315>
- Poveda, E., Monsalve, G., & Vargas, C. A. (2015). Receiver functions and crustal structure of the northwestern Andean region, Colombia. *Journal of Geophysical Research: Solid Earth*, 120(4), 2408–2425. <https://doi.org/10.1002/2014jb011304>
- Ramachandran, K., Hyndman, R. D., & Brocher, T. M. (2006). Regional P wave velocity structure of the Northern Cascadia Subduction Zone. *Journal of Geophysical Research*, 111(B12), B12301. <https://doi.org/10.1029/2005jb004108>
- Rodríguez, E. E., & Russo, R. M. (2020). Southern Chile crustal structure from teleseismic receiver functions: Responses to ridge subduction and terrane assembly of Patagonia. *Geosphere*, 16(1), 378–391. <https://doi.org/10.1130/ges01692.1>
- Rodríguez-Domínguez, M., Pérez-Campos, X., Montealegre-Cázares, C., Clayton, R. W., & Cabral-Cano, E. (2019). Crustal structure variations in south-central Mexico from receiver functions. *Geophysical Journal International*, 219(3), 2174–2186. <https://doi.org/10.1093/gji/ggz434>
- Rondenay, S., Bostock, M. G., & Shragge, J. (2001). Multiparameter two-dimensional inversion of scattered teleseismic body waves 3. Application to the Cascadia 1993 data set. *Journal of Geophysical Research*, 106(B12), 30795–30807. <https://doi.org/10.1029/2000jb000039>

- Ryan, J., Beck, S., Zandt, G., Wagner, L., Minaya, E., & Tavera, H. (2016). Central Andean crustal structure from receiver function analysis. *Tectonophysics*, 682, 120–133. <https://doi.org/10.1016/j.tecto.2016.04.048>
- Sakaguchi, K., Gilbert, H., & Zandt, G. (2006). Converted wave imaging of the Toba Caldera, Indonesia. *Geophysical Research Letters*, 33(20), L20305. <https://doi.org/10.1029/2006gl027397>
- Salmon, M. L., Stern, T. A., & Savage, M. K. (2011). A major step in the continental Moho and its geodynamic consequences: The Taranaki–Ruapehu line, New Zealand. *Geophysical Journal International*, 186(1), 32–44. <https://doi.org/10.1111/j.1365-246x.2011.05035.x>
- Sano, T., & Yamashita, S. (2004). Experimental petrology of basement lavas from Ocean Drilling Program Leg 192: Implications for differentiation processes in Ontong Java Plateau magmas. *Geological Society, London, Special Publications*, 229(1), 185–218. <https://doi.org/10.1144/GSL.SP.2004.229.01.12>
- Schlaphorst, D., Melekhova, E., Kendall, J.-M., Blundy, J., & Latchman, J. L. (2018). Probing layered arc crust in the Lesser Antilles using receiver functions. *Royal Society Open Science*, 5(11), 180764. <https://doi.org/10.1098/rsos.180764>
- Shiomi, K., Obara, K., & Sato, H. (2006). Moho depth variation beneath southwestern Japan revealed from the velocity structure based on receiver function inversion. *Tectonophysics*, 420(1–2), 205–221. <https://doi.org/10.1016/j.tecto.2006.01.017>
- Soudou, F., Kind, R., Hatzfeld, D., Priestley, K., Hanka, W., Wylegalla, K., et al. (2006). Lithospheric structure of the Aegean obtained from P and S receiver functions. *Journal of Geophysical Research*, 111(B12), B12307. <https://doi.org/10.1029/2005jb003932>
- Stefano, R. D., Bianchi, I., Ciaccio, M. G., Carrara, G., & Kissling, E. (2011). Three-dimensional Moho topography in Italy: New constraints from receiver functions and controlled source seismology. *Geochemistry, Geophysics, Geosystems*, 12(9), Q09006. <https://doi.org/10.1029/2011gc003649>
- Stratford, W., Peirce, C., Paulatto, M., Funnell, M., Watts, A. B., Grevemeyer, I., & Bassett, D. (2015). Seismic velocity structure and deformation due to the collision of the Louisville Ridge with the Tonga-Kermadec Trench. *Geophysical Journal International*, 200(3), 1503–1522. <https://doi.org/10.1093/gji/ggu475>
- Suhardja, S. K., Grand, S. P., Wilson, D., Guzman-Speziale, M., Gomez-Gonzalez, J. M., Dominguez-Reyes, T., & Ni, J. (2015). Crust and subduction zone structure of southwestern Mexico. *Journal of Geophysical Research: Solid Earth*, 120(2), 1020–1035. <https://doi.org/10.1002/2014jb011573>
- Takahashi, N., Kodaira, S., Klemperer, S. L., Tatsumi, Y., Kaneda, Y., & Suyehiro, K. (2007). Crustal structure and evolution of the Mariana intra-oceanic island arc. *Geology*, 35(3), 203–206. <https://doi.org/10.1130/g23212a.1>
- Takahashi, N., Kodaira, S., Tatsumi, Y., Yamashita, M., Sato, T., Kaiho, Y., et al. (2009). Structural variations of arc crusts and rifted margins in the southern Izu-Ogasawara arc–back arc system. *Geochemistry, Geophysics, Geosystems*, 10(9), Q09X08. <https://doi.org/10.1029/2008gc002146>
- Takahashi, N., Suyehiro, K., & Shinohara, M. (1998). Implications from the seismic crustal structure of the northern Izu–Bonin arc. *Island Arc*, 7(3), 383–394. <https://doi.org/10.1111/j.1440-1738.1998.00197.x>
- Thy, P., Leshner, C. E., & Fram, M. S. (1998). Low pressure experimental constraints on the evolution of basaltic lavas from site 917, southeast Greenland continental margin. *Proceedings of the Ocean Drilling Program—Scientific Results*, 152, 359–372. <https://doi.org/10.2973/odp.proc.sr.152.235.1998>
- Tsumura, N., Matsumoto, S., Horiuchi, S., & Hasegawa, A. (2000). Three-dimensional attenuation structure beneath the northeastern Japan arc estimated from spectra of small earthquakes. *Tectonophysics*, 319(4), 241–260. [https://doi.org/10.1016/s0040-1951\(99\)00297-8](https://doi.org/10.1016/s0040-1951(99)00297-8)
- Tuff, J., Takahashi, E., & Gibson, S. A. (2005). Experimental constraints on the role of garnet pyroxenite in the genesis of high-Fe mantle plume derived melts. *Journal of Petrology*, 46(10), 2023–2058. <https://doi.org/10.1093/petrology/egi046>
- Van Avendonk, H. J. A., Shillington, D. J., Holbrook, W. S., & Hornbach, M. J. (2004). Inferring crustal structure in the Aleutian island arc from a sparse wide-angle seismic data set. *Geochemistry, Geophysics, Geosystems*, 5(8), 4395. <https://doi.org/10.1029/2003gc000664>
- Wagner, D., Koulakov, I., Rabbel, W., Luehr, B. G., Wittwer, A., Kopp, H., et al. (2007). Joint inversion of active and passive seismic data in Central Java. *Geophysical Journal International*, 170(2), 923–932. <https://doi.org/10.1111/j.1365-246x.2007.03435.x>
- Wan, K., Lin, J., Xia, S., Sun, J., Xu, M., Yang, H., et al. (2019). Deep seismic structure across the southernmost Mariana trench: Implications for arc rifting and plate hydration. *Journal of Geophysical Research: Solid Earth*, 124(5), 4710–4727. <https://doi.org/10.1029/2018jb017080>
- Whitaker, M. L., Nekvasil, H., Lindsley, D. H., & McCurry, M. (2007). Can crystallization of olivine tholeiite give rise to potassic rhyolites?—An experimental investigation. *Bulletin of Volcanology*, 70(3), 417–434. <https://doi.org/10.1007/s00445-007-0146-1>
- Wu, H.-H., Tsai, Y.-B., Lee, T.-Y., Lo, C.-H., Hsieh, C.-H., & Toan, D. V. (2004). 3-D shear wave velocity structure of the crust and upper mantle in South China Sea and its surrounding regions by surface wave dispersion analysis. *Marine Geophysical Researches*, 25(1–2), 5–27. <https://doi.org/10.1007/s11001-005-0730-8>
- Yuan, X., Asch, G., Bataille, K., Bock, G., Bohm, M., Echtler, H., et al. (2006). Deep seismic images of the southern Andes. In S. M. Kay & V. A. Ramos (Eds.), *Evolution of an Andean margin: Tectonic and magmatic view from the Andes to the Neuque'n Basin (35°–39°S lat)* (Vol. 407, pp. 61–72). [https://doi.org/10.1130/2006.2407\(03\)](https://doi.org/10.1130/2006.2407(03))
- Zhang, P., & Miller, M. S. (2021). Seismic imaging of the subducted Australian continental margin beneath timor and the Banda Arc collision zone. *Geophysical Research Letters*, 48(4), e2020GL089632. <https://doi.org/10.1029/2020gl089632>